INFLUENCE OF ADDITIVES ON THE FOAMABILITY OF POTATO STARCH BASED BIOPOLYMERS

INFLUENCE OF ADDITIVES ON THE FOAMABILITY OF POTATO STARCH BASED BIOPOLYMERS

By
HITESHKUMAR OZA

A Thesis
Submitted to the School of Graduate Studies
In Partial Fulfillment of the Requirements
For the Degree
Master of Applied Science

McMaster University

MASTER OF APPLIED SCIENCE (2011) McMaster University

(Chemical Engineering) Hamilton, Ontario

TITLE: **Influence of Additives on the Foamability of Potato Starch based Biopolymers**

AUTHOR: Hiteshkumar Oza

B. Eng. (Dharmsinh Desai Institute of Technology, India)

SUPERVISORS: Dr. Michael Thompson

Dr. Andrew Hrymak

NUMBER OF PAGES: XXII – 199

ABSTRACT

Potato starch based bio-polymers are brittle, moisture sensitive, low modulus materials with limited suitable for short term disposable plastics applications. Foaming can overcome much of the brittle features of a resin but the stiffness of a material will directly impact foamability. Blending Polylactic acid (PLA) with starch will increases hydrophobicity and mechanical strength of the thermoplastic resin. Unfortunately, PLA/Starch blend remain brittle and exhibit insufficient melt strength to display suitable foamability attributes.

This thesis looked into the influence of additive like chain extenders to diversify the application of potato based novel biopolymers as foam-grade materials. To improve foamability, which is largely dependent on melt strength, it is possible to modify available blends by bulk modification with bi- and multi- functional epoxy chain extenders. The modification work was carried out using twin screw extruder (TSE) and an internal batch mixer (Haake Mixer) with four different chain extenders. The modified blends were characterized by Parallel Plate Rheometry, DSC, Intrinsic Viscosity and SEM techniques. Finally, foamability of modified blends was examined by using supercritical CO_2 as a physical blowing agent in a high-pressure batch vessel. Variables such as saturation pressure, saturation time and saturation temperature were adjusted to determine their influence on the cell morphology of the foamed parts.

It was found that the chain extension with multi-functional epoxy-styrene-acrylic chain extenders greatly reduced the crystalline content of the PLA phase in the Solanyl® biopolymers. The addition of multi-functional epoxy chain extenders significantly increased the melt viscosity of Solanyl® biopolymers compared to bi-functional epoxy chain extenders. Such improvement in the melt viscosity of modified blends helped stabilize the evolved cellular structure of foamed parts produced by a batch foaming process, yielding smaller cell size and higher cell density in comparison with neat foamed Solanyl® biopolymers. Finally, through use of Intrinsic Viscosity as a characterization method and solvent-selective separation of two polymer phases, it was determined that the chain extension reaction occurred preferentially in the PLA phase with no detectable change in value for the starch component.

ॐ

OM

भूर्भुवाः स्वः

BHURBHUVAH SVAH

तत्सवितुर्वरेण्यं

TATSAVITURVARENYAM

भर्गो देवस्य धीमही

BHARGO DEVASYA DHIMAHI

धियो योनः प्रचोदयात्

DHIYO YONAH PRACHODAYAT

Earth Atmosphere Heavens.
We meditate on the sacred light
of the effulgent source.
Let that inspire
our thoughts.

ACKNOWLEDGEMENTS

I would like to acknowledge my supervisor and my mentor, Dr. Michael Thompson for his constructive guidance, encouragement and never-ending supports throughout the course of this research work.

I would also like to acknowledge my special thanks to Dr. Andrew Hrymak for his continuous guidance on the discussion part of this thesis during two years period.

I would like to express my most sincere thanks to Agriculture Bioproducts Innovation Program (ABIP by Agriculture and Agri-Food Canada) for their funding of this research, and also, to Solanyl Biopolymers Inc. for providing materials for this project.

I would like to convey my special thanks to Dr. Alex D. Sokolowski from BASF (Business Development Manager- Joncryl® Functional Additives) for providing Joncryl® chain extenders for our research work.

I would like to express my thanks to Ms. Elizabeth Takacs (Lab Manager of MMRI) and Ms. Justyna Derkach (Lab Assistant) for their trainings and assistance to use lab instruments. Also, thanks to Paul Gatt for his technical support on my experimental apparatus.

I would also like to acknowledge my deepest thanks to the chemical engineering department staffs who are working hard to keep things running well.

Finally, but certainly not the least, I would like to thank my parents, my wife Rashmi , and my son Pranay for all the love, encouragement and faith they blessed me with.

TABLE OF CONTENTS

LIST OF FIGURES

LIST OF TABLES

NOMENCLATURE

AAC	Aliphatic or Aromatic Copolyester
a-PLA	Amorphous PLA
c-PLA	Semi-crystalline PLA
CE	Chain Extender
DGEBA	Diglycidyl Ether Bisphenol A
DP	Degree Of Polymerization
EBC	Easter Bio Co-polyester
EMC	Equilibrium Moisture Content
ISO	International Organization for Standardization
LDPE	Low-Density Polyethylene
MA-g-PLA	Maleic Anhydride grafted Polylactic Acid
PCL	Polycaprolactum
PE	Polyethylene
PEG	Poly (ethylene glycol)
PEG-DGE	Poly (ethylene glycol) Diglycidyl Ether
PET	Polyethylene Teraphthalate
PHA	Polyhydroxyalkanoates
PLA	Polylactic Acid
PP	Polypropylene
PVC	Polyvinyl Chloride
PVOH	Poly(vinyl alchohol)
RSD	Relative Standard Deviation
TPS	Thermoplastic Starch

CHAPTER: 1

INTRODUCTION

1.1 BACKGROUND

Today, a world without plastic is incomprehensive and it plays an important role in human life. The world production of plastics is estimated to be more than 150 million tonnes per year (Ren, 2003). Plastics with high mechanical strength, durability, low price and low density are usually made from petroleum resources. Thermoplastic foams can be made from petroleum based synthetic polymers by creating a cellular core structure in a polymer matrix by the expansion of a blowing agent. These thermoplastic foams have been extensively used in a variety of applications, such as impact and sound insulation, weight reduction, packaging and buoyancy devices. Traditional synthetic polymers used

for the manufacturing of thermoplastic foams are polyethylene (PE), polypropylene (PP), polystyrene (PS), polyvinyl chloride (PVC), polyethylene terephthalate (PET) etc. Due to the larger amount of usage and its non-biodegradable nature, disposal of these foams have caused concerns about their negative impact on the environment for last two or three decades. To overcome their non-biodegradability, one option is to recycle synthetic plastics. But, now a day it is more expensive to recycle plastic and bring them back into the market than it is to make new ones. In addition, the energetic plastic recycling processes omit toxic gas (e.g. dioxin) (Averous et al., 2009). As a result, a small portion of used thermoplastic foams has been recycled and most of the foams are disposed to landfills due to end-use contaminations. However, tougher environment laws and increasing disposal cost have forced research institutes and industries to develop materials that are renewables, degradable and recyclable, better known as "green materials".

Starch is a natural bio-polymer, abundant in supply, a low-cost alternative to the petroleum-based materials and better known among "green materials". Their use in plastic production would greatly reduce the demand for non-biodegradable plastics. Starch has been studied extensively as raw materials for making foam products. Starch based foamed products usually have poor physical and mechanical properties and they are highly water-soluble (Fang and Hanna, 2000; Zhang et al., 2007a). Water has been used as a plasticizer as well as a blowing agent in the manufacturing of breakfast cereals and insulation foams because it is inexpensive and environmental friendly solvent for

starch. However, those foams have more open-cell structure and low mechanical strength compared to expanded polystyrene based foams.

Starch often blended with hydrophobic petroleum-based polymers in order to reduce the usage of petroleum polymers and the moisture sensitivity (Bhatnager and Hanna, 1995; Zhang et al., 2007b). However, the use of non-biodegradable polymers significantly reduced the biodegradability of blend compared to pure commercial starch loose-fill packaging material (Bhatnagar and Hanna, 1995). To improve both water resistance and mechanical properties of the foamed materials, biodegradable polymers can be incorporated into starch-based foams. Such product should be completely biodegradable and possess excellent mechanical properties. Much attention has been given to biodegradable polymeric foam products made from renewable sources, such as polylactic acid (PLA).

PLA belongs to the family of aliphatic polyesters and is the first commercialized biodegradable polymer that is derived from renewable agriculture resources such as corn or sugar beets. The basic building block for PLA is lactic acid (2-hydroxy propionic acid), produced by fermentation of corn starch. Lactic acid can exist as one of two dimer stereoisomers, L-lactic acid and D-lactic acid. It is one of the few polymers, whose mechanical properties, permeability, heat deflection temperature and biodegradation rate in a composting environment can be easily modify by ring-opening polymerization of a controlled mixture of the L- and D-isomers (Mihai et al.,2007; Lim et al.,2008). This biodegradable thermoplastic polyester has functional properties comparable to those of

many petroleum-based plastics. However, PLA is expensive compared to the synthetic plastic due to its complicated synthesis and mostly used in high value films, thermoforms, food & beverage containers and biocompatible/bioabsorbable medical market. Recently its cost has been greatly reduced to the point that it can be now used for manufacturing of low end packaging products.

Incorporation of dry starch into PLA reduces the overall raw materials cost, improved water resistance and increased the biodegradation rate of PLA phase (Huneault et al., 2007; Ning et al., 2008; Shin et al., 2011). Blending of dry starch with PLA increases the rigidity of the material but at the same time increases the intrinsic brittleness of the PLA phase. The blend of hydrophilic starch and hydrophobic PLA is thermodynamically immiscible leading to poor interfacial adhesion between the two components, resulting in irreproducible and less than optimal mechanical properties (Zhang et al., 2004). However, the blend of gelatinized starch/PLA show much finer dispersed morphology than the native dry starch and the resulting foams retained its biodegradability and water resistance characteristics (Zhang et al., 2007a). In term of foaming, the use of water as a blowing agent in the starch/PLA blend result in poor cell morphology and it also promotes undesirable hydrolysis of PLA at elevated temperature, leading to loss of molecular weight. The depolymerisation of PLA can cause reduction in the melt viscosity and elasticity of starch/PLA blend. However, the higher melt viscosity and elasticity are required for the blow molding and foaming processes (Mihai et al.,

2007; Zhang et al., 2007b). In this research, the low cost and non-flammable supercritical CO_2 has been used as a blowing agent.

In order to increase the usefulness of starch/PLA blend in foaming processes, its melt strength must be increased during processing. Recently, considerable research has been devoted to the development of higher molecular weight polymers by post-polymerization reaction during compounding in extruders or injection-molding machines by using bi- or multi-functional chain extender (CE). Chain extension is largely obtained by bridging the hydroxyl or carboxyl reactive end groups with bi- or multi-functional epoxy molecules. This is especially useful to enhance the molecular weight and melt viscosity of a polymer yet has also been shown to increase strain-hardening behaviour which is beneficial to stabilizing foam morphology. Thus, chain extension enables the fine tuning of the material rheology for a foaming process.

1.2 RESEARCH OBJECTIVE

This research work is focused on methods to improve the foamability of new commercially available biopolymers, in this specific case, those incorporating starch such as the grades supplied by Solanyl® Biopolymer Inc. The influence of bi- and multi-functional epoxy chain extenders on the fomability of the Solanyl® blend 30R and model system of just hydrolyzed starch (Solanyl® 100 BP)/PLA will be studied with respect to their improvement on foamability by using a high-pressure batch foaming apparatus. The specific objectives of this research are:

- Determine the most effective chain extenders in affecting the thermal and rheological properties of a hydrolyzed potato starch/PLA blend (and its comparable commercial resin).
- Established the effectiveness in the rheological changes made to the blend by batch foaming, examining different parameters of saturation pressure, saturation time and saturation temperature on final foam properties.

1.3 THESIS OUTLINE

The following chapters outline the framework of research in this thesis:

- Chapter 1 presented the brief introduction to the background of subject, research objective and thesis outline
- Chapter 2 covered the literature review on biodegradable polymers, foaming process, starch/PLA foams and identified the importance of the chain extender
- Chapter 3 described the experimental procedures, melt processing of blends, batch foaming apparatus and characterization techniques
- Chapter 4 included the thermal analysis of the neat and the modified blends with chain extenders
- Chapter 5 included the SEM and intrinsic viscosity analysis of the neat and the modified blends with chain extender
- Chapter 6 included the parallel plate rheology study of the neat and the modified blends with chain extenders

- Chapter 7 included the effect of the batch foaming parameters on the foam morphology of the neat and the modified blends with chain extenders
- Chapter 8 included both the conclusion based on our experimental data analysis and possible future work related to this research work
- Chapter 9 included the list of references had been used for this research work

CHAPTER: 2

LITERATURE REVIEW

2.1 BIODEGRADABLE POLYMER

Using synthetic and long lasting polymers for short-lived items in food packaging, dinner utensils, trash bags, diapers, planting pots and agriculture films has raised concerns about disturbing and damaging the ecosystem. Specifically, resources for manufacture of synthetic polymers are being depleted while the price is constantly rising, and incineration of these synthetic polymers may generate toxic gases while satisfactory landfill sites are limited. As a consequence, there are both academic as well as industrial interests in developing biodegradable polymers from renewable resources. According to study by SRI Consulting company on "Biodegradable Polymers", the total consumption of biodegradable polymers in North America, Europe and Asia are forecast to grow at an

average annual rate of nearly 13% over the five-year period from 2009 to 2014 (GreenerPackage, 2010).

A product is considered biodegradable when it will degrade into water and carbon dioxide through naturally occurring micro-organisms. In addition, to be considered compostable, three criteria must be met: biodegradation—it has to break down into carbon dioxide, water and biomass at the same rate as cellulose; disintegration—the plastic must become indistinguishable in the compost; and non-toxicity—it has no harmful side effect on the environment. According to ISO 17088 standard, products are called compostable when at least 60% of biodegradation take place within 180 days in a compostable environment. The issue between bio-based and biodegradable materials has continued to attract attention worldwide. In the U.S. and Europe, industry sources comment that the idea of bio-based or "where it comes from" versus biodegradable or "where it goes" is currently driving or will drive the overall biopolymers market in the future (GreenerPackage, 2010).

2.2 CLASSIFICATION OF BIODEGRADABLE POLYMER

A biodegradable polymer can be classified by how it is synthesized and formed during its growth cycle. Based on that, it is classified as biosynthetic, semi-biosynthetic and chemosynthetic. Biosynthetic polymers are prepared directly from biomass (e.g. plants – starch), and are biodegradable within a reasonable time scale. However, semi-biosynthetic polymers, prepared from polymerization of renewable monomer feedstock (e.g. polylactic acid) and even chemosynthetic polymers, prepared from polymerization

of non-renewable monomer feedstock (e.g. poly (ε- caprlactone)), are also biodegradable if they contain chemical bonds which also occur in natural compounds (Steinbuchel, 1995). Thus, biodegradability not only depends on origin, but also on chemical structure and degradation conditions. Biodegradable polymers, classified on the basis of material class, are presented in Table 2.1 (Mohanty, 2000). When biodegradable polymer material is derived completely from renewable sources, it may be referred to as a green plastic. Renewable sources of polymeric materials offer an answer to maintaining sustainable development and ecologically attractive technology.

There are four different categories for biodegradable polymers based on the synthesis (Averous, 2004). Only first three categories (a-c) in which, polymer monomer derived from renewable resources.

a. **Agro-based Biodegradable Polymer**: Polymer obtained from agro-resources (starch and cellulose),
b. Polymer obtained from microbial production (polyhydroxyalkanoates (PHAs)),
c. **Agro-based Biodegradable Polyester**: Polymer monomers obtained from chemical synthesis or agro-resources (polylactic acid(PLA)),
d. **Petroleum Based Polyesters**: Polymer monomers obtained by conventionally chemical synthesis (polycaprolectum (PCL), aliphatic or aromatic copolyesters (AAC)).

Biodegradable polymers are classified into two main families: the agro-polymers (category a) and the biodegradable polyesters (category b-d).

Table 2.1 Classification of biodegradable polymers on the basis of material class (Mohanty, 2000)

Material Class	Manufacturer	Product name
Starch & starch blends	BioPlastic (Michigan)	Envar™
	BIOTEC	Bioplast®, Bioflex®, Biopur®
	Earth Shell	Starch-based composite
	Novamount	Mater-Bi™
	Novon	Poly-NOVON®
	Starch Tech	ST1,ST2,ST3
	Solanyl	Solanyl® BP
Poly(lactic acid) (PLA)	Birmingham Polymers	Poly(L-lactide) & Poly(DL-lactide)
	Boehringer Ingelheim	Resomer®
	Cargill Dow Polymers	EcoPLA®
	Chronopol	HeplonTM
	Neste	Poly(L-lactide)
Polycaprolactone (PCL)	Birmingham Polymers	Poly(ε- caprolactone)
	Planet Polymer	Enviroplastic®-C
	Solvey	CAPA®
	Union Carbide	TONE®
Polyhydroxyalkanoates (PHA)	Metabolix	PHA
	Biomer	Biomer™
	Monsanto	Biopol®
Copolyester	BASF	Ecoflex
	Eastman	Easter Bio™
Poly(vinyl alcohol) (PVOH)	Idroplast	Hydrolene®
	Novon	Aqua-NOVON®
	Planet Polymer	Aquadro™
	Texas Polymer	Vinex™

2.3 AGRO - BASED BIODEGRADABLE POLYMER

Agro-based polymers are derived from renewable natural sources, are often biodegradable, and their residues are not toxic to the eco-system. They can be produced by biological systems i.e. plants. There are different families of agro-based polymers such as polysaccharides and lignins. Plants store energy in the form of polysaccharide at the end of the photosynthesis process. Based on the glucose unit linkages in micromolecules, polysaccharides are mainly classified as cellulose or starch. Cellulose making up the cells walls of plants, and is used mainly in paper manufacturing. It is a linear polymer consisting of β (1-4) linked D-glucose units. Cellulose is mainly insoluble in water, has high tensile strength, and is indigestive by human. Another type of cellulose is lignin, which is a complex chemical compound most commonly found in wood and is an integral part of the secondary cell walls of plants and some algae. Lignins are by-products of pulp and paper manufacturing, and having low economical usage and value (Averous 2004). Starch on the other hand is the energy supply in biological systems. It is a polysaccharide consisting of α (1-4) and α (1-6) D-glucose units. Starch is soluble in water, has weak tensile strength, and is digestible by living organism.

2.3.1 NATIVE STARCH

Starch, the main polysaccharide of cereals, legumes and tubers, is a renewable and widely available raw material. Next to cellulose and chitin, starch is a carbohydrate of high natural abundance (Tharanathan, 2005). It is a part of the human diet, and represents a major source of energy required to support life. It is widely distributed in stems, leaves,

roots, grains, pollen, seeds and fruits, in the form of small granules. It can be found in cereal grains (corn, wheat and sorghum) and tubers (potato, tapioca and arrowroot). The starch macromolecule is polysaccharide composed of α-glucose units, and its molecular formula is $[C_6H_{10}O_5]_n$. It is semi-crystalline granules consists of two types of glucose polymer: amylose, which are linear or sparsely branched chains of α-D-glucopyranose units linked together by (1→4) bonds (Figure 2.1(a)) and contributes about 30% of storage starch, and amylopectin which are highly branched polymer of α-D-glucopyranose units linked together by (1→4) bonds but also on (1→6) linkages (Figure 2.1 (b)) and contributes the remaining 70% of storage starch. Starch also contains small

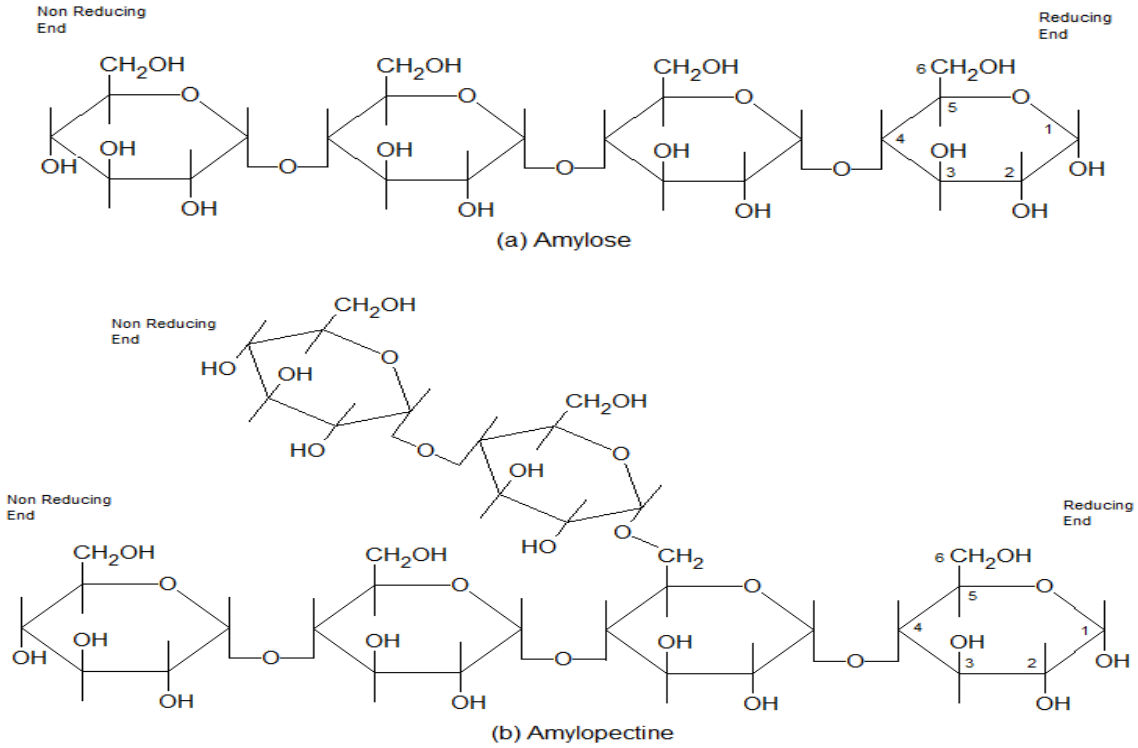

Figure 2.1 The glucopyranose unit linkage in amylase and amylopectin

amount of non-carbohydrate components, mainly lipids, proteins, non-starch polysaccharides and phosphorus (Liu, 2005). It is believed that in some cereal starches, small amount of lipids are complexed in the cavity of amylose double helix (Poutanen, 1996). Amylose with single or double helixes having a molecular weight of 10^5-10^6 grams/mol, while amylopectin with a highly multiple-branched structure have a molecular weight of 10^7-10^9 grams/mol (Averous, 2004). In most starches the degree of polymerization (DP) in amylose is between 800 to 3000, and each amylose macromolecule bears one reducing end (Glucose molecule with free –OH on C_1 – anomeric carbon) and one non-reducing end (Glucose molecule with free –OH on C_4). The degree of polymerization in amylopectin is about $2*10^6$ and each amylopectin macromolecule having one reducing ends and several non-reducing ends. Starch molecules have a complex structure mainly consists of a D-glucopyranosyl units which are hydrogen bounded, aligned radially and composed of granules having semi-crystalline structure (Swinkels, 1985).

Being linear macromolecules, amylose imparts hydrophilic characteristic due to there being hydroxyl groups along the polymer chain. Amylopectin molecules have a tendency to form hydrogen bonds with adjacent chains, and as a result, the polymer chains have less affinity towards water. Amylopectin molecules consist of various chain length structures. The outer chains (A) consist of about 20-30 α-glucose units, and are packed in regularly spaced double helices clusters (Figure 2.2 (a)). These clusters of small outer chains (A) are joined by longer chains about 40 or more α-glucose units (B)

which span into two, three or more double helices clusters. The single chain (C) carries other chains as branches, and contains only one reducing end per molecule as shown in Figure 2.2 (a). The possible positioning and interaction of free amylose chains, amylose-lipid complexes and short-chain amylopectin double helices in starch crystallite shown in Figure 2.2 (b).

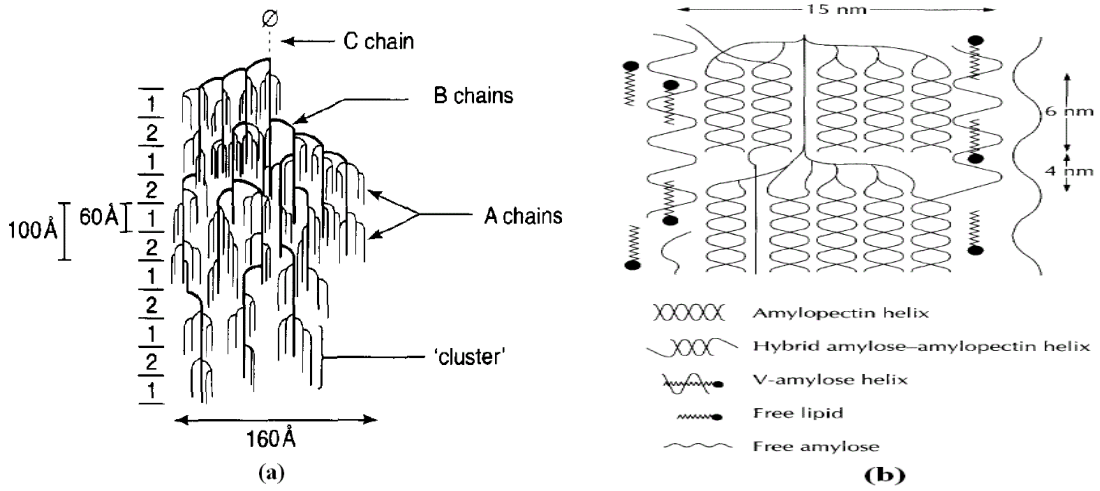

Figure 2.2 (a) Schematic representation of the crystalline clusters (van Soest et al. (1997)) (b) Model of starch crystallites showing the possible positioning and interaction of the various components (Blanshard, 1987)

Starch granule crystallinity mainly depends on botanical source and varies between 15-45% (Poutanen, 1996). The starch macromolecular structure is formed by inter-macromolecular hydrogen link between hydroxyl groups of polymer chains with the participation of water molecules. Amylopectin with highly branched molecules is the dominant crystalline part of the native starch. Amylose and branch region of amylopectin form the amorphous region in the granule (Averous, 2004).

Starch with a semi-crystalline structure varies in composition and appearance depending on the botanical source. Some mutant genotypes of maize, barley and rice have almost 70% of amylose, whereas other waxy genotypes such as maize, barley and rice contain less than 1% of amylose (maize, barley, rice). Table 2.2 shows the composition and macromolecular structure of different genotypes of starch. After different stages of refining, starch contains small amount of lipids, protein and phosphorus, which alter starch properties by formation of lipid complexes and Maillard reactions with proteins (Averous, 2004).

Table 2.2 Composition and characteristics of different starches (Swinkels 1985, Averous, 2004)

Starch	Potato	Maize	Wheat	Tapioca	Waxy Maize
Type of starch	tuber oval,	cereal	cereal	Root	cereal round,
starch shapes	Spherical	round, polygona	round, lenticular	truncated, round, oval	Polygonal
Diameter, range	5 - 100	2 - 30	1 - 45	4 - 35	2 - 30
Moisture at 65% RH and 20°C	19	13	13	13	13
Amylose	21	28	28	17	0
Amylopectin	79	72	72	83	100
Lipid*	0.05	0.7	0.8	0.1	0.15
Proteins*	0.06	0.35	0.4	0.1	0.25
Phosphorus*	0.08	0.02	0.06	0.01	0.01
Crystallinity (%)	25	39	36	n.d.	39

* % on dry substance

2.3.2 POTATO STARCH

Each year around one million tonnes of raw potatoes are processed in Britain and United States for the manufacturing of french fries, potato chips and instant potatoes. Potatoes contain approximately 81% water, 18% starch, and 1% cellulose, as well as contain dissolved organic compounds such as protein and carbohydrate. Large volumes of wastewater and organic solid wastes are generated in potato processing as result of washing, peeling, and additional potato processing operations (Wang et al., 2006). The resulting waste slurry from all processing operations contains partially gelatinized and ungelatinized starch, which constitutes the principle source of manufacturing grade starch or if cleaned further, food grade starch. Typical amylose and amylopectin contents in potato starch are 20-25% and 75-80% respectively. Potato starch has the highest swelling power (about 1100) in water compared to other commercial starches. It contains about 0.06% to 0.10% covalently bonded phosphate monoester groups. These negatively charged phosphate groups are exclusively linked to the amylopectin molecules of the potato starch molecules (Swinkels, 1985). The repulsion of like charges in aqueous solution helps to untangle the individual branches of the amylopectin molecules in potato starch, which assist in swelling of the potato granules. Also, the solubility of the potato starch in water is the highest compared to other starches.

Potato starch with higher molecular weights leads to higher melt viscosity during extrusion which correspondingly requires high mechanical energy by the motor and results in high die pressures (DellaValle et al., 1995). The extrusion of high amylose

potato starch can be more difficult than the processing of normal potato starch (Thuwell et al., 2006). This may be attributed to the high melting temperatures of amylose at low moisture contents. However, this can be compensate by processing at higher moisture content and a higher extrusion temperature. More entangled structure of the amylose in the molten state result in high melt pressure and viscosity. However, an increase in the amylose content in potato starch imparts higher strength and toughness in final product.

2.3.3 HYDROLYZED STARCH

Starch can be hydrolyzed to glucose in the presence of acid, acid-enzymes and enzyme-enzyme. Complete hydrolysis splits starch molecules quantitatively into dextrose. Starch hydrolysis occurs in three different stages. First, starch gelatinization - which involves the dissolution of starch granules to form a viscous suspension. Second, starch liquefaction - which partially hydrolyzes starch resulting in a loss of viscosity. Thirdly, starch saccharification - where further hydrolysis leads to full starch conversion to glucose and maltose (Wang et al., 2006). Starch in granular form cannot be hydrolyzed, so it is necessary to gelatinize the starch granules in the presence of hot water or steam first. Starch can be partially hydrolyzes to porous structure in the presence of enzymes, which can be further hydrolyzes to glucose and maltose. The most common types of enzymes used in hydrolysis are α-amylase and glucoamylase. α-Amylase specifically hydrolyzed the α-1,4 linkages present into starch to dextrins, maltose and a small amount of glucose. However, it cannot act on the α-1,6 links. While, glucoamylase can hydrolyzed on both, α-1,4 and α-1,6 linkages. It can convert maltose and higher DP

maltodextrins to glucose. It is believed that when partially gelatinized starch hydrolyzed by glucoamylase, the native starch granules degrade, and leaves behind porous starch granules (Liu, 2002).

Aggarawal et al. (1998) had obtained porous starch granules by partially hydrolysis of starch using glucoamylases. It was concluded that partially hydrolyzed starch showed a higher gelatinization temperature compared to their native counterparts. This was due to the hydrolyzed starch granules had shorter polymers chain length and required more energy to break compared to longer polymer chain length. Also, hydrolyzed starch appeared to be more crystalline compared to native starches suggesting that the enzymes attacked more on amorphous part of the starch granules and became more crystalline. However, in their research potato starch showed greater resistance to enzymatic attack than that of cereal starches.

2.3.4 STARCH GELATINIZATION

Starch gelatinization is a very important phenomenon in food processing and has been extensively studied in food science for decades with high water content (Hermansson and Svegmark, 1996). Starch based foods such as bread, steam bread and biscuits are processed under shearless condition. Initially, extruders had been used to prepare ready-to-eat cereals in early stage of development (Harper, 1989). In the 1970's, twin-screw extruders were used in food processing industries, and expanded substantially in the 1980's. Recently, starch has been considered as an important raw material for the manufacturing of biodegradable plastics. Starch gelatinization process has attracted much

attention because of their very important role in the processing of starch-based materials (Xie et al., 2006). Starch gelatinization is an irreversible process, and involves granule swelling, destroying the crystalline structure, crystalline melting, loss of birefringence and starch solubilization. Starch gelatinization is a multi-stage process which can be monitored by an order to disorder phase transition of starch granules. When enough water is present, this transformation is called "gelatinization". Starch gelatinization temperature depends on the botanical source of the starch (Donovan, 1979).

In the first stage, which occurs before the onset of gelatinization, water is reversibly complexed with the starch granule, and water mobility decreases until temperature reaches the onset gelatinization temperature. Still granules exhibit a birefringence under polar light (Lim et al., 2000). When a starch suspension is heated gradually, hydrogen bonds between the molecules weaken, and water is absorbed by the granules. This temperature is usually called the "initial gelatinization temperature". At this temperature, the granules swell irreversibly and begin to lose their birefringence. This transition involves dissociation of the double helices and expansion of the granules. This phenomena starts at the hilum or botanical centre, where hydrogen bonding between the molecules is weakest. As further heating above the gelatinization temperature, hydrogen bonding between the molecules continues to be disrupted, and water molecules become attached to hydroxyl groups, resulting in more swelling of starch granule. As a result, the starch become more soluble in water, and paste clarity increases. After the starch

molecules dissociate, the granules hydrate and swell irreversibly. During swelling amylose leaches out of the granule and forms a gel (Xie et al., 2006).

Starch gelatinization under wide range of water contents was studied by many researchers (Donovan, 1979; Eliasson, 1980; Burt and Russell, 1983; Qu and Wang, 1994). When starch cooked under higher moisture content (>61%), a single gelatinization endotherm was observed at a relatively low temperature range. This gelatinization endotherm was due to stripping of chains from starch crystallite and swelling of the amorphous regions of the granules. At decreasing moisture content, intensity of the gelatinization endotherm was diminished and shifted towards higher temperature range. This phenomenon observed as a result of insufficient water for the gelatinization process to be completed, and the remaining crystallite melted at higher temperature (Burt and Russell, 1983). Most starch applications in biodegradable plastics require moisture content of less than 20 wt%. At low moisture content, the melting temperature of starch (220-240°C) reaches to the beginning of the degradation temperature (220°C) of starch. To overcome with this issue, starch is often blended with higher boiling point and non-volatile plasticizers such as glycerol, sorbitol and PEG, in order to reduce its melting temperature (Averous, 2004). In the presence of low moisture content, high-boiling point plasticizers and thermo-mechanical treatment, starch semi-crystalline granules transfer to a homogenous amorphous material by using conventional plastic processing equipment. This plasticized starch is often known as "Thermoplastic starch" or TPS. In thermoplastic starch, semi-crystalline starch granules are converted to fully amorphous material by

processing at high temperature, high shear conditions and a limited amount of water in extruders; the term "destructurization" (loss of the native starch structure) has been used to describe this process. However, thermoplastic starch itself has several limitations due to its sensitivity to moisture and poor mechanical strength. In order to improve water resistance, mechanical strength, as well as maintain its biodegradability, thermoplastic starch is often blended with biodegradable polyester from renewable resources.

2.4 AGRO-BASED BIODEGRADABLE POLYESTERS (POLYLACTIC ACID)

In agro-based biodegradable polyesters, the monomer is derived from an agro-source, and the polymers are chemically synthesized by biotechnology, e.g., polylactic acid (PLA). Polylactic Acid is an aliphatic polyester made from 100% renewable resources, such as corn and sugar beets. The basic building block of PLA, lactic acid, can be produced by carbohydrate fermentation or chemical synthesis. Due to asymmetric carbon atoms, lactic acid has two optically active configurations as shown in Figure 2.3. L(-) - Lactic acid (2-hydroxy propionic acid) is produced by human and mammals, whereas both L(-) and D(+)- lactic acid are produced by microorganisms. PLA can be synthesized by simple condensation polymerization of lactic acid, which yields a low-molecular-weight, brittle and glassy polymer. Low-molecular-weight PLA is unusable for any applications unless used with coupling agents to increase the molecular weight of the polymer (Garlotta, 2001). High-molecular-weight PLA can be made by direct condensation or coupling polymerization, azeotropic dehydrative condensation and

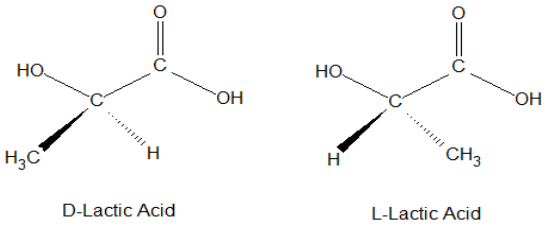

Figure 2.3 Lactic Acid Stereoisomers

polymerization through lactide formation (Auras et al., 2004). PLA molecular structure can be easily controlled by the ratio of D- and L- lactic acid. Poly (lactic acid) molecule structure is shown on Figure 2.4.

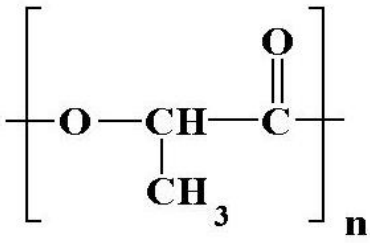

Figure 2.4 Poly(lactic acid) molecular structure

Direct condensation polymerization is the least expensive method to produce PLA. However, it is very difficult to obtain solvent free high-molecular-weight PLA. Therefore, chain coupling agents or esterification-promoting adjuvants needed, which add cost and complexity to the process. Azeotropic dehydration polymerization process yield high-molecular-weight polymers without using chain coupling agents or adjuvants. Ring opening polymerization of the cyclic lactide dimer process, developed and patented by Cargill Dow LLC, is a low-cost and continuous process for the production of PLA. The process uses lactic acid derived from fermentation of dextrose, which produces D-lactic

acid, L-lactic acid or mixture of both enantiomers. These are polymerized to obtain an intermediate low-molecular-weight polylactic acid. The low-molecular-weight prepolymer under low pressure and in the presence of a catalyst convert into a mixture of lactide sterioisomers. Lactide, the cyclic dimer of lactic acid is formed by the condensation of two lactic acid molecules. L-lactide is formed by two L-lactic acid molecules. D-lactide formed by two D-lactic acid molecules. Meso-lactide is formed by an L-lactic acid and a D-lactic acid molecule. The molten lactide mixture is then purified by vacuum distillation. Finally, high-molecular-weight polylactic acid is produced using an organo tin-catalyzed, ring-opening polymerization of lactides in a molten state. This process completely eliminates the use of costly and environmentally unfriendly solvents (Drumright et al., 2000; Garlotta, 2001; Auras et al., 2004). Manufacturing of polylactic acid is summarized in Figure 2.5.

Commercial PLA is a copolymer of poly (L-lactic acid) (PLLA) and poly (D,L-lactic acid) (PDLLA), which are produced from L-lactides and D,L-lactides, respectively. PLA produced from greater than 93% L-lactic acid is semi-crystalline, whereas between 93% to 50% L-lactic acid is strictly amorphous (Auras et al., 2004). As crystallizable L-lactic acid content decreases, the crystallinity and crystallization rate decreases. The crystallinity level in the PLA can alter its mechanical properties, permeability, heat deflection temperature and biodegradability in a composting environment. Semi-crystalline PLA exhibits both glass transition temperature (~56 to 63 °C) and melting temperature (~125 to 178 °C), depending on the optical purity and molecular weight of

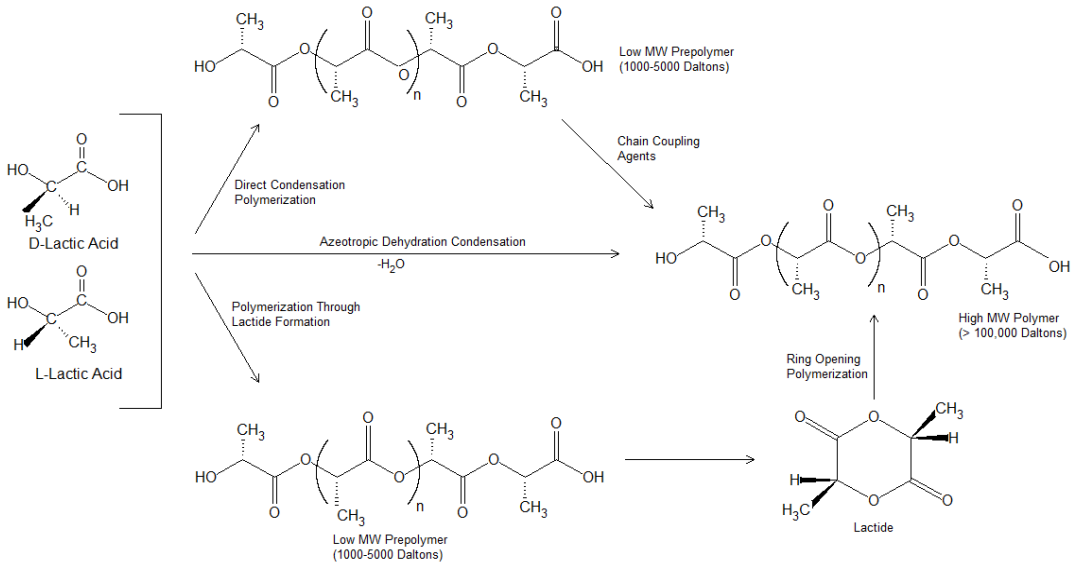

Figure 2.5 Manufacturing routes for Poly(lactic acid) (Garlotta, 2001)

the polymer. Pure PLLA has a melting temperature around 180°C, and the presence of meso-lactide in the PLA structure can reduce the melting temperature as much as 50°C, depending on the amount of D - and meso-lactide incorporated into the polymer (Lim et al., 2008). Semi-crystalline PLA below its glass transition temperature is very brittle.

2.5 PETROLEUM BASED POLYESTER

A large number of biodegradable polyesters such as poly (ε-caprolactone), polyesteramides and aliphatic-aromatic copolyesters (AAC) are based on petroleum resources, which are chemically synthesized from synthetic monomers. Aliphatic copolyesters are obtained by combinations of diols such as 1,2-ethanediol, 1-3-propanediol, 1,4-butadenediol, and dicarboxylic acid such as adiapic, sebacic or succinic acid. Compared to aliphatic copolyesters, aromatic polyesters are often based on

terephthalic diacids (Averous, 2004). A biodegradable aliphatic-aromatic copolymer (AAC) is based on monomers: 1,4-butanediol, adipic acid and terephthalic acid or dimethyltherephthalate in the polymer chain depending on the production process. Its representative structure is shown in Figure 2.6 (Witt et al., 2001). BASF commercialized aliphatic-aromatic copolyester with the Ecoflex® trademark. Due to its high molecular weight and long chain branched molecular structure, Ecoflex® has properties similar to LDPE (BASF, 2009). By having greater compatibility with polylactic acid, starch or cellulose, Ecoflex® is being used in production of packaging films, agricultural films and compost bags, by using a blown film, extrusion coating or cast film process.

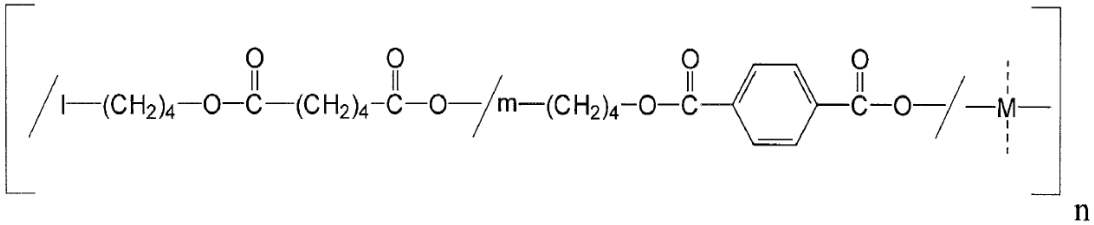

Figure 2.6 Structure of Ecoflex® F BX 7011. M and m represent monomers with branching and chain extension effect, respectively (Witt et al., 2001)

The glass transition temperature of Ecoflex® is -30°C and the crystalline melting temperature is 110-115°C (Yamamoto et al., 2002). Biodegradability of aliphatic-aromatic copolyesters depends on its structure. As terephthalic acid content is increased in the polymer chain, the degradation rate of aliphatic-aromatic is decreased (Muller et al., 1998). However, aliphatic-aromatic copolyesters are totally biodegradable and compostable in a micro-organism environment, and there is no indication of an environmental risk (ecotoxicity) when aliphatic-aromatic copolyesters are introduced into

the composting processes (Witt et al., 2001). Also, the addition of aliphatic-aromatic copolyester in PLA increases the toughness of the blend while maintaining the overall biodegradability (Jiang et al., 2006).

2.6 SOLANYL® BIOPOLYMER

Solanyl® is bio-based and biodegradable polymer made from potato starch reclaimed from the food processing industry. Solanyl® BP is a patented biodegradable product, and it contributes to a reduction of greenhouse gasses by completing the carbon neutral cycle during biodegradation process. Solanyl® BP is made by the Rodenburg process, in which potato starch is modified by fermentation process. The major portion of potato waste slurry contains starch, the rest being proteins, fats and oils, inorganic components and cellulose. The fermentation process is carried out in a storage silo, where the slurry is stored for about two weeks. The potato starch allows for stabilization and partial fermentation. During the fermentation process, a small fraction of the starch is converted to lactic acid by the lactic acid bacteria that are naturally present in the feedstock. The resulting product is dried in an oven to 10% water content, and then extruded (Bastioli, 2005). The lactic acid produced by the fermentation process is used for the production of poly (lactic acid) (Nampoothiri et al., 2010).

Solanyl® BP can be used as a replacement for petroleum-based plastic resins and can be injection molded for short life, disposable products such as packaging, planting pots and disposable cutlery. Different grades of Solanyl® BP available by the parent company Rodenburg Biopolymers B.V. from Netherlands. Among them, Solanyl® 100

BP consist of only partially hydrolyzed pre-gelatinized starch, and Solanyl® blend 30R consist of partially hydrolyzed and gelatinized starch, poly (lactic acid) and aliphatic-aromatic copolymer (AAC). It is believed that an aliphatic-aromatic copolymer, a ductile biodegradable polymer, used in Solanyl® BP/PLA blend, which modifies the brittle nature of hydrolyzed starch/PLA blend to ductile one, and increases the overall toughness of the Solanyl® blend 30R.

Solanyl® BP has many benefits including:

- Processing of Solanyl® BP requires 65% less energy compared to petroleum based plastics
- Solanyl® is biodegradable and compostable according to EN 13432 standards
- Solanyl® bioplastics are made from completely renewable resources

While there are numerous publications on starch and PLA blends, there are just a few literature publications available for Solanyl® biopolymer blends. Lee et al. (2008a) added natural fibers in Solanyl® biopolymers, which enhanced the mechanical properties of biocomposites compared to neat biopolymer. Solanyl® blend 30R is considered to be a ternary blend of hydrolyzed starch, PLAs and aliphatic-aromatic copolymer. Sarazin et al. (2008) and Liao et al. (2009) have studied the ternary blend of thermoplastic starch (TPS), poly (lactic acid) and polycaprolactone (PCL). The morphology of 50/50 thermoplastic starch/PLA blend was very coarse and a bimodal distribution of the dispersed TPS phase was found. After adding 10 wt % of PCL to a 50 wt % thermoplastic

starch blend, the dispersion of TPS in the PLA matrix was improved, and a smaller TPS phase domain was observed in the PLA matrix (Sarazin et al., 2008).

Foaming is a well-known process, which also enhance the ductility and impact resistance of polymer matrix. It also provides a significant weight and density reduction in plastic parts. The density reduction by the foaming process reduces the material cost without compromise to the required properties such as impact resistance, toughness and volume expansion ration (Matuana et al., 2009). However, there is no information available on the foamability of the ternary blend based on the hydrolyzed potato starch biopolymers. This research work looked into the foamability aspects of the hydrolyzed starch/PLA blends and its corresponding commercial biopolymer (Solanyl® blend 30R). The high-pressure batch foaming process had been used to evaluate the processing window for both Solanyl® biopolymer blends.

2.7 FOAMING PROCESS

The foam process is a physical phenomenon in which a gaseous blowing agent is diffused into and out of the polymer melt under certain processing conditions such as pressure, temperature or stress. Foaming can occur within polymer melt in a dynamic state such as extrusion and injection molding or in a static state such as batch foaming. Polymeric foamed material classified by its cell size, expansion ration and cell wall integrity. Under cell size categories, the conventional (cellular or coarse) foams have an average cell size above 100 μm, fine-celled foams with an average cell size between 20 to 100 μm, and microcellular foamed have an average cell size below 20 μm (Klempner and

Sendijarevic, 2004). Conventional cellular foam and microcellular foam are also characterized by its cell-population density (number of cells nucleated per unit volume of the un-foamed polymer). A cellular polymeric foamed material has a cell density around 10^4-10^6 cells/cm^3. While, a microcellular polymeric foamed material has a cell density in the range of 10^9-10^{15} cells/cm^3 (Matuana, 2008). The expansion ratio is defined by the ratio of polymer density to foam density. Foam material with an expansion ratio below 4 are known as high-density foams, between 4 and 10 known as medium-density foams, and above 10, as low-density foams. Regarding cell wall integrity, there are opened-cell and closed-cell foams. Open-cell foams have opening in the cell walls which interconnect the adjacent cell with each other, and closed-cell foams have complete cell walls and adjacent cells are not connected (Throne, 1996).

In 1980s, researchers in the Massachusetts Institute of Technology developed microcellular thermoplastic foam by creating a very large number of micro-bubbles in a polymer matrix. This approach could reduce total material cost and consumption of mass in plastic parts without compromising the mechanical properties of foamed parts such as impact strength, toughness, fatigue life and thermal stability (Waldman, 1982; Martini et al., 1984; Matuana, 2008). The improvements in mechanical properties are due to a high cell density of very small bubble cells. Also, the presence of small bubbles inhibits crack propagation by blunting the crack tip and increasing the amount of energy needed to propagate the crack (Waldman, 1982). Also, the presence of small cells can reduce the

bulk density of the polymer matrix and reduced the usage of the polymeric material. The foaming process can be divided in three major steps:

- Cell Nucleation
- Cell Growth
- Cell Termination and Stabilization

2.7.1 CELL NUCLEATION

Cell nucleation is a thermodynamic phenomenon, in which the formation of the bubble takes place in polymer melt. When system experienced thermodynamic disturbance, the external induced thermodynamic change produces a supersaturated state. As a result, the system automatically starts to re-establish the stable state by applying a sharp change necessary to the system, such as bubbling (Lee, 2000). By considering a polymer-gas melt, which is completely saturated with a blowing agent, the already saturated polymer-gas system becomes supersaturated as gas solubility is decreased by either increasing temperature or decreasing pressure. In order to restore a low-energy stable state, the polymer-gas solution tends to form bubbles (Throne, 1996).

The classical nucleation theory divides nucleation in two parts: homogenous nucleation and heterogeneous nucleation. In homogenous nucleation, cell nucleation occurs in the liquid bulk of a uniform polymer-gas solution. The formation of bubbles is driven by the effective diffusion of dissolved gas. The bubble size is smaller and uniformly distributed in the polymer melt (Lee, 2000). However, in heterogeneous nucleation, supersaturation of polymer-gas solution leads to formation of a bubble on

heterogeneous nucleating site (e.g., nucleating agents or impurities). The size of the microbubbles is mainly dependant on the differential pressure of gas inside and outside the bubble, and is defined by the Rayleigh equation.

$$R_{bcr} = 2*\sigma/(P_g-P_l) \quad 2.1$$

where, R_{bcr} is the critical bubble radious, σ is surface tension of the polymer melt, P_g and P_l is the internal gas pressure and surrounding polymer/gas pressure, respectively (Throne, 1996).

When high pressure gas is dissolved in a polymer melt, the melt phase becomes saturated. Smaller bubbles are nucleated when internal gas pressure is greater than the polymer/gas melt pressure. As the saturated polymer melt passes through a die in an extruder or spruce-runner system in an injection molding machine, the pressure of the polymer/gas falls below the point where bubble nucleation can begin. As per the Rayleigh equation, the critical bubble diameter is dependent on the melt temperature through the internal gas pressure (P_g) and the surface tension (σ). As the melt temperature increases, the critical bubble diameter decreases and smaller cells are nucleated and grow. However, at high temperature, melt viscosity decreases and bubble coalescence increases, and over all bubble count decreases (Throne, 1996).

2.7.2 CELL GROWTH

After the cell nucleation stage, the bubbles begin to grow as the excess gas is diffused into the nucleated bubble from the polymer melt. The foaming growth process is controlled by the viscosity of the polymer, the gas concentration in polymer melt, the

foaming temperature and the amount of nucleating agent. Cell growth stage can be divided in three steps.

- Inertial bubble growth
- Diffusional bubble growth
- Membrane formation

Inertial bubble growth is controlled by external mechanical forces such as viscous and elastic forces, surface tension and inertial forces. Initially the bubble growth phenomenon is dominant by rapidly diffusing gas molecules to the growing bubble interface, and the surrounding polymer melt is stretched away from the nucleant site. The stretching resistance is inversely proportional to the viscosity of the polymer melt. However, it is unclear at this point which viscosity is playing dominant role in bubble growth phenomenon. As the local region is stretched away from the nucleant site during bubble growth phenomenon, it may be local shear viscosity becomes dominant. The expansion rate is very small in the early stage of the bubble growth, so it may be zero-shear viscosity. Finally, it may be extensional viscosity as the polymer melt is stretched by bubble growth in biaxial directions. Also, at high temperature viscosity of the polymer melt decrease significantly so it will favour bubble growth (Throne, 2002).

During diffusion growth, the region around the growing bubble is quickly depleted of the gas from the polymer melt surrounding the bubbles. As a result, gas molecules from the higher gas concentration region must diffuse to the growing bubble site. Diffusion of gas through a polymer melt is very slow phenomenon. The bubble

growth slows down and this bubble growth is known as diffusional bubble growth. Bubble coalescence, where two bubbles merge into one, occurs during this period of time (Throne, 2002).

The final stage in the bubble growth phenomena is the formation of a membrane between two bubbles. The membrane can be formed by biaxial stretching of polymer melt between two bubbles and it is strongly depend on the melt elasticity of the polymer melt (Throne, 2002).

2.7.3 CELL TERMINATION AND STABILIZATION

The cell growth can be inhibited or stopped by quickly cooling the foamed polymeric material. According to the Rayleigh's principle, when the difference between the gas pressure inside the bubble and the pressure on the liquid surrounding the bubble equal to the surface tension term, the bubbles should stop growing (Throne, 2002). Nonlinear viscoelastic property (strain hardening behaviour), polymer deplasticization (the separation of blowing agent by diffusion from polymer phase) and polymer crystallization play an important role during foam stabilization. Strain hardening is a rapid increase in extensional viscosity with time during the cell growth period of the polymer foaming process, and it is observed when the macromolecular chain disentanglement rate is too low compared to the deformation rate (Mihai et al., 2010). Cell stabilization can also affected by number of factors such as blowing agent concentration, and type as well as a number of polymer matrix properties such as viscosity, elasticity and surface tension (Throne, 2002).

2.8 BLOWING AGENTS

Blowing agents are necessary ingredients in the manufacturing of thermoplastic foamed material. In general, a blowing agents in its vapor phase, expands thermoplastic melt upon reduction in pressure during processing. There are two types of blowing agents: Physical and Chemical

2.8.1 PHYSICAL BLOWING AGENTS

Physical blowing agents are volatile liquids or gases that are directly injected into the process and are dissolved into the polymer melt by processing at higher pressure. At atmospheric conditions, the dissolved blowing agent expands and creates a foamed product. In the early years of foaming technology, the low boiling points liquids such as hydrocarbons, chlorohydrocarbons and chlorofluorohydrocarbons has been used as blowing agents because they were nonflammable and performed well in the process. However, being expensive and contributing to the destruction of the earth's ozone layers, the use of these materials for foaming are considered to be unsafe (Lee, 2000).

Permanent or atmospheric gas such as nitrogen and carbon dioxide also has been used as a blowing agent in thermoplastic foam. Nitrogen is less expensive, non-flammable, non-toxic and environmentally safe inert gas. Also, it has low molecular weight, a smaller molecular profile, non-polar and easily diffuse through polymer melts. However, due to its lower solubility in most of the polymers, it requires higher operating pressure to get higher dosage into the polymer melt. Carbon dioxide, which has a reasonably good solubility in most of the polymer melt. Carbon dioxide has a relatively

low critical point (31°C and 7.39 MPa) and is available as a semi-cryogenic liquid. However, it has some inherent handling problems. Improper throttle of CO_2 vapor into the extruder can generate solid CO_2 during processing. Also, sudden phase change during metering can change dosage condition dramatically (Throne, 1996).

2.8.2 CHEMICAL BLOWING AGENTS

Chemical blowing agents (CBAs) are solid or liquid materials that generate gas during a chemical reaction at elevated temperature. The generated vapor then behaves as a physical blowing agent in the processing environment. Chemical blowing agents are in the form of finely divided solid particles, and most decompose within a specific temperature range. The decomposition temperature range of CBA should be within the same range as the melt temperature of the polymer being processed. This ensures that the CBA does not prematurely decompose and escape through feed zone (Lee, 2000). CBAs which generate carbon dioxides are more favourable in processing because they have more solubility in the polymer melt, and generate finer cells and lower density compared to CBAs which generate nitrogen (Throne, 1996).

Chemical blowing agents are generally divided into exothermic and endothermic categories. Exothermic CBAs generate heat (energy) during their decomposition and evolve mainly nitrogen gas. Endothermic CBAs consume thermal energy during their decomposition and evolve mainly carbon dioxide gas. Once exothermic CBAs begins to decompose, it is very difficult to control it before it reaches full decomposition. This results in faster decomposition within a narrow temperature range. Endothermic CBAs

require additional heat to continue their decomposition, and these result in a broader decomposition time and temperature range (Lee, 2000).

2.9 STARCH BASED FOAMS

There has been great interest in replacing synthetic thermoplastic based foam material such as expanded polystyrene (EPS) with those made from biopolymers which are considered to be more environmentally friendly. Expanded polystyrene create major disposal problems for companies and municipalities because of its light weight, bulky nature, and non-biodegradability. One of the major concerns of polystyrene foam for single use food containers is that very few containers can be recycled due to economic and food hygiene issues. Also, expanded polystyrene foam used in packaging is an environmental concern due to its non-biodegradability (Glenn et al., 2007). Thus, bio-based and biodegradable foams made from starch and other biopolymers can overcome these recycling and biodegradability problems.

Starch based foam products were first made for food industries from extrusion processing, popping and puffing. In extrusion processing, starch and water are heated under elevated temperature and pressure in an extruder. Suddenly releasing the elevated pressure at the die end creates steam, which acts as a blowing agent and produces starch foam. However, in starch foam made by water as a blowing agent, the foam cell size and density is not uniform due to the explosive nature of steam (Glenn et al., 2007). Starch-based foam can also be made through the solvent exchange method (Glenn et al., 1995), baking technology (Glenn et al., 2007) and the oven-puffing process. In the solvent

exchange method, starch aquagel is hydrated in an ethanol solvent; evaporating the solvent in a dryer produces foam. In baking technology, starch dough with more than 50% moisture is placed in a preheated (120–200°C) mold which has a steam vent. Once the mold is closed, the dough is gelatinized by rapidly heating the starch component. The moisture in the dough converts to steam and acts as a foaming agent. The foam structure solidifies in place as moisture is quickly driven out of the dough in the form of steam. By this method, the low density starch containers were commercialized. The oven-puffing process utilizes lower moisture content then the baking technology, and is operated at ambient pressure. The process involves densifying a starch-based sample by compression, equilibrating to desired moisture content, and then rapidly heating the sample to cause expansion. In order to improve mechanical strength, mineral and wood fillers have been used. Also, to improve moisture resistance, the starch foam surface is coated with wax and other materials (Shogren et al., 2002).

Wang et al. (1995) compared the physical characteristics of two biological cushioning material foams made from wheat and corn starches with those of commercial polystyrene cushioning material. Both starch samples were mixed with 3% polyethylene glycol and 0.5% silicon dioxide, and extruded through a single screw extruder. Both wheat and corn starch foams had bulk density much higher than the expanded polystyrene foam. Also, wheat and corn starch foam had bigger cell size than polystyrene foam. The equilibrium moisture content (EMC) of starch based foam was increased significantly with the increase in relative humidity. Starch based foam showed more unrecoverable

plastic deformation. Starch and water based foams have weak mechanical properties, are brittle and readily absorb moisture in a humid environment. The addition of PLA to starch contributes to an increase in the elasticity of the cell walls, prevents cell structure collapse, and improves the ultimate tensile strength and percentage of elongation at break of the foamed products (Fang and Hanna, 2000). However, starch is often blended with non-biodegradable polymers such as polyethylene (Shah et al., 1995), polystyrene (Oliveira et al., 2010), polycarbonate (Pushpadass et al., 2008) and polyurethane (David et al., 2010) in order to lower the density and increase resistance to water absorption of the foams. The addition of a synthetic polymer to starch increase the porosity of the blend after the starch phase has been consumed by microorganisms and the synthetic polymer loses its structural integrity by increasing the surface to volume ratio. The other environment factors, such as oxygen, sunlight, heat etc. trigger auto oxidation of chemically unstable pro-oxidants, generating free radicals which attack the molecular structure of the synthetic polymer. To maintain biodegradability of the foams, various biodegradable polymers have been studied. Among them poly (lactic acid) (PLA) is a particularly interesting biopolymer.

2.10 POLY(LACIC ACID) BASED FOAMS

PLA is more expensive, brittle and has a lower impact resistance compared to other petroleum-based commodity plastics. In addition, PLA has a narrow processing window due to their sensitivity to moisture and heat (Matuana et al., 2009). All these factors may greatly limit its application in packaging industries. In order to broaden its

applications and lower the cost, PLA is blended with fillers such as cellulosic fibers (Huda et al. 2006; Pilla et al., 2008) or starch (Ke and Sun 2000; Ning et al., 2008). Also, in order to compete with flexible commodity synthetic polymers, PLA has been plasticized with biocompatible plasticizers. Citrate ester, which is normally derived from naturally occurring citric acid, has been used as a plasticizer for PLA (Labrecque et al., 1997). Recently, poly (ethylene glycol) (PEG) has been used as a plasticizer for PLA (Jacobsen and Fritz, 1999; Martin and Averous, 2001; Li and Huneault, 2007). The resulting plasticized PLA materials show improved ductility and drawability, which broadens its potential application in packaging. However, addition of fillers, second polymers and plasticizers could increase the manufacturing cost due to costs associated with the additives.

Efforts have been made to improve the ductility and impact resistance of PLA by foaming technology, which also reduced unit density. PLA has been foamed by microcellular batch foaming technology (Fujimoto et at., 2003; Wang et al., 2007; Matuana, 2008). The batch foaming is also called two-stage solid state foaming process. In the first stage, the polymer is saturated with non-reacting supercritical gas (usually CO_2 or N_2) at high pressure in a high-pressure vessel. During the saturation period, the gas diffuses into the polymer matrix and attains a uniform concentration throughout the polymer specimen. When this material is removed from the pressure vessel and brought to atmospheric pressure, a "supersaturated" specimen that is thermodynamically unstable due to the excessive gas dissolved into the polymer is produced. In the second stage, the

specimen is heated to what is termed the foaming temperature, which is well below the polymer melting point. This step is typically carried out in a heated bath with temperature control. Since the polymer is still in a solid state, the foams thus produced are called "solid-state foams" to distinguish them from the conventional foams that are produced in an extruder from a polymer melt (Wang et al., 2007).

Fujimoto et al. (2003) have studied the batch foaming of neat PLA and PLA/layered silicate nanocomposites by using supercritical CO_2 as a foaming agent in an autoclave at elevated temperature and pressure. In resulting nanocomposites, the foam density was reduced to 0.5 g/cm^3 and cell size was around 0.36 to 2.59 μm. Also, larger cell density compared to neat PLA was due to dispersed silicate particles in PLA matrix which acted as nucleating sites for cell nucleation. Batch foaming is a good technique for studying absorption or desorption isotherms of supercritical gas, cell nucleation and cell growth in polymer matrix. However, it is not likely to be implemented in the industrial production scale because it is a time consuming process involving different steps in the batch foaming process as mention before (Matuana, 2008).

To overcome the shortcomings of microcellular batch foaming and scale-up towards industrial applications, PLA foams have been manufactured through a continuous extrusion (Reignier et al., 2007; Lee et al., 2008b, Mihai et al., 2010) and injection molding (Kramschuster et al., 2007) processes using supercritical CO_2 as a physical blowing agents. Reignier et al. (2007) investigated the processing window for continuous extrusion foaming of amorphous poly (lactic acid) by using supercritical CO_2

as a blowing agent. Above 7 wt % CO_2 concentration, low density foam (<30 kg/m^3) was achieved and foam density did not change significantly with increasing CO_2 concentration. The cell population density increased slightly from 10^7 to 10^8 cell/cm^3 with CO_2 concentration. It appeared that a critical gas concentration of 7 wt % was required for a favourable nucleation and expansion process leading to low-density foams (Reignier et al., 2007). Mihai et al. (2010) also obtained low-density foam (35 to 41 kg/m^3) for semi-crystalline and amorphous PLA, when CO_2 concentration exceeded a threshold of 7 wt % and 9 wt %, respectively.

Using supercritical CO_2 for continuous microcellular foaming process requires modification to the existing equipment by adding a supercritical fluid (SCF) delivery system. It provides high pressure and accurately metered mass flow of SCF to the processing equipment. Also, modification to the screw and die are needed to achieve a single melt-gas phase solution. Matuana et al. (2009) studied the effect of the endothermic chemical blowing agent (CBA), PLA melt flow index and extruder's rotational speed. He quantified the foamed product by density reduction and cell-population density. It was concluded that a homogenous and finer cellular morphology can be obtained in PLA foam by controlling the extruder's processing speed and CBA content. Since PLA has lower molecular weight, processing at higher temperature (about 170°C to 180°C) can initiate chain unzipping and scission reactions, leading to a loss of molecular weight and thermal degradation. The depolymerisation of PLA can change its physical properties, including reducing the melt viscosity, melt elasticity as well as

thermal and mechanical properties (Pilla et al., 2009). Chain extension is a method to obtain a high molecular weight of virgin, reprocessed or recycle thermoplastics. Chain extension is a post polymerization reaction carried out either in the final polymerization processing steps or during melt compounding in an extrusion or injection molding machine (Villalobos et al., 2006).

2.11 STARCH AND PLA FOAMS

As we discussed earlier, starch based packaging foams have the advantages of being biodegradable, inexpensive and derived from renewable agriculture resources. However, starch based foams do not have sufficient physical and mechanical properties, and are highly moisture sensitive. To improve moisture resistance and maintain functional properties, biodegradable polymers can be incorporated into starch-based foams. The resulting starch based foams have excellent functional properties and are completely biodegradable in a biodegradable environment. Research has been focused by using biodegradable polymer from renewable sources, such as polylactic acid (PLA) and polycaprolactone (PCL) (Fang and Hanna, 2000; Fang and Hanna, 2001). Due to higher manufacturing cost, these resins are limited in their applications to packaging. Biodegradable aliphatic polyesters or aliphatic-aromatic co-polyesters are manufactured from petroleum resources and manufacturing cost is comparable to that of conventional plastic resins. The use of those biodegradable polymers into starch can improve blend properties.

Fang and Hanna (2000) improved the physical and mechanical properties of starch-based plastic foams by blending starch with poly (lactic acid). The effect of starch type, ratio of starch to polymer and moisture content on expansion ratio, bulk density, water solubility index and compressibility were examined. An increased in PLA content improved the radial expansion ratio, and reduced the bulk density and compressibility significantly. The higher PLA contents (40 wt %) may have contributed to an increase in elasticity of the cell walls and prevented the cell from collapsing. This helped to trap more gas in the cells, and increased the radial expansion ratio and reduced bulk density. The addition of PLA in starch-based foams did not improve the water solubility index. In another study by the same researchers (Fang and Hanna, 2001), PLA was replaced by Eastar Bio Co-polyesters® 14766 (EBC) and the effect of starch type, ratio of starch to polymer, and moisture content on the functional properties of extrudates were examined. It was found that, at lower EBC contents (10 wt % and 25 wt %), the extrudates foam samples had a higher radial expansion ration and lower bulk density (32.5 kg/m^3). Alternatively, foams containing higher EBC contents (40 wt %) had a lower radial expansion ratio and higher bulk density (52 kg/m^3). Higher polyester contents reduced the melt strength, and the cell collapsed after exiting from the die, which resulted in reduced radial expansion and an increase bulk density. Willett and Shogren (2002) concluded that the addition of as little as 10 wt % of PLA significantly reduced the foam density by altering the rheological properties of the melt during bubble growth.

Zhang et al. (2007a) has been used water as a physical blowing agent and talc as a nucleating agent for starch/PLA (40/60 wt %) extruded foams. The optimum expansion ratio with lowest foam density was obtained with 15% moisture contents. They found that water acted as a plasticizer in starch/PLA blend and lowered the melting temperature. Excess water reduced the melt viscosity of blend and this favoured cell collapse at the exit of die. In another study from the same researchers Zhang et al. (2007b), they examined starch/PLA foamed cell structure with various ratios of the blends. They concluded that the cell structure tended towards a closed structure as the starch ratio of the matrix was reduced, with the cell wall mainly composed of the PLA phase. The starch/PLA blend showed a lake of affinity between the hydrophilic starch and the hydrophobic PLA polymers, which resulted in extremely coarse blend morphologies and brittle materials (Martin and Averous, 2001). However, thermoplastic starch and PLA can be reactively compatibilized by adding maleic anhydride grafted PLA (MA-g-PLA) to the blend (Huneault and Li, 2007). By doing interfacial modification, the dispersed TPS phase size was decreased by one order of magnitude and the elongation at break was increased from 5-20% to 150-250% range.

Mihai et al. (2007) had evaluated the foamability of PLA/TPS blend with interfacial modification of PLA by MA-g-PLA and introducing supercritical CO_2 in the extruder. In their study, glycerol has been used as a plasticizer and water free thermoplastic starch has been used to avoid hydrolysis of PLA at elevated temperature. Low density foam (25 kg/m^3) was obtained in 33%TPS/PLA blend, where 67 wt % PLA

blend was consist of 50/50 PLA/MA-g-PLA blend. The foamed cell size was reduced to 40 μm compared to 150-200 μm with unmodified 33%TPS/PLA blend. The foamed morphology was characterized by fine cell and high open-cell content, which was caused by rupturing the cell wall during rapid CO_2 foam cell expansion.

To our knowledge, there is a little information available on batch foaming of starch/PLA with supercritical CO_2. However, Hao et al. (2008) studied the batch foaming of PLA/starch pellets with supercritical CO_2 in high-pressure stainless steel reactor at 150°C. The pellets were composed of 60:40 weight ratio of PLA and corn starch. They studied the effect of saturation pressure on the foamability of PLA/starch pellets and concluded that at 12 MPa and 1 hr saturation time was optimum for lowest bulk density (about 400 kg/m^3) and largest cell size. They also concluded that as PLA/starch pellets were exposed to supercritical CO_2 for longer periods of time, more gas absorbed by pellets and consequently a larger cell size and reduced foam density were obtained.

2.12 CHAIN EXTENDERS

Many efforts have been made to enhance the properties of virgin polymers by using chain extenders (CEs), with the expectation of improving the melt strength or viscoelastic properties of polymers during foaming process. Chain extension is the use of bi-functional or multi-functional chemical compounds for rebuilding the molecular weight and physical properties of polymers by bridging the end functional groups of polymers (Villalobos et al., 2006). Bi-functional (f_n=2) chain extenders with hydroxyl, amine, epoxy, anhydride and carboxylic functional groups have limited success in

restoring the molecular weight. Bi-functional CEs will only couple two end groups of polymer chains, leading to a linear polymer with relatively low molecular weight. A high percentage of loading is required for any substantial increase in molecular weight. Too excessive of a loading of bi-functional CEs will narrow the processing window and can lead to long chain branching, possibly catastrophic gelation. To overcome with these limitations, CEs with both high and low functionalities are needed to enhance molecular weight at much broader processing windows (Pilla et al., 2009). The general structure and chain extension mechanism of multiple chain extenders is given in Figure 2.7. BASF Joncryl® uses non-linear chain extension technology. It is an epoxy-functional, styrene-acrylic or styrene-free acrylic based reactive chain extenders use to modify the initial polymer with a long chain branched structure.

High melt viscosity and elasticity requires the use of PLA resin in thermoforming, blow-molding and foaming process. In the early stage of research, the PLA resin was

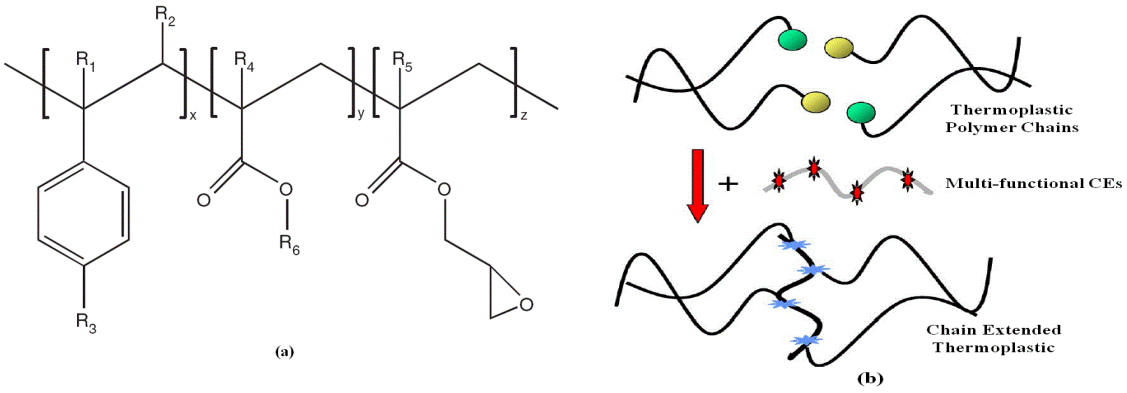

Figure 2.7 (a) General structure of the multi-functional epoxy-based chain extenders. (where R1 to R5 are H, CH3, a higher alkyl group, or combinations of them; R6 is an alkyl group) (b) Chain Extenders Mechanism (Villalobos *et al.*, 2006)

reactively modified by using low-molecular weight chain extenders for foam processing (Di et al., 2005). 1,4-butanediol (BD) and 1,4-butane diisocynate (BDI) has been used as low-molecular weight chain extenders. In the study by Di et al., BD was added in the PLA melt as an acid value reducer by reacting BD with the carboxyl groups. When the reaction over, BDI was added, and it reacted with the hydroxyl end groups of PLA. The change in mixing torque was considered as the extent of the reaction, and the time at maximum torque was considered as the final reaction end time. This was followed by batch foaming in a high-pressure stainless steel autoclave. The reactively modified PLA has a lower foam density, smaller cell size and higher cell density when compared to plain PLA. In current research, bi-functional epoxy based chain extenders have been used to evaluate their effectiveness on the foamability of the hydrolyzed starch based biopolymer (Solanyl® blend 30R) and hydrolyzed starch/PLA blends.

For microcellular foaming, the supercritical CO_2 acts as a plasticizer, thereby reducing melt viscosity. The research has been targeted on adding multi-functional CEs (BASF-Joncryl®) in PLA, which increases the melt strength during extrusion and the injection molding foaming process (Pilla et al., 2009; Mihai et al., 2010). Pilla et al. (2009) concluded that adding CE in PLA melt decreased the degree of crystallinity by formation of a branched PLA molecular structure, which inhibited the crystallization process. The fractured surface on PLA-CE showed more plastic like deformations. By adding CEs, the tensile properties such as specific toughness, strain-at-break and specific tensile strength have been increased compared to plain PLA. The PLA-CE blend showed

improved thermal stability, which enhanced processability of PLA. Pilla et al. (2009) also studied the effect of CEs and processing condition on cell morphologies. Mihai et al. (2010) recently studied extrusion foaming of amorphous and semi-crystalline PLA by using epoxy-styrene-acrylic oligomer (CesaExtend OMAN698493) as a reactive chain extender, and supercritical CO_2 as a blowing agent. The effect of CEs was quantified by increases in shear viscosity, melt elasticity and most important strain-hardening behaviour upon uniaxial deformation in the molten state during foaming process. Low density foam was obtained for c-PLA with 5 wt % CO_2 content and for a-PLA with 9 wt % CO_2 content. The difference between foaming behaviour was attributed to crystallites formation during the foaming process. The studies showed that c-PLA can fully crystallize in a very short period of time when CO_2 concentration was 5 wt % and those crystallites play an important role in foam nucleation and stabilization during foaming process.

Yuan et al. (2010) studied the effect of epoxy based multi-functional CEs (Joncryl®) in a starch/PLA blend on mechanical as well as water resistance properties. When small amount of CEs (1 wt %) were added to starch/PLA blend, there was an improvement in the tensile strength, elongation at break and tensile modulus for the whole range of blends. Also, Joncryl® improved the water resistance of starch bioplastic film by enhancement of the hydrophobic property of the blend systems. Li et al. (2011) investigated the effect of a multifunctional epoxy-acrylic-styrene chain extender (CESA-Extend OMAN698493) on the properties of glycerol plasticized TPS/PLA blends. The

use of chain extender effectively increased the melt viscosity of the TPS/PLA blend, which compensated for the molecular weight loss of PLA due to thermal hydrolysis during compounding. The effect of chain extender on the tensile properties of TPS/PLA blends was not significant, which indicated that the chain extender effectively linking PLA end groups and did not play any particular interfacial role. However, improved ductility in the modified blend with chain extender was due to the improved PLA molecular weight and chain entanglement at the interface, which improves the stress transfer between PLA and the ductile glycerol-TPS phase.

To our knowledge, there is no information on the effect of chain extenders on the foamability of a hydrolyzed potato starch/PLA and its comparable commercial resin (Solanyl® blend 30R) blends. In this research, two types of epoxy-styrene-acrylic oligomer chain extenders and two types of low-molecular weight epoxy chain extenders were used to evaluate their effect on the foamability of the hydrolyzed starch(Solanyl® BP)/PLA and Solanyl® blend 30R blends.

CHAPTER: 3

EXPERIMENTATION

3.1 MATERIALS

The Solanyl® blend 30R and Solanyl® 100 BP were procured from Solanyl Biopolymers Inc. (Carberry, Manitoba, Canada).A commercial mix of the Solanyl® blend 30R containing granules of partially hydrolyzed/gelatinized potato starch, poly(lactic acid) (PLAs) and an aliphatic-aromatic copolymer (AAC). The Solanyl® 100 BP contains only the pure partially hydrolyzed/gelatinized potato starch granules. The L-lactide and D-lactide contents in PLAs were not disclosed by the supplier due to confidentiality agreement. Therefore, PLAs could differentiate by only its optical properties. The Solany® blend 30R contains mixture of transparent and opaque PLA. PLA

(NatureWorks™ PLA 7000D) was purchased from Jamplast Inc. (MO, USA), which contains only opaque granules. Chain extenders of epoxy functional styrene-acrylic oligomer (Joncryl® ADR 4370S and Joncryl® ADR 4380) were supplied by BASF (MI, USA). Joncryl® ADR 4370S is available in the form of solid clear flakes with the average molecular weight (M_w), glass transition temperature (Tg) and Epoxy Equivalent Weight (EEW) of 6800 g/mol, 54°C and 285 g/mol respectively. Joncryl® ADR 4380 is available in clear viscous liquid form with the average molecular weight (M_w), glass transition temperature (Tg) and Epoxy Equivalent Weight (EEW) of 3300 g/mol, -41°C and 450 g/mol respectively. General structure of epoxy functional styrene-acrylic oligomers chain extender is shown in Figure 3.1.

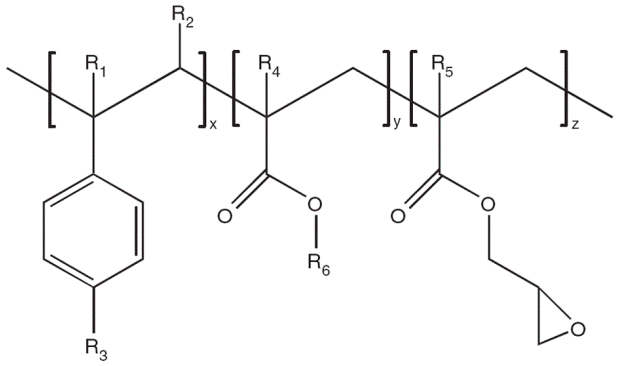

Figure 3.1 General structure of the multi-functional epoxy-based chain extender.
(where R1 to R5 are H, CH_3, a higher alkyl group, or combinations of them;
R6 is an alkyl group, and x, y and z are each between 1 and 20.
(Villalobos et al., 2006))

Two bi-functional epoxy chain extenders Diglycidyl Ether Bisphenol A (DGEBA) and Poly (ethylene glycol) Diglycidyl Ether (PEG-DGE) were purchased from

SigmaAldrich Canada. DGEBA with a number average molecular weight (Mn) and melting temperature (Tm) of 340 g/mol and 40°C respectively. The number average molecular weight (Mn) of PEG-DGE was 640 g/mol. The general structures of the di-epoxy chain extenders are shown in Figure 3.2. Supercritical CO_2 (7.39 MPa and 31.1°C) with a purity of 99.9% was used as a physical blowing agent in the batch foaming process and purchased from Air Liquide Canada.

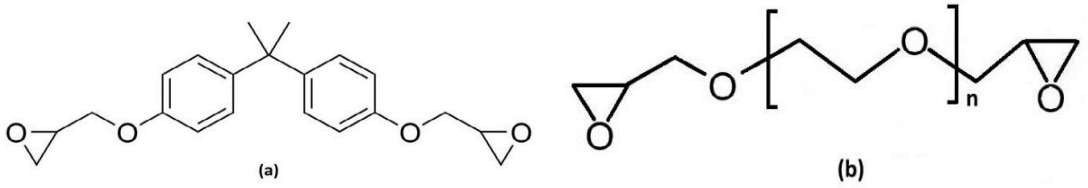

Figure 3.2 General structures of the bi-epoxy functional chain extenders.
(a) Diglycidyl Ether Bisphenol A (DGEBA)
(b) Poly (ethylene glycol) Diglycidyl Ether (PEG-DGE)

3.2 MELT PROCESSING OF BLENDS

A co-rotating intermeshing twin screw extruder (Leistritz ZSE-HP) with a L/D ratio of 40 and screw diameter (D) of 27 mm equipped with heating zones was used for blending. The temperature profile maintained at the 8 heating zones from the feed section to the metering zone section was in the sequence of 85-105-150-160-160-160-170-170-160°C. The screw speed was fixed at 150 rpm for all formulations. The material was extruded through a cylindrical die with an aperture diameter of 3 mm set at 150°C. The material was fed at 5 kg/hr by Brabender DDSR20 gravimetric feeder into the extruder feed throat.

The components in the Solanyl® blend 30R were blended in the twin screw extruder (TSE) and granulated into 2-3 mm pellets by using a 66SRE-Extreme (Rapid Granulators Inc.) granulator. The resulting Solanyl® blend 30R granules were melt blended with different amount of chain extenders (CEs) in an internal mixer (Haake Reomix 3000P). The capacity of the batch mixer with co-rotating roller rotors was 310 cm^3 and about 250 g of Solanyl® blend 30R granules was charged with CEs and melt processed at 170°C with a mixing speed of 75 rpm for about 10 min. The type and level of CEs contents used in formulation are presented in Table 3.1. The amounts of CEs

Table 3.1 Solanyl® blend 30R with different types and contents of CEs in the internal mixer (Haake mixer) (SL: Solanyl® blend 30R)

Type of Chain Extenders	Experiments	% of Chain Extenders
Joncryl® ADR 4370-S	SL-0.5-4370S-Internal	0.5 wt %
	SL-1.5-4370S- Internal	1.5 wt %
	SL-2.0-4370S-Internal	2.0 wt %
Joncryl® ADR 4380	SL-0.5-4380-Internal	0.5 wt %
	SL-1.5-4380-Internal	1.5 wt %
	SL-2.5-4380-Internal	2.5 wt %
Diglycidyl Ether Bisphenol A (DGEBA)	SL-0.5-DGEBA-Internal	0.5 wt %
	SL-1.5-DGEBA-Internal	1.5 wt %
	SL-2.5-DGEBA-Internal	2.5 wt %
Poly(ethylene glycol) diglycidyl ether (PEG-DGE)	SL-0.5-PEG-DGE-Internal	0.5 wt %
	SL-1.5-PEG-DGE-Internal	1.5 wt %
	SL-2.5-PEG-DGE-Internal	2.5 wt %

added to blends were based on the total weight of Solanyl® blend 30R granules. After processing in an internal mixer, the samples were cooled to room temperature and granulated into 2-3 mm granules by granulator. Each sample was molded into standard 10 mm x 40 mm x 2 mm rectangular shape bars by using a hot press at 170 °C for 3 min. The rectangular bars were used for the batch foaming process.

In another formulation, CEs were dissolved in acetone and coated on Solanyl® blend 30R granules. The resulting granules were dried overnight at room temperature and directly extruded in TSE at above mentioned extrusion processing conditions. The samples formulation is shown in Table 3.2. The extruded samples were cooled to room temperature, granulated into 2-3 mm granules by Rapid granulator and stored in sealed plastic bags.

Table 3.2 Composition of different types of chain extenders used with Solanyl® blend 30R and hydrolyzed starch/PLA blends in TSE (SL: Solanyl® blend 30R, SP: hydrolyzed starch/PLA)

Type of Chain Extenders	Experiments		% of Chain Extenders
Joncryl® ADR 4370-S	SL-0.5-4370S-TSE	SP-0.5-4370S-TSE	0.5 wt %
	SL-2.0-4370S-TSE	SP-2.0-4370S-TSE	2.0 wt %
Joncryl® ADR 4380	SL-0.5-4380-TSE	SP-0.5-4380-TSE	0.5 wt %
	SL-2.5-4380-TSE	SP-2.5-4380-TSE	2.5 wt %
Diglycidyl Ether Bisphenol A (DGEBA)	SL-0.5-DGEBA-TSE	SP-0.5-DGEBA-TSE	0.5 wt %
	SL-2.5-DGEBA-TSE	SP-2.5-DGEBA-TSE	2.5 wt %
Poly(ethylene glycol) diglycidyl ether (PEG-DGE)	SL-0.5-PEG-DGE-TSE	SP-0.5-PEG-DGE-TSE	0.5 wt %
	SL-2.5-PEG-DGE-TSE	SP-2.5-PEG-DGE-TSE	2.5 wt %

For comparison purposes, the hydrolyzed starch/PLA (Solanyl® 100 BP/PLA 7000D) were first blended in TSE and then tried to modify in the internal mixer. But, the excessive degradation of hydrolyzed starch without any plasticizers in the blend prevented further processing in the internal mixer with CE. Therefore, the hydrolyzed starch/PLA blend was directly modified in the TSE with CE. Solanyl® 100 BP (hydrolyzed starch) and PLA 7000D mixed with 40/60 ratio by weight. This blend subsequently called as the hydrolyzed starch/PLA blend in our rest experimental and discussion parts. The granules were coated with different CEs as above mentioned coating procedure. The coated granules were extruded in TSE at above mentioned extrusion processing conditions. The types and levels of CEs contents used in formulation are presented in Table 3.2. The samples were cooled to room temperature and granulated into 2-3 mm granules by granulator. Each sample was molded into standard 10 mm x 40 mm x 2 mm rectangular shape bars by using a hot press at 170 °C for 3 min. The rectangle bars were used in the batch foaming process.

3.3 BATCH FOAMING APPARATUS

The foaming process was carried out in a 75 mL high-pressure batch foaming vessel. The high-pressure syringe pump (ISCO Model 260D) was used to charge supercritical CO_2 (P_c=7.39 MPa, T_c=31.1°C) into the vessel. A schematic of the set-up used for the experiments shown in Figure 3.3. The syringe pump was attached to the vessel via high pressure stainless steel tubing and couplings. The built-in pressure transducer in the syringe pump accurately controls the pressure inside the high- pressure

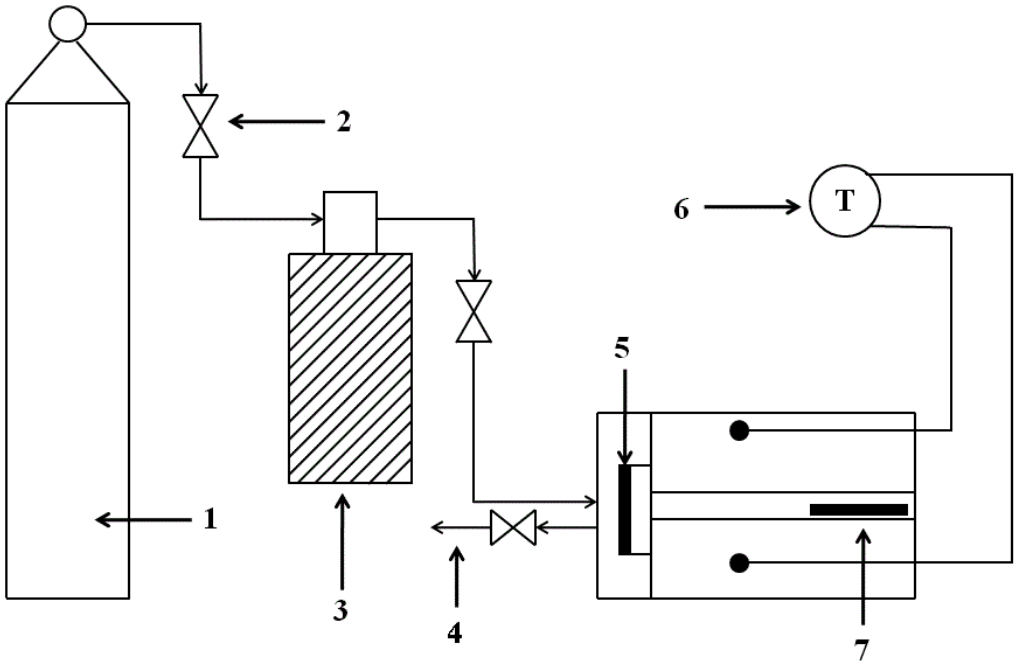

Figure 3.3 High-pressure batch foaming vessel diagram: 1, Supercritical CO_2 gas cylinder; 2, valve; 3, high-pressure syringe pump; 4, vent; 5, o-ring; 6, temperature controller; 7, sample

vessel chamber. The temperature of the vessel (170°C) was controlled by the temperature control module and the fluctuation of temperature in the vessel was less than ± 2°C. The Teflon o-ring was used to prevent leakage between the main body of the vessel and cap.

3.4 BATCH FOAMING PROCESS

The foaming process on the samples was carried out by placing them on a small aluminum tray inside the high-pressure vessel to facilitate easy removal of the foamed samples. The vessel was preheated to 170°C before placing the sample and a control module was used to control the temperature. The rectangle sample bars were placed in an

aluminum tray and kept inside the high-pressure vessel. The vessel was saturated with supercritical CO_2 at different pressures and saturation times. Finally, the vent valve of the vessel was opened and depressurized to atmospheric pressure in less than 2 sec for all the foamed samples. After the foamed sample removed from the chamber, it cooled by ambient air then stored in plastic bags at room temperature. For Solanyl® blend 30R and CEs, three different saturation pressures and two different supercritical CO_2 saturation time were used to evaluate the foam bulk density, cell size and cell density. Details of the batch foaming parameters for Solanyl® blend 30R with different chain extenders are given in Table 3.3.

For hydrolyzed starch and PLA blends, two different saturation pressures and one identical supercritical CO_2 saturation time of 60 min was used to evaluate the foam physical characteristics. Detail batch foaming parameters for Solanyl® BP/PLA blends with different chain extenders are given in Table 3.4.

Table 3.3 Batch foaming parameters for Solanyl® blend 30R with different types and contents of chain extenders (SL: Solanyl® blend 30R)

Experiments #	Saturation Time (min)	Saturation Pressure (MPa)		
SL-0.5-4370S-Internal	30 and 60	10	15	20
SL-1.5-4370S-Internal				
SL-2.0-4370S-Internal				
SL-0.5-4380-Internal	30 and 60	10	15	20
SL-1.5-4380-Internal				
SL-2.5-4380-Internal				
SL-0.5-DGEBA-Internal	30 and 60	10	15	20
SL-1.5- DGEBA-Internal				
SL-2.5- DGEBA-Internal				
SL-0.5-PEG-DGE-Internal	30 and 60	10	15	20
SL-1.5-PEG-DGE-Internal				
SL-2.5-PEG-DGE-Internal				

Table 3.4 Batch foaming parameters for hydrolyzed starch/PLA with different types and contents of chain extenders (SP:hydrolyzed starch/PLA)

Experiments #	Saturation Time (min)	Saturation Pressure (MPa)	
SP-0.5-4370S-TSE	60	15	20
SP-2.0-4370S-TSE			
SP-0.5-4380-TSE	60	15	20
SP-2.5-4380-TSE			
SP-0.5- DGEBA-TSE	60	15	20
SP-2.5- DGEBA-TSE			
SP-0.5-PEG-DGE-TSE	60	15	20
SP-2.5-PEG-DGE-TSE			

3.5 CHARACTERIZATION

3.5.1 DIFFERENTIAL SCANNING CALORIMETRY (DSC)

Differential scanning calorimetry (DSC) measurements were conducted on all component polymers and extruded blend samples by using a Q200 differential scanning calorimeter equipped with a refrigerated cooling system (TA Instruments, USA). Around 10-12 mg samples were sealed in an aluminum Tzero hermetic DSC pan and heated up from 0°C to 200°C at 10°C/min, and then subjected to isothermal stage at 200°C for 3 min in order to erase the previous processing history. Sample was cooled to - 60°C, and finally reheated to 200°C. A nitrogen flow was maintained at 50 mL/min during DSC tests. The second heating cycle was used for the thermal analysis. The TA Universal Analysis 2000 software was used to analyze the DSC curves for studying the glass transition and melting temperature. The percentage of error in measuring the glass transition temperature (T_g), the re-crystallization temperature (T_{ch}) and the melting temperature (Tm) was 1.82%, 1.26% and 0.86% RSD (Relative Standard Deviation) respectively based on three repeats.

3.5.2 INTRINSIC VISCOSITY

The Intrinsic Viscosity (IV) [η] measurements were done for the samples prepared by TSE. Cannon 25K 867 series (CANNON Instrument Company, State College, PA) Ubbelohde viscometer was used to measure the intrinsic viscosity of PLA/AAC and PLA phases. This Ubbelohde viscometer had Kinematic Viscosity range of 0.5-2 mm^2/s (cSt) and ASTM size code of 25. The samples processed in the TSE had

been used for the intrinsic viscosity measurement of the PLA/AAC or PLA phase. The PLA/AAC or PLA phases from the modified blends were first extracted by dissolving it in chloroform for 24 hr. Then, the solution was filtered through a coarse filter (Dimaglass Type: C) to separate the starch phase. The extracted starch phase was dried in a vacuum oven at 50°C overnight and stored in sealed glass vials. The chloroform was evaporated from the solution and PLA/AAC or PLA phase was completely dried by using vacuum oven overnight at 50°C. The samples of different concentration were prepared by dissolving about 0.01 - 0.03 g of PLA/AAC or PLA extract in 10 mL chloroform. The samples were kept overnight for complete dissolution of PLA/AAC or PLA extract in chloroform. The Ubbelohde viscometer kept in the water bath for 15 min at 25 ± 0.5 °C until thermal equilibrium and then the sample was loaded in the Ubbelohde viscometer. The samples were kept at that temperature for a minimum of 30 mins to reach thermal equilibrium. Each sample solution was rinsed once through the capillary tube before flow time (t) was measured. Flow time recorded was used to calculate the relative viscosity (η_r) and specific viscosity (η_{sp}). The intrinsic viscosity of each sample was calculated by using the Solomon and Ciuta equation of a single point measurement:

$$[\eta] = \frac{\sqrt{2\left(\eta_{sp} - \ln \eta_r\right)}}{c} \qquad 3.1$$

where, $\eta_r = t_{solution}/t_{solvent}$ is relative viscosity, $\eta_{sp} = \eta_r - 1$ is specific viscosity and c is polymer solution concentration (g/100mL).

For comparison purposes, intrinsic viscosity of individual components of Solanyl® blend 30R were also measured to determine the intrinsic viscosity of pristine PLAs, PLA 7000D and aliphatic-aromatic copolyester(AAC). About 0.01-0.03 g of virgin components were dissolved in 10 mL of chloroform and the sample were kept overnight for complete dissolution in chloroform. The same procedure was used for the measurement of intrinsic viscosity values of the pristine components as well.

Solanyl® blend 30R and hydrolyzed starch/PLA blend samples with and without 4370S CE were also used for the investigation of intrinsic viscosity of the starch phase. Intrinsic viscosity of pristine partially hydrolyzed/gelatinized starch measured and used as a reference for the comparison. About 0.02 – 0.03 g of hydrolyzed starch or extracted starch phase were dissolved in 10 mL DMSO for 48 hrs. Then, the solution was filtered through pre-weight wired mesh (200x 200) to separate undissolved particles in Starch/DMSO solution. The wired meshes was dried in vacuum at 70°C overnight and re-weighed in order to measure approximate concentration of starch in 10 mL DMSO solution. The Ubbelohde glass viscometer (Technical Glass Product, Sr. No. 2292) were used to measure flow time for the intrinsic viscosity of starch phase. This Ubbelohde viscometer had Kinematic Viscosity range of 2-10 mm^2/s (cSt) and ASTM size code of 1. The same procedure was adopted to measure the intrinsic viscosity of starch phase.

3.5.3 SCANNING ELECTRON MICROSCOPY(SEM)

The blend morphology of Solanyl® blend 30R and hydrolyzed starch/PLA blend samples with and without 4370S CE were investigated by JEOL 7000F FE scanning

electron microscope (SEM). The samples were cryo-fractured in liquid nitrogen and starch phase was etched in hydrochloric acid (HCl, 1N) at ambient temperature for 12 h. The samples were then cleaned by washing with demineralized water using ultrasound for 5 min and then dried overnight in vacuum oven at 50°C. Each sample was mounted on an aluminum stub with graphite filled tape, sputter coated with a 9 nm layer of Platinum done with Gatan Model 682 Precision Etching Coating System (PECS), and examined with a scanning electron microscope at an accelerated voltage of 1 kV.

3.5.4 RHEOLOGICAL MEASUREMENT IN PARALLEL PLATE RHEOMETER

Rheological measurements were done in dynamic oscillatory mode under strain-controlled conditions on a parallel plate TA Instruments ARES rheometer. The diameter of the plates was 25 mm and the gap between the plates was set to 1.5 mm for all measurements. The test sample disks were prepared by using hot press at 170°C for 3 min. The temperature of the heat chamber was maintained at 170 °C by two thermocouples within the heat chamber. After placing sample between two discs, the gap between disk was adjusted to 1.5 mm and extra molten sample was trimmed off for a smooth edge around the sample. The strain sweep test (range 0.1-100%) was done in order to determine the strain in the linear visco-elastic region at frequency of 1 rad/sec. The range of strain in linear visco-elastic region was 2%- 6% for Solanyl® blend 30R and 1%- 5% for hydrolyzed starch/PLA blends. Then, dynamic frequency sweep tests were carried out in the interval of 0.1-100 rad/sec. At least 3 runs were performed for each sample and the experimental results were averaged.

3.5.5 PHYSICAL CHARACTERISTIC OF FOAMS

The bulk density of foamed sample was determined by digital electronic densimeter (MIRAGE MD-200S) that measures the density value based on Archimedes's principle. The determination of the density value is based on the density of water at 4°C (1 g/cm^3). First, the foamed sample was weighed in the air and then by submerging them in water. Based on these two weights, the density of the foam sample was determined by the densimeter. The measurements were repeated three times and average values were reported.

The foamed samples were cryogenically fractured by dipping them into liquid nitrogen. The fractured surface was observed under Greenough type stereoscope (Stemi-2000C, Carl Zeiss AG, Germany). The image of the sample's foam cell size was analyzed by Sigma Scan Pro software. The cell population density (n) was calculated as the number of cells per unit volume with respect to the unfoamed samples. The number of cells (N) in the defined area (ℓ x ℓ) was first calculated from stereoscope images. The total number of cells per cubic centimetre was calculated by the following equation (Mihai et al., 2010).

$$n = \left(\frac{N}{l^2}\right)^{3/2} * Va \quad \text{Where } Va = \rho_{sample}/\rho_{foam} \tag{3.2}$$

Where, Va is the radial expansion ratio, ρ_{sample} and ρ_{foam} are the density of unfoamed and foamed samples respectively.

CHAPTER: 4

RESULTS AND DISCUSSION –

DIFFRENTIAL SCANNING CALORIMETRY

4.1 THERMAL PROPERTIES OF HYDROLYZED STARCH /PLA BLENDS

Differential Scanning Calorimetry (DSC) tests were done on partially hydrolyzed potato starch and virgin PLA7000D beads in order to evaluate an appropriate thermal processing window of the mix in the TSE. Typical DSC thermographs of partially hydrolyzed potato starch (Solanyl® 100 BP) and PLA 7000D are shown in Figure 4.1 corresponding to the second heating cycle for the materials. From the thermographs, the partially hydrolyzed starch showed a single melting peak at 178°C. The disappearance of

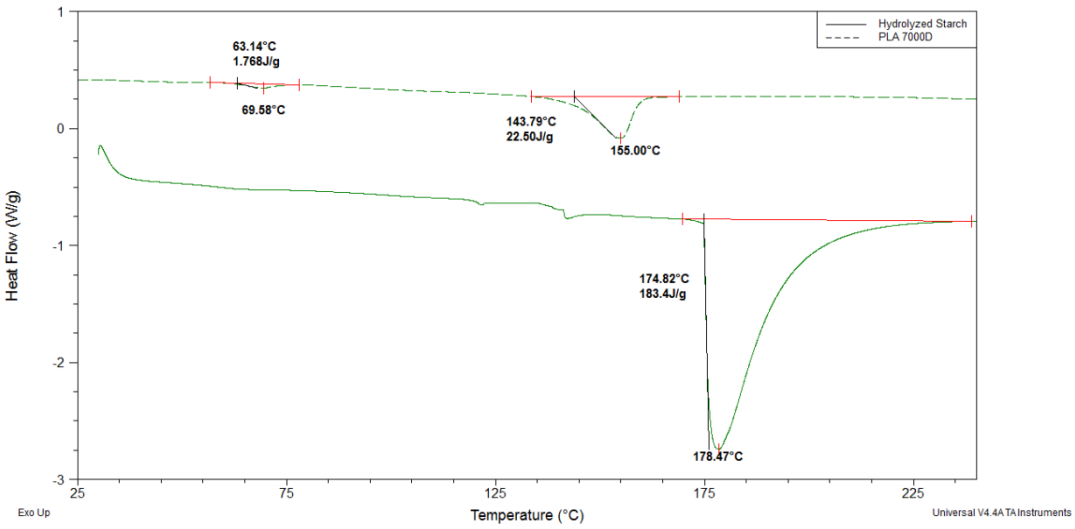

Figure 4.1 DSC thermographs pristine components of hydrolyzed starch (Solanyl® 100 BP) and PLA 7000D

the starch melting peak in subsequent starch/PLA blends were due to complete starch gelatinization during thermal processing. The virgin opaque PLA 7000D beads showed a glass transition temperature (T_g) at 70°C and a melting temperature (T_m) at 155°C; the glass transition for PLA is different than for many other polymers showing a peak rather than a step transition. Those characteristic peaks of PLA were in agreement with the results published by Guan et al. (2005), Jang et al. (2007) and Shin et al. (2011) for PLA polymer.

The hydrolyzed starch/PLA (40/60 wt %) was processed at 170°C in the TSE, relying on mechanical energy to complete melting of both resins and maximize mixing of two phases, while minimizing thermal degradation of PLA in stagnant regions of the screw, which certainly would occur at higher temperature. Jang et al. (2007) observed the

presence of moisture in starch decreased the number and weight average molecular weight to about half compared to that of pure PLA due to hydrolysis. In the present work, hydrolyzed starch had an inherent moisture content of 8 wt % (measured by Mettler-Toledo HG63 moisture analyzer), which unable complete melting of starch granules during processing. However, no plasticizer such as glycerol or sorbitol has been used in any of the blends investigated.

4.1.1 HYDROLYZED STARCH/PLA AND ADR 4370S

Typical DSC melting thermographs of hydrolyzed starch/PLA blend with 0.0 wt %, 0.5 wt % and 2.0 wt % of CE (ADR 4370S) are shown in Figure 4.2. Each sample displayed a glass transition (T_g), a melt endotherm (T_m) and now a re-crystallization exotherm (T_{ch}), all typical of the transitions for PLA observed within dry starch/PLA blends (Zhang and Sun, 2004; Jang et al., 2007).

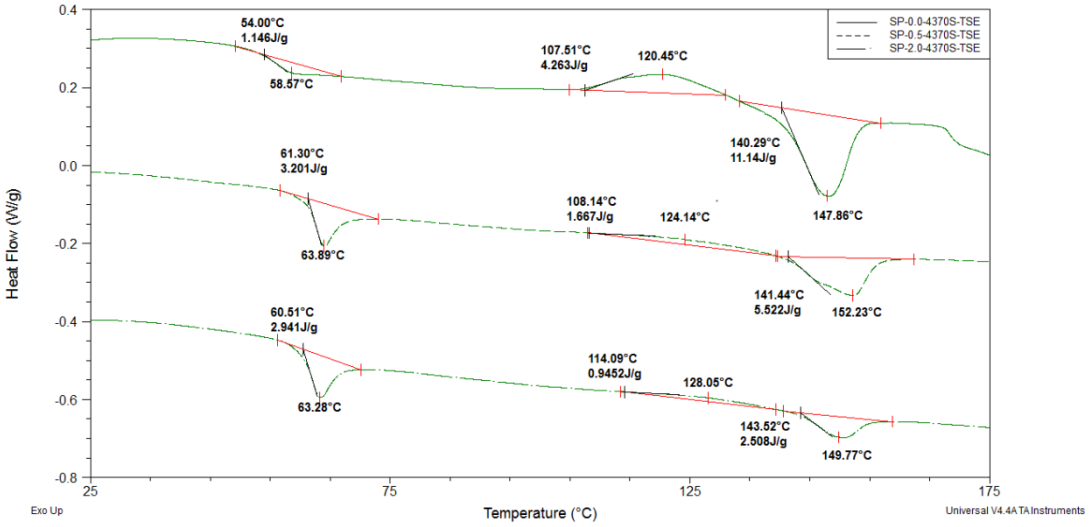

Figure 4.2 DSC thermographs of hydrolyzed starch/PLA blend with different contents of ADR 4370S CE

The neat blend without CE showed a glass transition temperature of the PLA phase at 59°C, which was about 11°C lower than the neat PLA. Thermal degradation, especially hydrolysis during compounding due to the inherent moisture of the hydrolyzed starch was likely a contribution to the shifted T_g with rheological evidence of degradation was noted by the intrinsic viscosity measurement described in the following section (Section 5.1). However, this shift in glass transition was not noted by others studying corn starch blends with PLA (Ke and Sun, 2000; Jang et al., 2007) and in the case of Jang et al. (2007), measurement by gel permeation chromatography of the extracted PLA phase confirmed chain degradation had occurred (i.e. 54% reduction in M_n). Therefore, it is believed the main cause for the decreased T_g found in Figure 4.2 was a result from using hydrolyzed potato starch in place of a native variety. Hydrolysis of the starch was intended by the vendor to improve its interaction with PLA, which evidently enhanced chain mobility of the PLA phase in the blend. Conversely, the addition of CE decreased a glass transition temperature of the PLA phase by about 6°C to ~64°C compared to the neat PLA, regardless of its concentration. This transition appeared better defined in the thermograms by the inclusion of CE. The higher T_g found for these two concentrations of CE compared to the neat blends indicated retardation in chain mobility but also showed that at least some reaction with the epoxy functional CE was taking place in the PLA phase. These results differ from those of Li et al. (2011), who did not observe any shift in their T_g values by using a similar multi-functional epoxy-styrene-acrylic copolymer CE

with a blend of glycerol plasticized TPS/PLA, but their use of glycerol in the trials may have obscured this outcome.

The thermograph of neat blend showed an endothermic peak at 148°C corresponding to the melting peak of PLA. The reduced melting temperature of the PLA phase from 155°C to 148°C was not in agreement with results reported by Ke and Sun (2000) or Jang et al. (2007), who found the melting transition of different blends were similar to that of pure PLA. In their results the melting peak remained at 170°C with varied weight ratios of either corn or wheat starch blended with semi-crystalline PLA. Jang et al. (2007) also implied that starch acted as a nucleating agent towards crystallization in the PLA phase based on their observations of increased heat of fusion with the addition of starch to the blends. Comparatively, the neat blend in our work showed a decrease in enthalpy compared to pure PLA (11 J/g versus 23 J/g, respectively) by addition of starch. Though our results differ from those of other researchers, such comparisons helped to reaffirm that the hydrolyzed starch used in the present work had a plasticizing influence on the PLA phase, altering its crystalline morphology as well as reducing its crystalline content. With the addition of 0.5 wt % CE to the blend, the melting peak was found at 152°C but still showed a shoulder corresponding to 148°C. For 2 wt % CE, the transition remained broad with a peak temperature of 150°C, but the shoulder was no longer distinctly evident. The heat of fusion for the modified blends decreased with CE concentration, reduced to 3 J/g by 2.0 wt % CE. The progressive loss of the shoulder in the melting transition suggested that a different crystalline morphology

was produced in the materials with CE though not matching the neat PLA either. Also, the lowering of crystalline content for the PLA phase was expected as chain alignment would become increasingly difficult from branching with the epoxy moieties of CE. This result was in agreement with Pilla et al. (2009) and Li et al. (2011).

A new crystallization exotherm was observed in Figure 4.2 at 120°C for the neat blend which had been absent in the original PLA material. The broad peak was present for each of the modified blends as well, and appeared to shift to higher temperatures with increasing CE concentration, though that may have been partially an artefact of detecting the decreasing peak height. The heat of crystallization varied in proportion to the subsequent melting peak for the trials with CE but was always smaller (30-38% of ΔH_m) than the enthalpy of fusion (ΔH_m). The peak has been detected consistently in starch/PLA blends observed by Jang et al. (2007) and also been observed in pure PLA that has been quenched rapidly in fiber spinning (Yuan et al., 2001). The presence of the peak points to slowed crystallization kinetics of the PLA during the first heat-cool cycle in the DSC caused by the presence of starch. With incomplete crystallization prior to reaching the glass transition temperature of the polymer phase, a highly amorphous structure with frozen-in stresses resulted until the second heating cycle allowed re-crystallization to occur. The CE species reduced the crystallinity of the PLA phase through chain extension, leaving less content for re-crystallization upon the second heating cycle. Ke and Sun (2003) reported increased crystallization rates with corn starch for the PLA phase, but such a finding cannot be reconciled with the hydrolyzed potato starch.

However, our results were not in agreement with Mihai et al. (2010), who blended c-PLA with similar type multifunctional epoxy-styrene-acrylic copolymer (CESA-Extend OMAN698493) CE. The peak crystallization temperature on heating decreased by 10°C as the CE content was increased up to 2% and leads to increase the rate of crystallization in the presence of CE.

4.1.2 HYDROLYZED STARCH/PLA AND ADR 4380

Typical DSC thermographs of blend with 0.0 wt %, 0.5 wt % and 2.0 wt % of CE (ADR 4380) are shown in Figure 4.3. The description of glass transition (T_g), a re-crystallization exotherm (T_{ch}) and a melt endotherm (T_m) of neat blend was given in section 4.1.1.

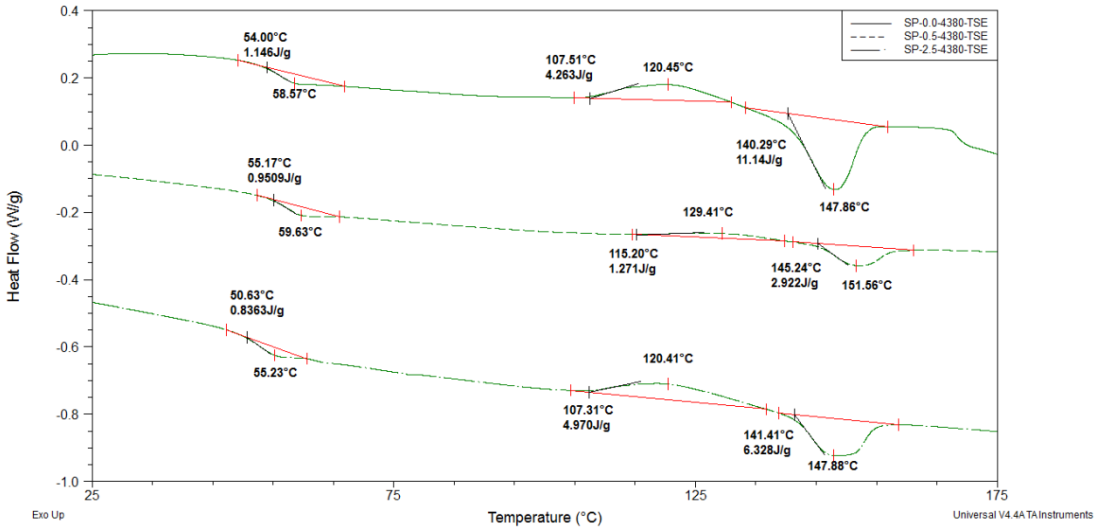

Figure 4.3 DSC thermographs of hydrolyzed starch/PLA blend with different contents of ADR 4380 CE

The glass transition temperature of the blend with 0.5 wt % CE was increased by only 1°C to 60°C compared to the neat blend. This result was significantly different from the previously investigated CE (ADR 4370S, Section 4.1.1), which may be due to the lower epoxy functionality of the ADR 4380 CE. However, further addition of CE to 2.5 wt % decreased the glass transition temperature of the PLA phase to 55°C, which was lowered then the neat blend. The addition of low molecular weight CE at 2.5 wt %, might work as a plasticizer in the blend.

The thermographs of blend with 0.5 wt % CE showed melting peak at 152°C and it was higher by 4°C compared to neat blend. Which was comparable with the results from the previous CE (ADR 4370S, Section 4.1.1). The neat blend had estimated melting enthalpy of 11 J/g and the addition of the CE decreased the melting enthalpy to around 3 J/g for 0.5 wt % CE. Different crystalline morphology compared to neat blend would result in higher melting point of blend with 0.5 wt % CE. Also, the lowering of crystalline content was expected as some of the PLA chains linearity was disrupted by branching of polymer chains with epoxy moieties of CE. However, further addition of 2.5 wt % CE did not show any significant changed in the melting transition but developed less crystalline endotherm compared to neat blend. This was evident by the lower epoxy functionality of ADR 4380 CE.

The peak re-crystallization temperature on heating increased by around 9°C as the CE content was increased to 0.5 wt % compared to neat blend. The re-crystallization enthalpy of blend with 0.5 wt % CE was decreased to 1 J/g. From the obtained results, it

seems that the rate of crystallization was decreased in the presence of the CE and blend could crystallize at higher temperature. There results were comparable to previously investigated CE (ADR 4370S, Section 4.1.1). However, further increased in CE content to 2.5 wt % did not show any significant improvement in the re-crystallization exotherm compared to neat blend.

4.1.3 HYDROLYZED STARCH/PLA AND DGEBA

Typical DSC thermographs of blend with 0.0 wt %, 0.5 wt % and 2.5 wt % of CE (DGEBA) are shown in Figure 4.4. The description of glass transition (T_g), a re-crystallization exotherm (T_{ch}) and a melt endotherm (T_m) of neat blend was given in section 4.1.1.

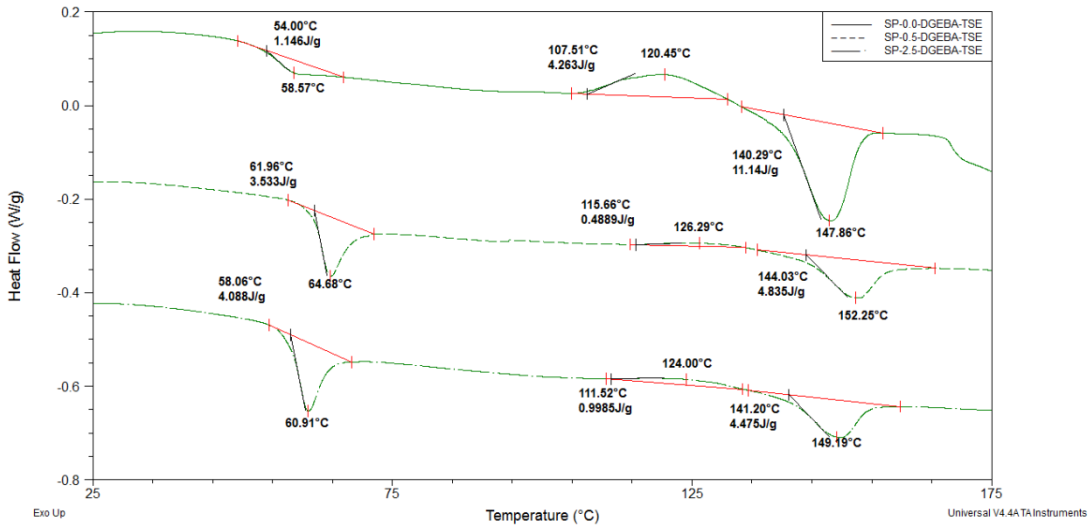

Figure 4.4 DSC thermographs of hydrolyzed starch/PLA blend with different contents of DGEBA CE

The blend with 0.5 wt % CE had a glass transition temperature at 65°C, which was 6°C higher than the neat blend. The incorporation of bi-functional CE also hampered the activity of polymer chains by polymeric chain extension. The chain extension reaction between blend and CE was noted by intrinsic viscosity measurement in the following section (Section 5.1). However, the addition of 2.5 wt % CE increased the glass transition temperature by only 2°C compared to neat blend. It was possible that at higher content of CE, the excess low-molecular weight CE worked as a plasticizer in the polymer matrix and enhanced the segmental chain mobility of modified polymer chains compared to 0.5 wt % CE, which in turn, decreased the glass transition temperature of blend at 2.5 wt %. However, Haralabakopoulos et al. (1998) observed the glass transition temperature of PET continuously decreased with increased DGEBA content.

The addition of CE increased the melting peak to 152°C and 149°C for 0.5 wt % and 2.5 wt % CE respectively. However, increasing in melting peak and decreasing melting enthalpy compared to neat blend was the evidence of creating new and less crystalline structure which melted at higher temperature. Haralabakopoulos et al. (1998) also observed decreased in melting peak of PET as concentration of DGEBA increased.

The re-crystallization exotherm temperature increased to 126°C and 124° for 0.5 wt % and 2.5 wt % of CE respectively. Also, the re-crystallization enthalpy was decreased to about 0 - 1 J/g for blends with both levels of chain extender. The reason for increased in re-crystallization temperature and decreased in enthalpy can be explained by chain extension reaction between bi-functional epoxide and polymer chains, which

decreased heating re-crystallizability of PLA phase. However, those differences in thermal transitions in blend with DGEBA can be attributed to the low levels of branching with bi-functional CE.

4.1.4 HYDROLYZED STARCH/PLA AND PEG-DGE

Typical DSC thermographs of blend with 0.0 wt %, 0.5 wt % and 2.5 wt % of CE PEG-DGE are shown in Figure 4.5. The description of glass transition (T_g), a re-crystallization exotherm (T_{ch}) and a melt endotherm (T_m) of neat blend was given in section 4.1.1.

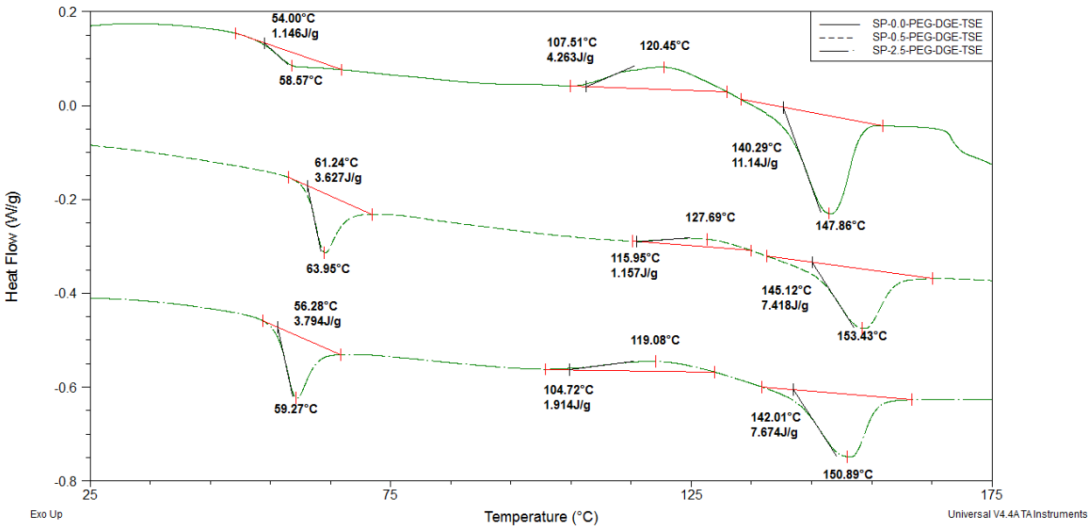

Figure 4.5 DSC thermographs of hydrolyzed starch/PLA blend with different contents of PEG-DGE CE

The blend with 0.5 wt % CE had a glass transition temperature at 64°C, which was 5°C higher than the neat blend. The incorporation of bi-functional CE also hampered the activity of polymer chains by polymeric chain extension. The chain extension reaction between blend and CE was noted by intrinsic viscosity measurement in the following

section (Section 5.1). However, the addition of 2.5 wt % CE did not improved glass transition temperature and remained at same level as the neat blend. It was possible that the excess concentration of low-molecular weight CE worked as a plasticizer in the polymer matrix and enhanced the segmental chain mobility of modified polymer chains compared to 0.5 wt % CE, which in turn, decreased the glass transition temperature of blend at 2.5 wt %.

The addition of CE increased the melting peak to 153°C and 151°C for 0.5 wt % and 2.5 wt % CE respectively. However, increasing in melting temperature and decreasing melting enthalpy is evidence of creating new and less crystalline structures, which melt at a higher temperature compared to neat blend.

The re-crystallization exotherm temperature increased to 128°C for 0.5 wt % of CE and further addition of 2.5 wt % CE did not change re-crystallization temperature compared to neat blend. Also, the re-crystallization enthalpy was decreased to about 1-2 J/g for blends with both levels of chain extender. The reason for decreased in enthalpy can be explained by chain extension reaction between bi-functional epoxide and polymer chains, which decreased re-crystallizability of PLA.

4.2 THERMAL PROPERTIES OF SOLANYL® BLEND 30R BLENDS

Differential scanning calorimetry (DSC) tests were also done on individual components of the commercial Solanyl® blend 30R in order to evaluate an appropriate thermal processing window in the TSE and internal mixer. Typical DSC melting thermographs of hydrolyzed starch, transparent PLA, opaque PLA and aliphatic-aromatic

copolyester are shown in Figure 4.6 corresponding to the second heating cycle for the materials.

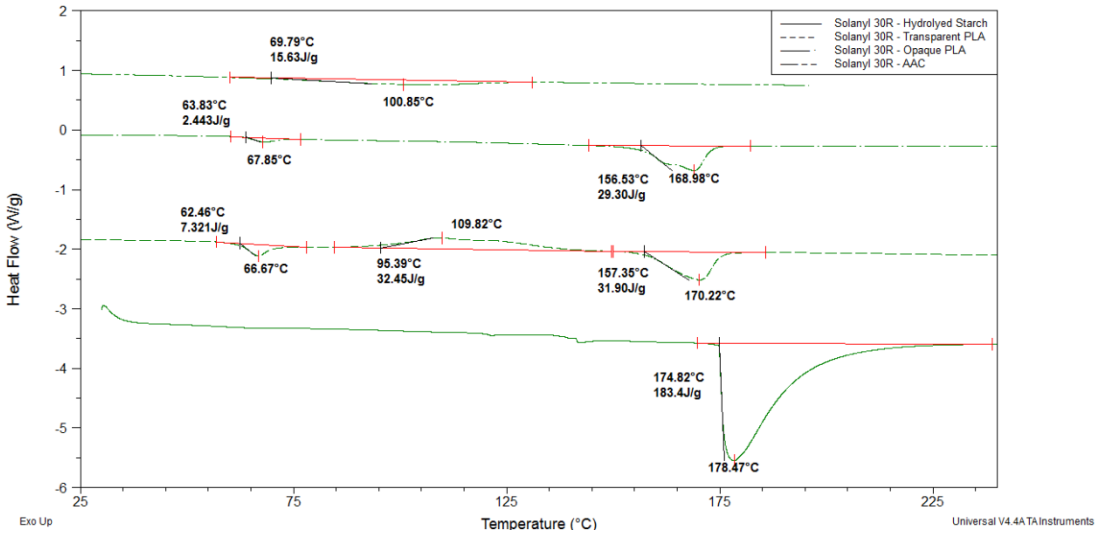

Figure 4.6 DSC thermographs of Solanyl® blend 30R pristine components of hydrolyzed potato starch, Transparent PLA, Opaque PLA and aliphatic-aromatic copolyester (AAC)

The thermograph description of partially hydrolyzed starch was already given in section 4.1. The virgin transparent PLA beads showed a glass transition peak (T_g) at 67°C and a broad melting peak (T_m) at 170°C. The transparent PLA beads also showed an unusual transition peak which assumes corresponded to recrystallization at 110°C. These characteristic peaks of PLA beads were in agreement with the results published by Ke and Sun (2000) for transparent PLA beads. The virgin opaque PLA beads showed only a glass transition peak at 68°C and a melting peak at 169°C. In contrast, one can barely find the melting peak of aliphatic-aromatic copolyester (AAC) at around 101°C. Jiang et al. (2006) also did not observe the glass transition of aliphatic-aromatic copolyester (poly

(butylene adiapate-co-terephthalate) (PBAT)) by DSC method. However, they measured the glass transition temperature of aliphatic-aromatic copolyester (PBAT) at -30°C by dynamic mechanical analysis (DMA) and a melting temperature at 115°C by DSC analysis. Even though hydrolyzed potato starch has a higher melting peak of 178°C compared to other components, the blends were processed at maximum 170°C in the TSE as well as in the internal mixer in order to avoid hydrolysis of PLA chains at the higher temperature in presence of moisture as explained in section 4.1.

4.2.1 SOLANYL® BLEND 30R AND ADR 4370S

Typical DSC thermographs of Solanyl® blend 30R with 0.0 wt %, 0.5 wt %, 1.5 wt % and 2.0 wt % of CE (ADR 4370S) are shown in Figure 4.7. Each sample displayed a glass transition (T_g), a melt endotherm (T_m) and a re-crystallization exotherm (T_{ch}).

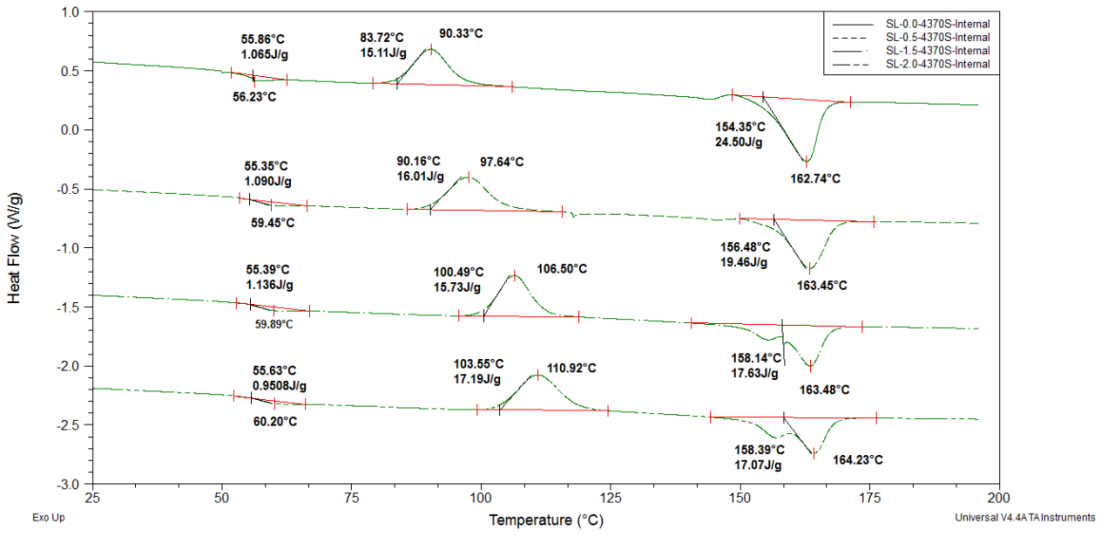

Figure 4.7 DSC thermographs of Solanyl® blend 30R with different contents of ADR 4370S CE

The neat blend without CE showed a glass transition temperature of PLA phase at 56°C, which was 11°C and 12°C lowered compared to transparent and opaque PLAs, respectively. The reduction in glass transition temperature was due to thermal degradation during hydrolysis of PLA phase in presence of inherent moisture content in the hydrolyzed starch as explained in section 4.1. The thermal degradation further evidenced by intrinsic viscosity measurement in the following section (Section 5.2). It is also believed that the presence of elastomeric (soft) aliphatic-aromatic copolyester in Solanyl® blend 30R enhanced the chain mobility of PLA molecules and could also lowered its glass transition temperature. However, Sarazin et al. (2008) did not observe any shift in glass transition by addition of 10 wt % poly (ε-caprolactum) (PCL) in glycerol plasticized wheat starch/PLA (50/40 wt/wt) blend. The use of glycerol as a plasticizer in the blend may have reduced the thermal degradation of PLA chains. Conversely, the addition of CE decreased a glass transition temperature of the PLA phase by about 8°C to ~60°C compared to the neat PLAs, regardless of its concentration. The higher T_g of PLA phase with CE compared to the neat blend indicated chain extension reaction with epoxy functional CE and PLA phase. These results were in aligned with our previously studied hydrolyzed starch/PLA blend with ADR 4370S CE (Section 4.1.1).

The thermograph of the neat blend showed an endotherm peak at 163°C corresponding to the melting transition of both transparent and opaque PLAs. The reduction in melting temperature of the PLA phase from 170°C to 163°C was in agreement with results reported by Liao et al. (2009), who studied the effect of starch

content on melting transition of PLA phase in $PLA_{70}PCL_{30}$ blend. However, the decreased melting transition was only about 2°C as starch content was increased to 50 wt % compared to our neat blend (7°C). The neat blend in our work also showed a decreased in enthalpy compared to pure PLAs (25 J/g versus 32 J/g and 29 J/g for transparent and opaque PLAs, respectively). The hydrolyzed starch had a plasticizing influence on the PLA phase and prohibited the movement of that phase, which caused polymer chain arrangement more difficult and less crystalline structure was created. The addition of CE to the blend did not change the melting peak of blends (164°C). The heat of fusion for the modified blends decreased to 19 J/g with 0.5 wt % CE compared to neat blend (25 J/g) suggesting lowered crystalline content for the PLA phase. As it was expected as chain alignment would become increasingly difficult from branching with the epoxy moieties of CE. Also, the progressively increase in CE concentration to 2.0 wt % clearly separated two individual peaks in melting endotherm, suggesting the presence of new crystalline morphology in the blend (e.g. thickness of lamellar structure and size of the spherulities) introduced by the higher percentage of CE. The different crystalline morphology was obtained from different crystallization processes such as melt-crystallization (from cooling) and cold crystallization. Those crystalline structures with different morphologies melt at different temperatures, thereby producing two different melting peaks. The similar two melting peaks were also observed by Pilla et al. (2009), who studied the melt blending of PLA with similar type of multifunctional epoxy-styrene-acrylic copolymer (CESA-Extend OMAN698493) CE.

A crystallization exotherm was observed in Figure 4.7 at 90°C for the neat blend, which was 20°C lower than the peak seen in neat transparent PLA thermograph (Figure 4.6). Park et al. (2000) and Wang et al. (2001) observed a similar crystallization exotherm transition for PLA phase in PLA/Starch blends. Park et al. (2000) implied starch act as a nucleating agent for PLA phase and enhanced crystallization of that phase by observing increased in heat of fusion. However, in our work heat of fusion was decreased compared to neat PLA. While, Wang et al. (2001) stated PLA molecules suffered chain degradation during hydrolysis and shearing when mixed at high temperature. The increased short chains portion in the blend shifts the crystallization exotherm to a lower value and enhanced crystallization. In our work thermal degradation and hydrolysis of PLA chains in presence of inherent moisture content of hydrolyzed starch was the contributing factor for enhanced crystallization in the neat blend. Also, starch granules might restrict the molecular motion of the PLA matrix and result in a decreased crystallization and fusion enthalpies (32 J/g for neat transparent PLA vs. 15 J/g for neat blend). However, neat blend also developed small re-crystallization exotherm peak prior to the major melting endotherm peak in the heating cycle. This small exothermic peak was an additional crystallization that occurred at higher temperature, which was in agreement with the results from Ke et al. (2000, 2003).

As the CE content increased, the small exotherm peak gradually disappeared and a shoulder melting peak prior to the major melting peak appeared instead. This was due to different crystallization morphology development in presence of CE during

crystallization process. The peak re-crystallization temperature on heating increased by 21°C as the CE content was increased to 2.0 wt %. The re-crystallization enthalpy for blends were around 15 – 17 J/g regardless of CE concentrations. It is believed that the chain linearity was disrupted by branching of polymer chains with epoxy moieties of CE, which depressed the crystallizability of the blend and consequently the blend could crystallize at a higher temperature. This result was also in agreement with the study done by Pilla et al. (2009).

4.2.2 SOLANYL® BLEND 30R AND ADR 4380

Typical DSC thermographs of blend with 0.0 wt %, 0.5 wt %, 1.5 wt % and 2.5 wt % of CE (ADR 4380) are shown in Figure 4.8. The description of glass transition (T_g), a re-crystallization exotherm (T_{ch}) and a melt endotherm (T_m) of neat blend was given in section 4.2.1.

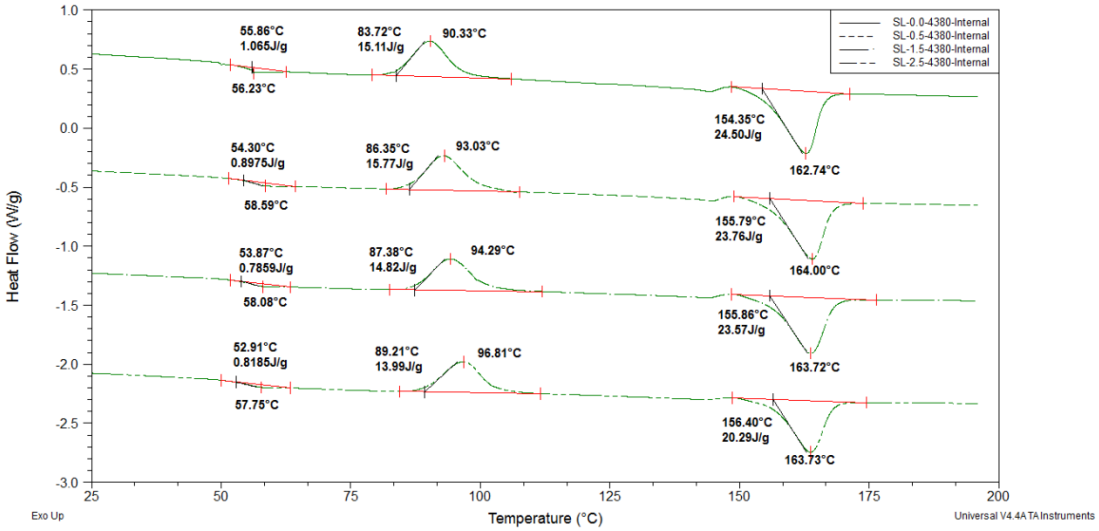

Figure 4.8 DSC thermographs of Solanyl® blend 30R with different contents of ADR 4380 CE

The glass transition temperature of the blend with 0.5 wt % CE was increased by only 3°C to 59°C compared to the neat blend. This result was not significantly different from the previously investigated CE (ADR 4370S, Section 4.2.1) with Solanyl® blend 30R, even the epoxy functionality of ADR 4380 CE was lower than ADR 4370S CE. However, further addition of CE did not change the glass transition temperature of the PLA significantly.

The melting peak of blend increased to 164°C, which was only 1°C higher compared to the neat blend regardless of CE concentration. These results were comparable with the previously investigated ADR 4370S CE (Section 4.2.1). The enthalpy of fusion progressively decreased to only 20 J/g as CE concentration increased to 2.5 wt %. The enthalpy of fusion comparatively higher than the modified blend with 2.0 wt % ADR 4370S CE (17 J/g, Section 4.2.1). This was expected as ADR 4380 have the low epoxy functionality compared to ADR 4370S. The crystalline content of the neat blend was less affected by the low epoxy functionality ADR 4380 CE and higher enthalpy of fusion was observed in the modified blend with ADR 4380 CE.

The peak re-crystallization temperature on heating progressively increased to 97°C as the CE content was increased to 2.5 wt %. From the obtained results, it seems that the rate of crystallization decreased in the presence of the CE and blend could crystallize at higher temperature. However, increased re-crystallization temperature was less pronounced in the blend with 2.5 wt % ADR 4380 CE compared to 2.0 wt % ADR 4370S (Section 4.2.1). It was believed that due to lower epoxy functionality of ADR

4380 compared to ADR 4370S, the chain linearity was less disrupted by branching of polymer chains by CE and consequently the blend could crystallize at a higher temperature. However, blend with 0.5 wt % CE developed small re-crystallization exotherm peak prior to the major melting endotherm peak in the heating cycle. As the CE content increased, the small exotherm peak remained at the same temperature and did not develop any secondary melting peak as it was developed in the blend with ADR 4370S (Section 4.2.1). This result may be due to lower epoxy functionality of ADR 4380 that did not develop any new crystalline morphology, which could melt at two different temperatures.

4.2.3 Solanyl® BLEND 30R and DGEBA

Typical DSC thermographs of blend with 0.0 wt %, 0.5 wt %, 1.5 wt % and 2.5 wt % of CE (DGEBA) are shown in Figure 4.9. The description of glass transition (Tg), a re-crystallization exotherm (Tch) and a melt endotherm (Tm) of neat blend was given in section 4.2.1.

The addition of 0.5 wt % CE in blend increased the glass transition temperature of the PLA phase from 56°C to 59°C. Higher glass transition temperature implied a hampered activity of PLA polymer chains and some extent of reaction between bi-functional epoxy DGEBA CE and reactive groups in blend, which can be further evidenced by intrinsic viscosity measurement in the following section (Section 5.2). Zhang et al. (2009) observed increased in glass transition by addition of glycidyl methacrylate (T-GMA) into PLA/PBET (70/30 wt %) blend. However, further addition of

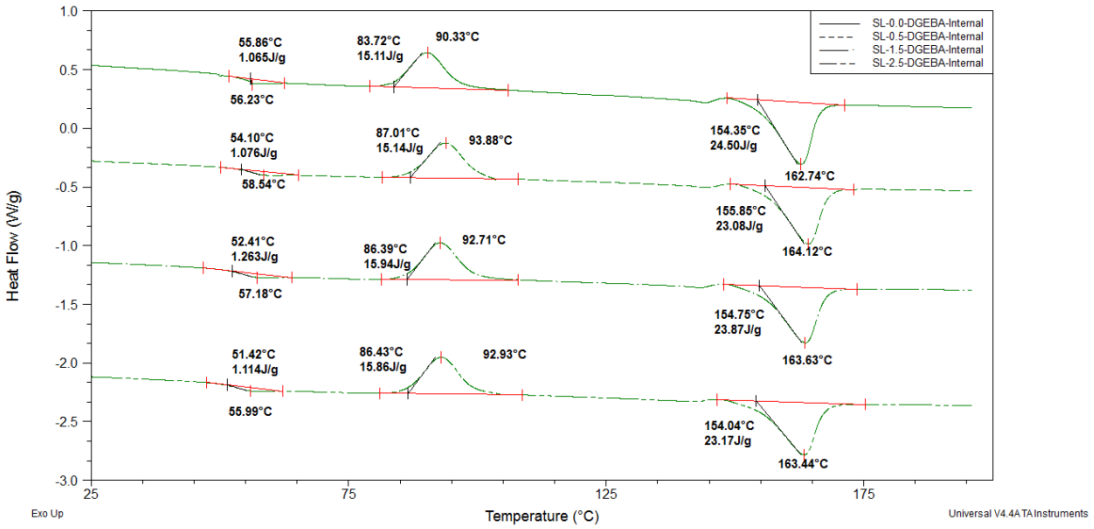

Figure 4.9 DSC thermographs of Solanyl® blend 30R with different contents of DGEBA CE

CE did not improve the glass transition and remained at same level as the neat blend in our work.

The addition of CE did not change the melting peak and melting enthalpy of the blends significantly. However, a small decrease in fusion enthalpy of 23 J/g compared to the neat blend (25 J/g) was the indication of some type of interaction between blend and bi-functional epoxy DGEBA CE, which created different crystalline morphology. The addition of CE increased the re-crystallization exotherm by 3°C compared to neat blend, which is also an indication of hampered crystallizability of the PLA chains. However, the re-crystallization enthalpy did not change significantly compared to the neat blend by increasing CE concentration.

4.2.4 SOLANYL® BLEND 30R AND PEG-DGE

Typical DSC thermographs of blend with 0.0 wt %, 0.5 wt % and 2.5 wt % of CE (poly (ethylene glycol) diglycidyl ether (PEG-DGE)) are shown in Figure 4.10. The description of glass transition (T_g), a re-crystallization exotherm (T_{ch}) and a melt endotherm (T_m) of neat blend was given in section 4.2.1.

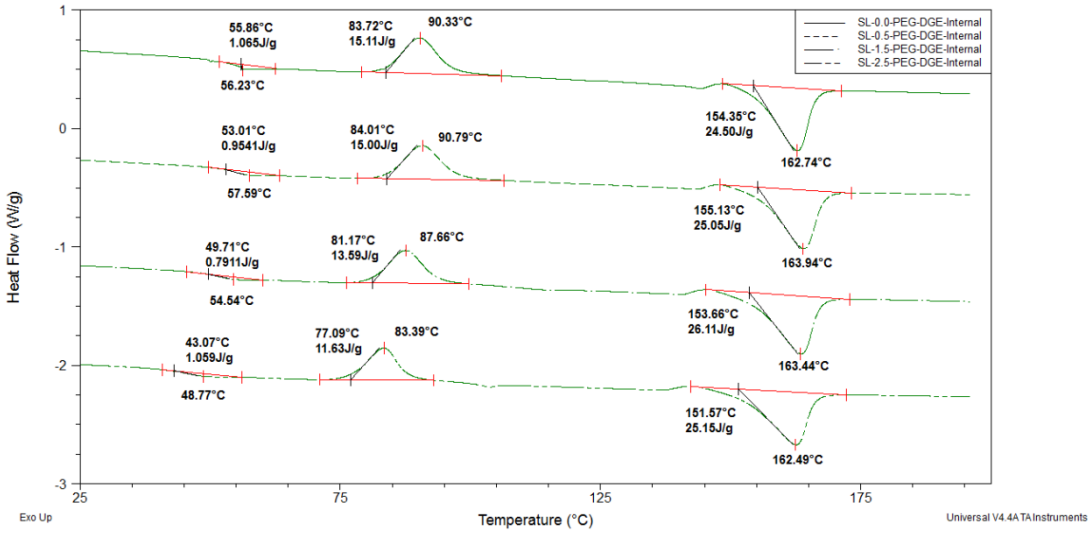

Figure 4.10 DSC thermographs of Solanyl® blend 30R with different contents of PEG-DGE CE

The addition of 0.5 wt % CE in blend increased the glass transition temperature of the PLA phase from 56°C to 58°C. Higher glass transition temperature implies a hampered activity of PLA polymer chains. However, the addition of more CE lowered the glass transition temperature to 49°C. It is possible that at higher contents of CE, this low molecular weight bi-functional PEG-DGE CE largely worked as a plasticizer in the blend and enhanced the segmental chains mobility of polymer chains, which in turn, decreased the glass transition temperature.

The addition of CE did not change the melting peak and melting enthalpy of the modified blends significantly. However, it decreased the re-crystallization exotherm by 7°C compared to neat blend for 2.5 wt % CE, which further reflect the enhanced crystallization of the PLA phase. Also, re-crystallization enthalpy progressively decreased to 12 J/g at 2.5 wt % CE is the indication of less crystallite was developed during heating cycle.

CHAPTER: 5

RESULTS AND DISCUSSION –

SCANNING ELECTRON MICROSCOPY (SEM) AND

INTRINSIC VISCOSITY

Our Differential Scanning Calorimetry (DSC) study concluded that the multi-functional epoxy CEs were effective in reducing crystalline content of blends by chain extension or branching reaction in neat blend with epoxy moieties of CE. As explained by Mihai et al. (2010), the chain extension reaction in polyesters increased the molecular weight of polymer chains by bridging the hydroxyl or carboxyl reactive end groups by using bi- or multi-functional chain extenders. There are a few studies targeted for

increasing molecular weight of PLA or glycerol plasticized TPS/PLA blend by using bi- or multi-functional epoxy CEs (Deenadayalan et al., 2009; Pilla et al., 2009; Mihai et al., 2010; Lie et al., 2011). To our knowledge, no one quantify the chain extension reaction in PLA and starch/PLA blends with bi- and multi-functional CEs. In our work, we employed the intrinsic viscosity technique to gain insight into which phase the chain extension reaction preferentially occurred.

The intrinsic viscosity can be related to the average molecular weight of linear polymers in a dilute (non-entangled) state by the Mark-Houwink relation:

$$[\eta] = KM^{a} \qquad 5.1$$

where, η= intrinsic viscosity (dL/g), M=molecular weight, "K" and "a" are constant that are specific to the particular solvent-solute pair and that is related to the shape of the solute molecule. For comparison of a modified resin relative to the neat material, one can assume these two constants are not significantly different allowing the change in intrinsic viscosity to be interpreted as a corresponding change in primary chain length. Table 5.1 presents the intrinsic viscosity values of the unprocessed pristine hydrolyzed starch, PLA 7000D and Solanyl® blend 30R components for reference only.

Table 5.1 Intrinsic viscosity values of the as-received Hydrolyzed starch, PLA 7000D and Solanyl® blend 30R components

Components Types	Intrinsic Viscosity (dL/g)	Solvent Used
Hydrolyzed Starch (Solanyl® 100 BP)	2.03 ± 0.08	DMSO
PLA 7000D	1.60 ± 0.03	Chloroform
Transparent PLA (Solanyl® blend 30R)	1.56 ± 0.01	Chloroform
Opaque PLA (Solanyl® blend 30R)	1.66 ± 0.05	Chloroform
AAC (Solanyl® blend 30R)	0.62 ± 0.04	Chloroform

5.1 BLEND MORPHOLOGY AND INTRINSIC VISCOSITY OF HYDROLYZED STARCH/PLA BLEND

The Scanning Electron Microscopy (SEM) was used to investigate the blend morphology of the neat blend and the blend modified with 2.0 wt % ADR 4370S CE. In SEM micrographs of its unfoamed neat blend and its modified material, the starch phase was selectively etched from the cross-section of a rectangular specimen which appeared as the dark holes in the micrographs (Figure 5.1 (a), (b)). As seen from the micrographs, a dispersed morphology occurred with discrete irregular shaped domains of starch present in the PLA matrix. For neat blend, very coarse morphology was observed with domain size of starch phase ranging from 20-150 µm (Figure 5.1 (a)). This phase separated morphology was obviously due to the poor adhesion and compatibility between the hydrophobic PLA and the hydrophilic starch molecules. The similar phase separated morphology reported by Martin and Averous (2001) for unmodified starch/PLA blend.

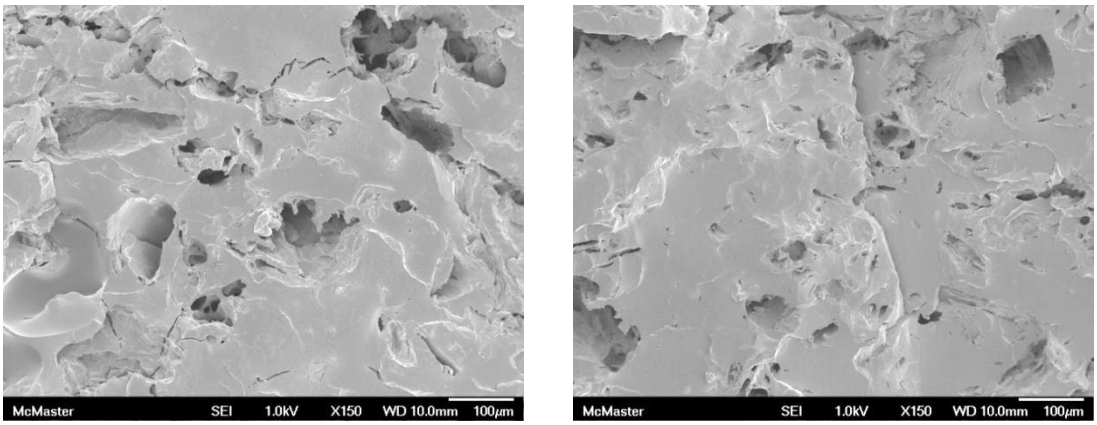

(a) SP-0.0-4370S-TSE (b) SP-2.0-4370S-TSE

Figure 5.1 Scanning Electron Micrographs of (a) neat hydrolyzed starch/PLA blend (b) the modified hydrolyzed starch/PLA blend with 2.0 wt % ADR 4370S CE

Addition of 2.0 wt % ADR 4370S CE did not change the blend morphology of the modified blend compared to the neat blend. The domain size was comparable ranging from 10 – 160 µm of the starch phase (Figure 5.1 (b)). Our morphology result on the modified blend with the multi-functional epoxy CE was also in agreement with one reported by Li et al. (2011) for the glycerol plasticized TPS/PLA blend with similar type of epoxy-styrene-acrylic multi-functional CE. Therefore, it was concluded that the presence of the multi-functional epoxy CE could not improve the blend's interface (i. e. grafting copolymer of PLA with starch amylose/amylopectin macromolecules) and did not sufficient alter the blend morphology during dispersive mixing.

Figure 5.2 presents the intrinsic viscosity measurement of the PLA phase for the modified hydrolyzed starch/PLA blend with different types and contents of CEs. The intrinsic viscosity measurements were done on the highest content of CE of each modified blend in TSE except for the modified blend with ADR 4370S and ADR 4380. The neat hydrolyzed starch/PLA blend processed in the TSE showed the low intrinsic viscosity of the PLA phase (1.45±0.03 dL/g) compared to unprocessed pristine PLA (1.60 ± 0.03 dL/g) (Table 5.1), which indicted some thermo-mechanical and/or hydrolytic degradation of the PLA phase had been occurred during extrusion. The addition of 0.5 wt % of ADR 4370 CE in the blend increased the intrinsic viscosity of the PLA phase to 1.62±0.02 dL/g. The increased in the intrinsic viscosity which is directly related to the increased in the molecular weight of PLA phase by equation 5.1 indicated that the chain extension reaction had been occurred between reactive groups on PLA chains and epoxy

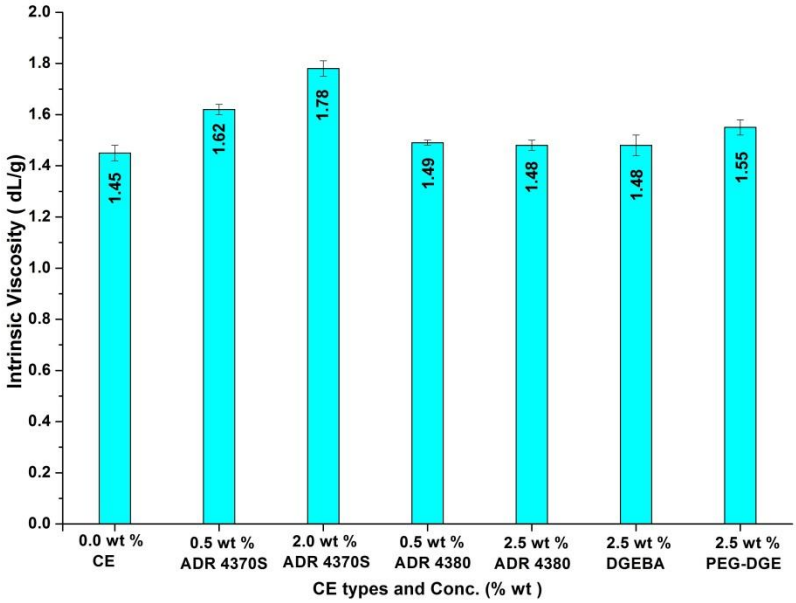

Figure 5.2 Effect of different types and contents of CEs on the intrinsic viscosity of the PLA phase for hydrolyzed starch/PLA blend

moieties of the CE. The presence of 0.5 wt % ADR 4370S CE in the neat blend compensated for the molecular weight loss of PLA phase during thermal processing. With increased CE content to 2.0 wt %, the intrinsic viscosity of the PLA phase increased to 1.78±0.03 dL/g, showing further reaction between the PLA chains and the epoxy moieties of the CE. From these results, it was concluded that the chain extension reaction between the reactive groups of the PLA chains and epoxy moieties of the CE were the major contributing factor in the increase in bulk melt viscosity for the modified blends with multi-functional ADR 4370S CE in a following section (Section 6.2.2).

The PLA phase of the modified blends with ADR 4380 CE at 0.5 wt % and 2.5 wt % concentrations did not show any significant change in the intrinsic viscosity, which

was comparable with the other CEs (DGEBA and PEG-DGE) at 2.5 wt % concentration levels (Figure 5.2). This finding suggested that the other CEs (ADR 4380, DGEBA and PEG-DGE) were not effective for increasing the molecular weight of the PLA phase in the corresponding modified blends. Also, the similar intrinsic viscosity of the PLA phase for the both modified blends with 0.5 wt % and 2.5 wt % ADR 4380 CE contents indicated that the presence of excess epoxy moieties of CE in modified blends did not further react with the reactive groups on the PLA chains. Consequently, the presence of unreacted low-molecular weight of ADR 4380 CE in the modified blends largely acted as a plasticizer and reduced the melt viscosity at higher CE concentration in a following section (Section 6.2.1). The low degree of chain extension in other modified blends with 2.5 wt % CEs (DGEBA and PEG-DGE) were also due to the plasticization or limited reactivity of the low-molecular weight bi-functional CE in the neat blend, which could hindered the chain extension reaction between PLA chains and epoxy moieties of the CEs.

We further extend our intrinsic viscosity study to the extracted hydrolyzed starch phase from the unmodified and modified blends with ADR 4370S CE only since this was the only blend to show a major change in the melt rheology. The neat hydrolyzed starch/PLA blend processed in the TSE showed significantly low intrinsic viscosity of the extracted starch phase (1.11±0.04 dL/g) compared to unprocessed pristine hydrolyzed starch (2.03 ± 0.08 dL/g) (Table 5.1). This indicated that the starch phase also suffered excessive degradation, with loss of molecular weight during thermal processing. The

same intrinsic viscosity reduction was observed in the extracted starch phase from the blends with 2.0 wt % ADR 4370S CE (1.10±0.01 dL/g). The result suggested that the epoxy reaction preferentially targeted the hydroxyl groups of PLA and the starch phase made no contribution to the increase melt viscosity noted in Chapter 6.

5.2 BLEND MORPHOLOGY AND INTRINSIC VISCOSITY OF SOLANYL® BLEND 30R

SEM micrographs were once again used to examine the blend morphology, in this case evaluating the neat commercial Solanyl® blend 30R and its modified blend with 2.0 wt % ADR 4370S CE. As seen from micrographs (Figure 5.3 (a) (b)), the PLA/AAC phase (neither polymer being extracted by 1N HCl) was observed as a continuous phase and starch as dispersed domains in the system. The neat Solanyl® blend 30R showed very coarse morphology with domain size of starch phase ranging from 25 – 220 µm (Figure 5.3 (a)). The same blend morphology was observed for the modified Solanyl® blend 30R

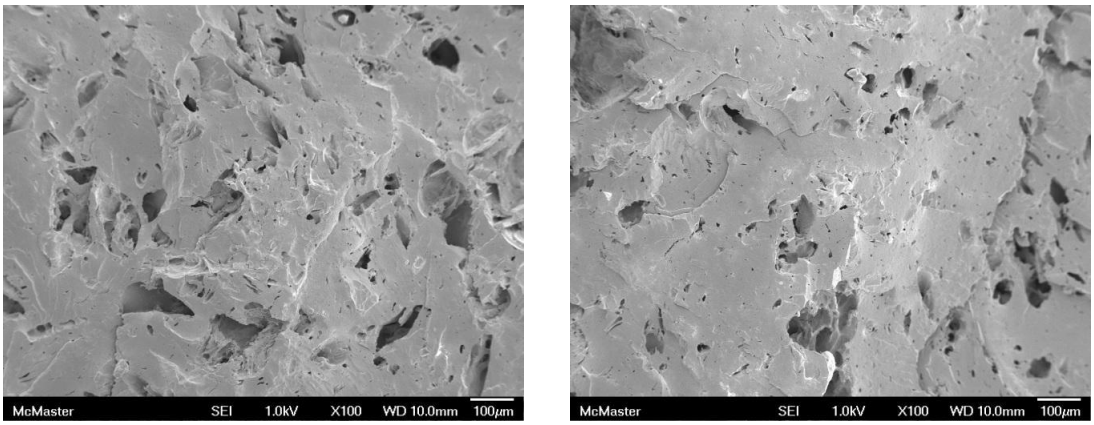

(a) SL-0.0-4370S-TSE (b) SL-2.0-4370S-TSE

Figure 5.3 Scanning Electron Micrographs of (a) neat Solanyl® blend 30R (b) the modified Solanyl® blend 30R with 2.0 wt % ADR 4370S CE

with 2.0 wt % ADR 4370S CE. The domain size was now found to be ranging from 25 – 150 µm of the starch phase (Figure 5.3 (b)). This indicated that the ADR 4370S CE did not worked as s compatibilizer for the Solanyl® blend 30R either.

Figure 5.4 presents the intrinsic viscosity measurement of the PLA/AAC phase for the modified Solanyl® blend 30R with different types and contents of CEs. The intrinsic viscosity measurements were done on the highest content of CE content of each modified blend in TSE except for the modified blend with ADR 4370S and ADR 4380. The similar trend of the intrinsic viscosity was also observed for the PLA/AAC phase of the neat and the modified Solanyl® blend 30R with different types and content of CEs compared to the intrinsic viscosity of the PLA phase of the neat and the modified

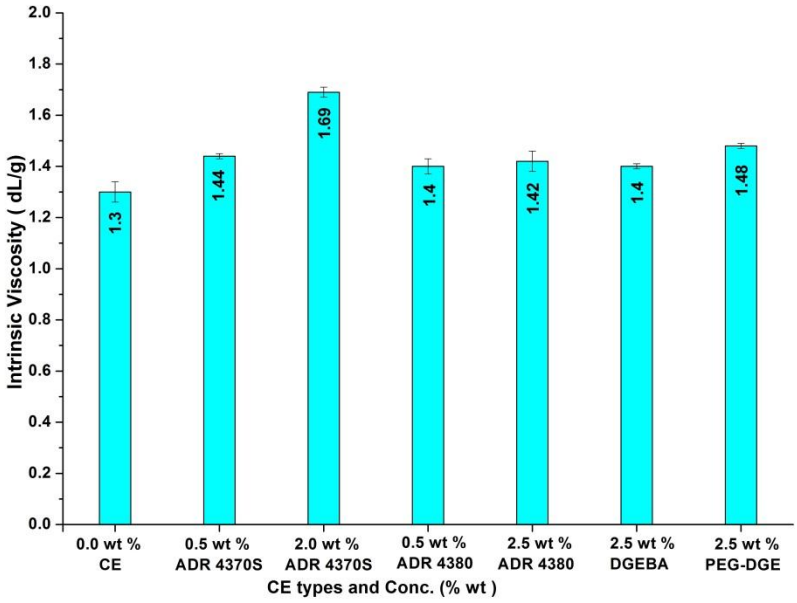

Figure 5.4 The effect of different types and contents of CEs on the intrinsic viscosity of the PLA/AAC phase for Solanyl® blend 30R

hydrolyzed starch/PLA blend (Figure 5.2). However, the low intrinsic viscosity of the PLA/AAC phase compared to the PLA phase of the modified hydrolyzed starch/PLA blend was due to the presence of the flexible AAC components in Solanyl® blend 30R. The low degree of chain extension in other modified blends with 2.5 wt % CEs (ADR 4380, DGEBA and PEG-DGE) was also observed due to the plasticization of the low-molecular weight CE in the neat blend at higher concentration (2.5 wt %), which could have hindered the chain extension reaction between PLA chains and epoxy moieties of the CEs. Consequently, it did not significantly contribute in increasing the melt viscosity of the corresponding modified blends either (Chapter 6).

The intrinsic viscosity measurement of the extracted starch phase for the neat Solanyl® blend 30R and its modified blend with ADR 4370S showed excessive starch degradation during thermal processing. The intrinsic viscosity of the extracted starch phase for the neat blend was 1.24±0.01 dL/g and for the modified blend with 2.0 wt % ADR 4370S was 1.19±0.02 dL/g. However, the intrinsic viscosity of the extracted starch phase of Solanyl® blend 30R was higher than that found for the hydrolyzed starch/PLA blend (Section 7.1) due to the presence of low viscosity AAC, which acted as a plasticizer during extrusion for the blend and lowered the shear stress on the natural polymer and lowered the starch degradation.

CHAPTER: 6

RESULTS AND DISCUSSION –

PARALLEL PLATE RHEOLOGY

Rheological measurement is a tool to evaluate the melt properties of the chain extended materials. Dynamic rheology provides information about the visco-elastic shear dependency and chain relaxation profile of polymer in the molten state.

6.1 RHEOLOGICAL PROPERTIES OF SOLANYL® BLEND 30R

Preliminary trials of processing Solanyl® blend 30R were done in an internal mixer. However, due to incomplete melting of partially hydrolyzed starch in those tests, the final practice adopted for the experiments required the neat blend be first processed in

the TSE and subsequently, the well mixed Solanyl® blend 30R modified by the different CEs within the internal mixer. Due to the two steps process, some extent of chain degradation due to thermal shearing and hydrolysis of PLA chains was anticipated within these trials (Wang et al., 2001). Initial rheological comparison of the original components of the Solanyl® blend 30R were not possible by parallel plate rheometer due to the intact hydrolyzed starch granules; such a measurement required plasticizer and high shear mixing action to gelatinized starch.

Typical frequency dependence of the complex viscosity (η*) of the neat blend processed in TSE and subsequently for 10 minutes in the internal mixer, are shown in Figure 6.1. The blend from the first stage in the TSE showed a higher η* at all frequencies level compared to the final blend processed in the second stage using the internal mixer; no CE was present in this comparison. The blend processed by TSE

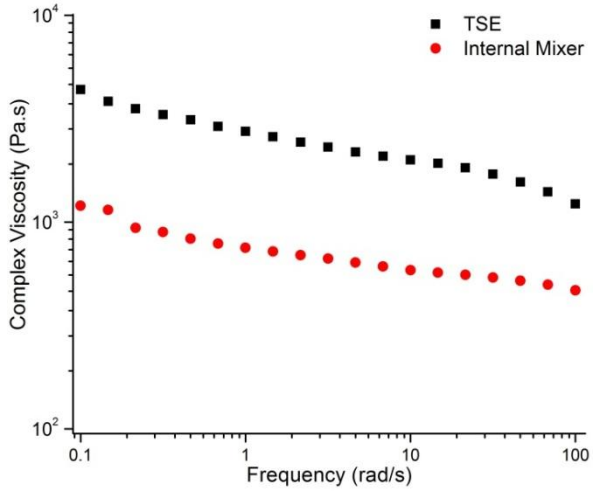

Figure 6.1 Frequency dependency of the complex viscosity (η*) of Solanyl® blend 30R after processed in the TSE and internal mixer for 10 min at 170°C
(Error for η*: TSE = 31.2% RSD and Internal Mixer = 5.3% RSD)

only showed a low frequency shear viscosity (η) (0.1 rad/s) = 4.4 kPa.s and non-Newtonian behaviour in the tested frequency range. In our work, blends processed in TSE were found to have suffered thermal and shear degradation, noted by intrinsic viscosity measurement in section 5.2. Li et al. (2011) obtained the plateau η*of 2.4 kPa.s and well defined Newtonian plateau for glycerol plasticized TPS/PLA blend. However, such a finding cannot be reconciled with blend with hydrolyzed starch without any plasticizers.

After Solanyl® blend 30R processed in TSE, the well mixed blend was further processed in an internal mixer for 10 min, setting the rheological baseline for subsequent comparison to the modified blend with CEs. The blend processed in the internal mixer exhibited lower viscosity, η (0.1 rad/s) = 1.2 kPa.s indicative of unzipping and chain scission reactions due to thermal hydrolysis in presence of moisture at higher temperature, and blend showed shear thinning tendency with increasing frequency. Mihai et al. (2010) who processed c-PLA in TSE found similar degradation, with the η of the extruded c-PLA reduced in half compared to unprocessed c-PLA pallets.

6.1.1 SOLANYL® BLEND 30R AND ADR 4380

The effect of CE (ADR 4380) addition on blend viscosity was evaluated on samples prepared in the internal mixer with different content of CE (Table 3.1). Figure 6.2 presents the complex viscosity (η*) as a function of frequency for blends with different content of CE. As discussed previously, the blend without CE showed η (0.1 rad/sec) = 1.2 kPa.s. The addition of 0.5 wt % CE did not show any significant increase in the η* at

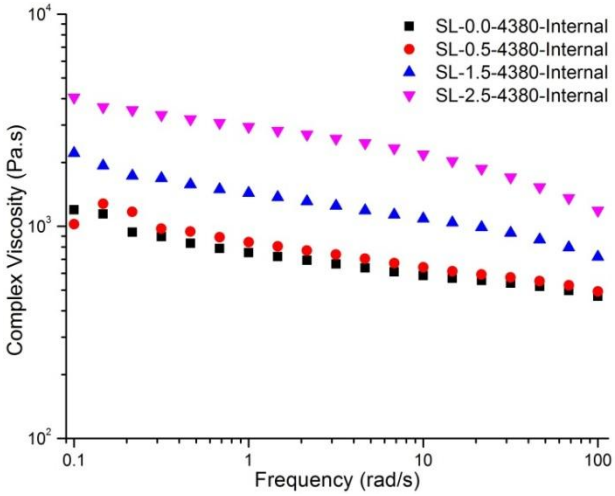

Figure 6.2 Frequency dependency of complex viscosity (η*) of Solanyl® blend 30R with different contents of ADR 4380 CE at 170°C
(Error for η*: SL-0.0-4380-Internal = 5.3% RSD, SL-0.5-4380-Internal = 4.5% RSD, SL-1.5-4380-Internal = 6.3% RSD, SL-2.5-4380-Internal = 3.7%RSD)

all frequencies compared to the neat blend, which may be due to the lower epoxy functionality of the ADR 4380 CE.

The addition of 1.5 wt % CE had a significant influence on the η* and η (0.1 rad/s) increased to 2.2 kPa.s for the modified Solanyl® blend. The modified blend also showed more shear thinning behaviour at higher frequency (> 25 rad/s). Di et al. (2005) stated that linear polymer should exhibit typical Newtonian behaviour in the low frequency region and shear thinning behaviour in the high frequency region. Conversely, strong shear thinning behaviour over most frequencies is typical for cross-linked or branched polymers. Our results were consistent with Sungsanit et al. (2010), who compared the rheological properties of the linear and branched PLA at 180°C. Branched PLA exhibited higher η* and stronger shear thinning behaviour at all frequencies

compared to the linear material. As a result, the stated conclusion from this analysis was that ADR 4380 produced more complex molecular structures in our blend, either branching or chain extension, though this analysis does not distinguish in which phase.

The further addition of 2.5 wt % CE, the η (0.1 rad/sec) increased to 4.1 kPa.s and shear thinning behaviour now spanned more of the frequency range (> 10 rad/s). The blend rheology continued to be influenced by the addition of more CE. Our results were consistent with Li et al. (2011), who observed similar increases in the η* compared to their neat glycerol plasticized TPS/PLA blend by the addition of similar type of epoxy-styrene-acrylic multi-functional CE (CESA-Extend OMAN698493).

Unfortunately, the effect of CE contents on the storage moduli (G') and loss moduli (G") of a starch/PLA blend was not reported by any other researchers, making comparison of the following rheological data to the literature impossible. G' and G" are used to characterize the viscoelastic properties of polymer melts (Dealy and Wissbrun, 1989). G' and G" are sensitive to the melt elasticity and viscosity of a polymer network respectively. The storage moduli (G') and loss moduli (G") of the blend with different contents of CE are shown in Figure 6.3. The G' lies below the G" curve for neat blend (i.e. G" > G') at all frequencies indicating a dominant viscous deformation response at the analysis temperature (170^{o}C). The blend with CE have higher G' and G" at all frequencies compared to the neat blend. This trends of G" > G' was observed for all modified Solanyl® blend with CE. However, the change in G' and G" were not pronounced in the modified blend with different levels of CE, which indicated a less stiff structure of the

modified blends due to the low epoxy functionality of the CE. As explained by Dealy and Wissbrun (1989), the dominance of melt elasticity over the viscous counterpart indicated the formation of a more rigid structure in the polymer matrix due to branching or cross-linking often referred to G'-G" cross-over, which was not observed with currently investigated CE within the tested frequencies range.

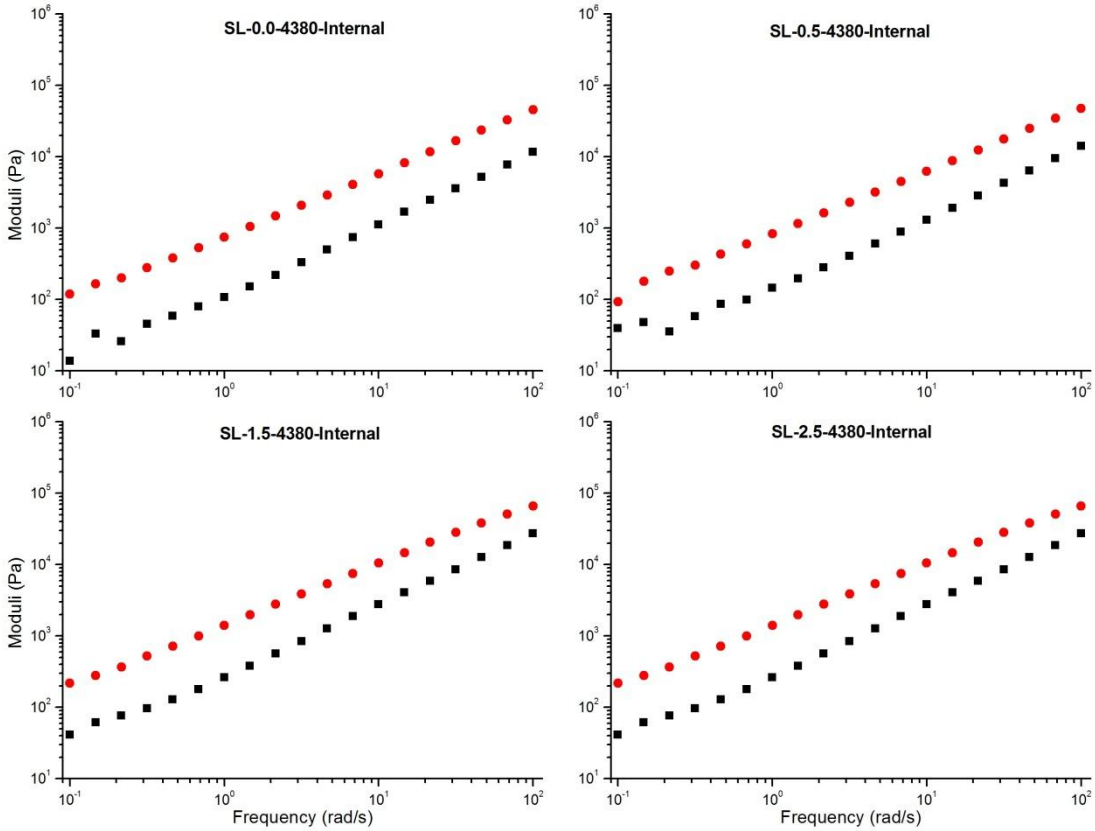

Figure 6.3 Frequency dependency of storage moduli G' (■) and loss moduli G" (●) of Solanyl® blend 30R with different contents of ADR 4380 CE at 170°C (Error for G' and G": SL-0.0-4380-Internal = 13.1% RSD and 5.4% RSD, SL-0.5-4380-Internal = 12.2% RSD and 4.5% RSD, SL-1.5-4380-Internal = 6.4% RSD and 6.3% RSD, SL-2.5-4380-Internal = 4.4% RSD and 3.6% RSD)

6.1.2 SOLANYL® 30R BLEND WITH ADR 4370S

The effect of CE (ADR 4370S) addition on blend viscosity was evaluated on samples prepared in the internal mixer with different content of CE (Table 3.1). Figure 6.4 presents the complex viscosity (η*) as a function of frequency for blend with different content of CE. The addition of CE resulted in much higher η* at nearly all frequencies. After addition of 0.5 wt % CE, the η (0.1 rad/s) increased to almost 7.5 kPa.s and enhanced the shear thinning tendency of the blend. The blend rheology was highly influenced by the presence of only 0.5 wt % CE and the significant change in the η* compared to modified blend with ADR 4380 (Section 6.1.1) was due to higher epoxy functionality of ADR 4370S compared to ADR 4380 CE.

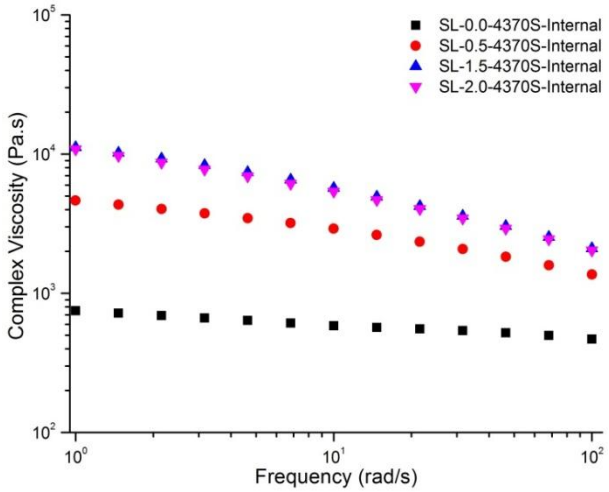

Figure 6.4 Frequency dependency of the complex viscosity (η*) of Solanyl® blend 30R with different contents of ADR 4370S CE at 170°C
(Error for η*: SL-0.0-4370S-Internal = 5.3% RSD, SL-0.5-4370S-Internal = 5.6% RSD,SL-1.5-4370S-Internal = 1.6% RSD, SL-2.0-4370S-Internal = 2.8% RSD)

Moreover, the addition of 1.5 wt % CE in blend increased the η (0.1 rad/s) to 19 kPa.s, which was significantly higher than the modified Solanyl® blend with 1.5 wt % ADR 4380 CE (η (0.1 rad/s) = 2.2 kPa.s). This indicated a higher extent of chemical reaction between the reactive groups had occurred in the blend with the epoxy moieties of the CE. However, further increasing CE content to 2.0 wt %, the η* did not change. This suggested that a threshold of CE concentration was reached and no more reactive groups were available in blends to further react with the epoxy moieties of the excess CE. A similar threshold value of 1.4 wt % was reported by Mihai et al. (2010), who blended PLA with a similar type of epoxy-styrene-acrylic multi-functional CE (CESA-Extend OMAN698493). Even though, they used only neat PLA and we used the Solanyl® blend, the threshold value was similar for both systems – not surprising as our results from intrinsic viscosity suggested that the majority of CE reacted with the PLA phase (Section 5.2). As a consequence of this threshold, the addition of more CE was determined to be completely ineffective in further improving the melt viscosity. Excess concentrations of the low-molecular weight CE were feared to plasticize the polymer matrix and obscured any effects of branching that had occurred. Therefore, the 2.0 wt % concentration level was considered for ADR 4370S, differing from all other CE studied.

The storage moduli (G') and loss moduli (G") of the blend with different contents of CE are shown in Figure 6.5. The G' lies below the G" curve for neat blend (i.e. G" > G') at all frequencies indicating a dominant viscous deformation response at the analysis temperature (170°C). Blend with 0.5 wt % CE showed higher G' and G" compared to neat

blend at all frequencies. Similar, increased in G' and G" was observed by Sungsanit et al. (2010) in branched PLA compared to neat liner PLA. For blend with 1.5 wt % and 2.0 wt % CE, G' actually increased above G" at higher frequency (~ 100 rad/s). The increased in G' above G" (G'-G" cross-over) reflects the dominance of melt elasticity of blends and formation of a more rigid structure in the blends, presumable from branching and chain extension by the CE. The similar G'-G" cross-over did not observe in the modified blends

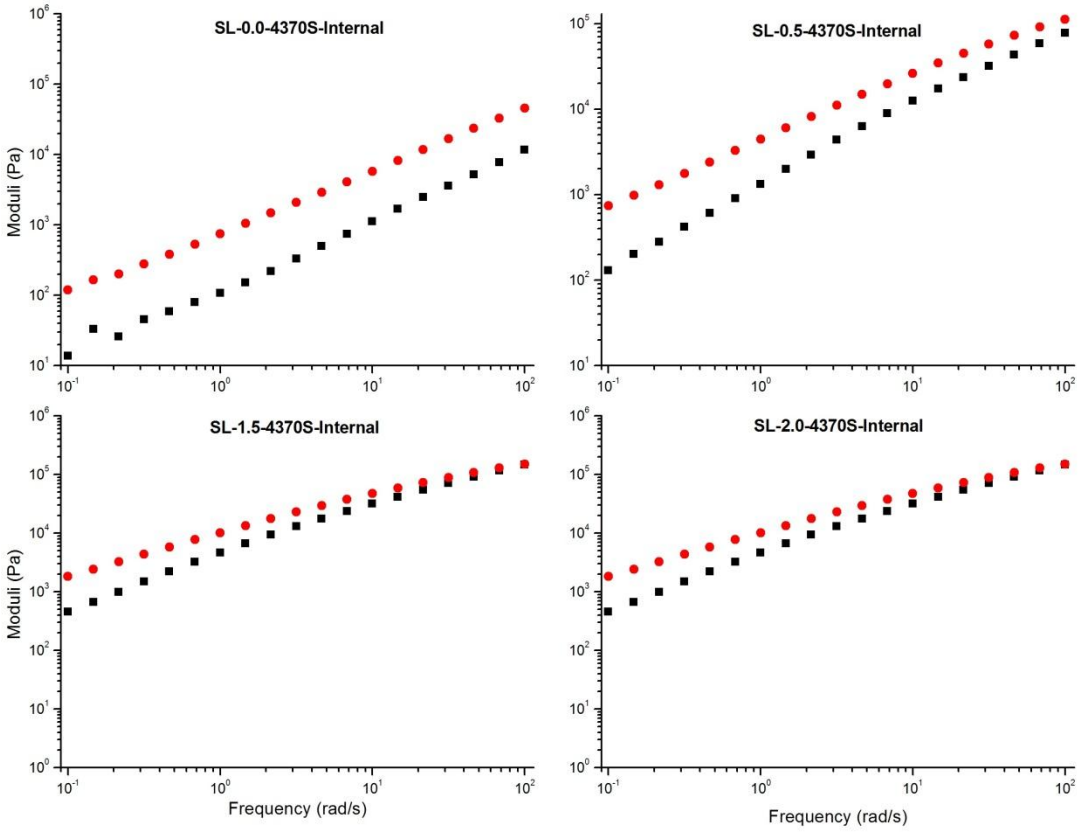

Figure 6.5 Frequency dependency of storage moduli G' (■) and loss moduli G" (●) of Solanyl® blend 30R with different contents of ADR 4370S CE at 170°C (Error for G' and G": SL-0.0-4370S-Internal = 13.1% RSD and 5.4% RSD, SL-0.5-4370S-Internal = 7.7% RSD and 5.5% RSD, SL-1.5-4370S-Internal = 2.2% RSD and 1.5% RSD, SL-2.0-4370S-Internal = 3.1% RSD and 2.8% RSD)

with ADR 4380 CE (Section 6.1.1) indicating low epoxy functionality of the ADR 4380 CE did not create more rigid structure in the modified blends.

6.1.3 SOLANYL® 30R BLEND WITH DGEBA

The effect of CE (DGEBA) addition on blend viscosity was evaluated on samples prepared in the internal mixer with different content of CE (Table 3.1). Figure 6.6 presents the complex viscosity (η*) as a function of frequency for blend with different content of CE. The addition of bi-functional epoxy CE did not improve η* of the blend as compared to other two previously investigated multifunctional CEs (Section 6.1.1for ADR 4380 and Section 6.1.2 for ADR 4370S). The addition of the bi-functional CE showed a linear decreasing trend of η* with some noisy effect at very low frequency range. The addition of 0.5 wt % and 1.5 wt % CE in blend lowered the η* at all

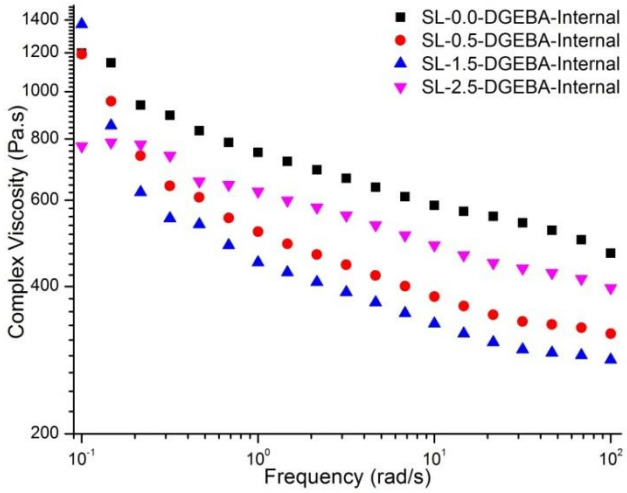

Figure 6.6 Frequency dependency of complex viscosity (η*) of blend with different contents of DGEBA CE at 170°C
(Error for η*: SL-0.0-DGEBA-Internal = 5.3% RSD, SL-0.5-DGEBA-Internal = 5.6% RSD,SL-1.5-DGEBA-Internal = 5.1% RSD, SL-2.0-DGEBA-Internal = 5.8% RSD)

frequencies and increased shear thinning behaviour, suggesting plasticization rather than chain extension of the matrix. The addition of 2.5 wt % CE showed some change in the η* of the blend compared to the blend with 0.5 wt % and 1.5 wt % CE which indicated the chain extension phenomena was beginning to dominate over the plasticization effect.

The storage moduli (G') and loss moduli (G") of the blend with different contents of CE are shown in Figure 6.7. The addition of bi-functional CE did not have any significant influence on the values of G' and G" compared to the neat blend. However, the G' was decreased as the initial concentration of CE increased to 1.5 wt % and then again increased as concentration of CE increased to 2.5 wt %. The same trend was observed for G" as well. This supported our previous argument on dominating chain extension over the plasticization effect at 2.5 wt % CE concentration.

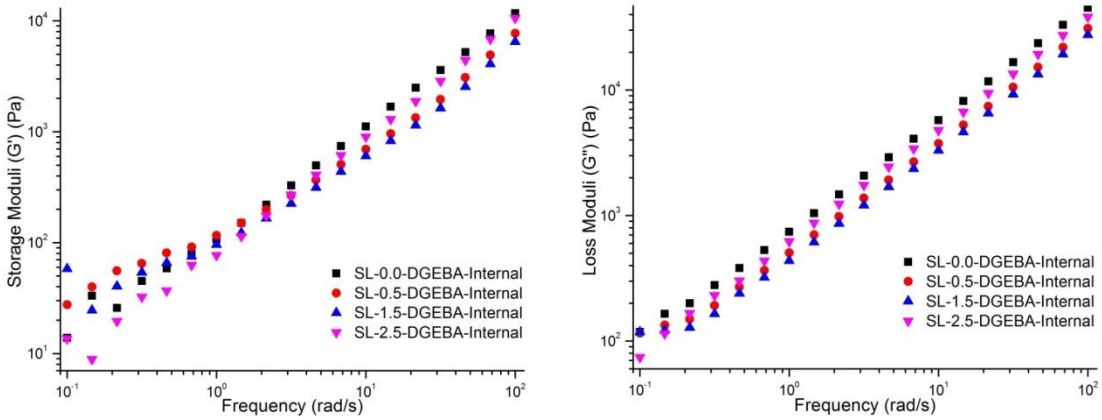

Figure 6.7 Frequency dependency of storage moduli (G') and loss moduli (G") of Solanyl® blend 30R with different contents of DGEBA CE at 170°C (Error for G' and G": SL-0.0-DGEBA-Internal = 13.1% RSD and 5.4% RSD, SL-0.5-DGEBA-Internal = 8.2% RSD and 5.8% RSD, SL-1.5-DGEBA-Internal = 11.1% RSD and 6.2% RSD, SL-2.5-DGEBA-Internal = 7.5% RSD and 3.0% RSD)

6.1.4 SOLANYL® 30R BLEND WITH PEG-DGE

The effect of CE (PEG-DGE) addition on blend viscosity was evaluated on samples prepared in the internal mixer with different content of CE (Table 3.1). Figure 6.8 presents the complex viscosity (η*) as a function of frequency for blend with different content of CE. Overall, little improvement was observed in η* of blends with the addition of this bi-functional epoxy CE. The viscosity increased rather than decreased as seen with DGEBA, but the change was certainly not so significant as compared to other two previously investigated multifunctional CEs (Section 6.1.1 for ADR 4380 and Section 6.1.2 for ADR 4370S). The addition of 0.5 wt % CE showed little increased in η* compared to the neat blend at nearly all frequency range, which showed some chain extension reaction, noted by intrinsic viscosity measurement in section 5.2. However,

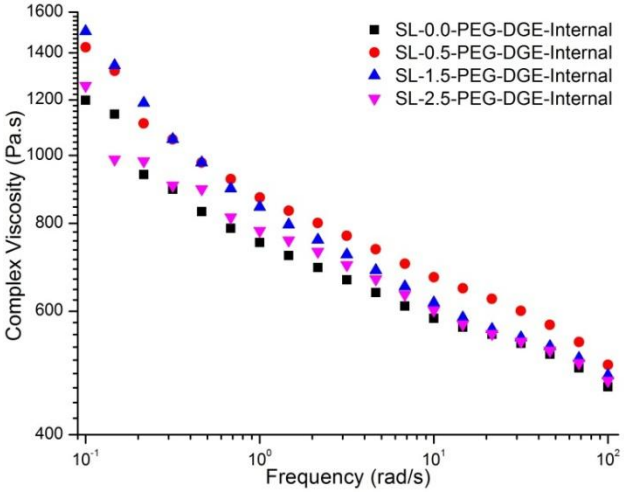

Figure 6.8 Frequency dependency of complex viscosity (η*) of Solanyl® blend 30R with different contents of PEG-DGE CE at 170°C
(Error for η* : SL-0.0-PEG-DGE-Internal = 5.3% RSD, SL-0.5-PEG-DGE-Internal = 11.5% RSD, SL-1.5-PEG-DGE-Internal = 5.9% RSD, SL-2.5-PEG-DGE-Internal = 5.5% RSD)

the addition of 1.5 wt % and 2.5 wt % CE showed lower η* compared to blend with 0.5 wt % CE, which indicated that plasticization effect was beginning to dominant over the chain extension at higher contents of CE.

The storage moduli (G') and loss moduli (G") of the blend with different contents of CE are shown in Figure 6.9. Overall, no significant change in G' and G" was observed with different contents of this bi-functional CE.

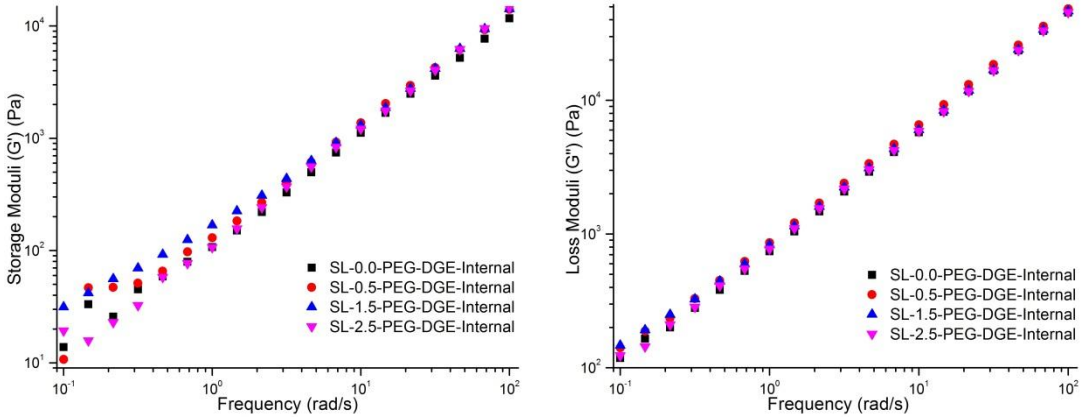

Figure 6.9 Frequency dependency of storage moduli (G') and loss moduli (G") of Solanyl® blend 30R with different contents of PEG-DGE CE at 170°C
(Error for G' and G": SL-0.0-PEG-DGE-Internal = 13.1% RSD and 5.4% RSD,
SL-0.5-PEG-DGE-Internal = 12.0% RSD and 11.6% RSD,
SL-1.5-PEG-DGE-Internal = 7.72% RSD and 6.04% RSD,
SL-2.5-PEG-DGE-Internal = 10.94% RSD and 5.62% RSD)

6.2 RHEOLOGICAL PROPERTIES OF HYDROLYZED STARCH/PLA BLEND

The Solanyl® blend 30R was processed in a two-step process but that blend contained an aliphatic-aromatic copolymer (AAC) which was very flexible and had a low viscosity at 170°C, which worked as an internal plasticizer for Solanyl® blend 30R.

Therefore, its polymer chains were partially protected from mechanical degradation. When the same processing trials were done on the hydrolyzed starch/PLA blend, excessive degradation of the hydrolyzed starch occurred due to the absence of any plasticizers if two-step procedure was followed. Therefore, the modification of hydrolyzed starch/PLA blends was done directly in the TSE to minimize the mechanical degradation.

6.2.1 HYDROLYZED SATRCH/PLA BLEND AND ADR 4380

The effect of CE (ADR 4380) addition on blend viscosity was evaluated on samples prepared in the TSE with different content of CE (Table 3.2). The effect of CE (ADR 4380) contents on the complex viscosity (η*) as a function of frequency for the samples prepared in the TSE are presented in Figure 6.10. The blend without CE processed in TSE showed the η (0.1 rad/s) of 7.2 kPa.s, which was much higher than the Solanyl® blend 30R processed only in the TSE (4.4 kPa.s, Section 6.1). The presence of aliphatic-aromatic copolyester (AAC) used in Solanyl® blend 30R significantly reduced the blend viscosity as compared to the neat hydrolyzed starch/PLA blend. The neat blend showed non-Newtonian behaviour in the tested frequency range with shear thinning for frequencies greater than 10 rad/s. However, Li et al. (2011) also observed plateau viscosity of 2.4 kPa.s at low frequency and shear-thinning behaviour at higher frequency for glycerol plasticized TPS/PLA blend. Addition of 0.5 wt % CE in the blend increased the η (0.1 rad/s) to 30 kPa.s., which was higher η* and relatively more shear thinning

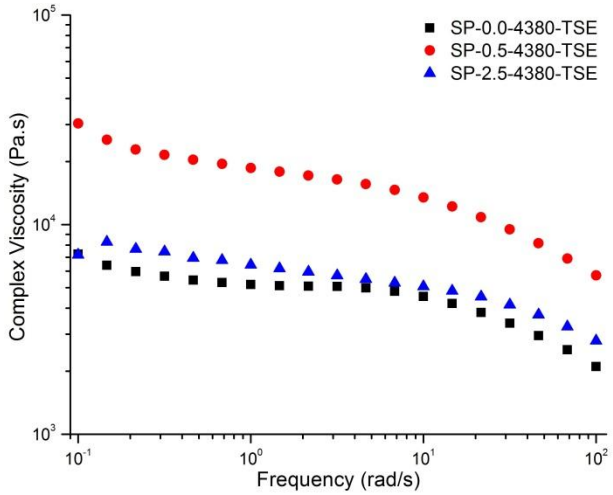

Figure 6.10 Frequency dependency of complex viscosity (η*) of hydrolyzed starch/PLA blend with different contents of ADR 4380 CE at 170°C (Error for η* : SP-0.0-4380-TSE = 2.9% RSD, SP-0.5-4370S-TSE = 3.2% RSD, SP-2.5-4380-TSE = 5.3% RSD)

behaviour compared to the neat blend, which indicated the formation of branched structure in the presence of CE. This significant change in the η* was once again due to the reaction between reactive groups in the blend with the epoxy moieties of the CE. Further addition of 2.5 wt % CE to the blend did not show any improvement in the η* compared to the blend. The relative similar η* was obtained may be due to dominance of plasticization over the chain extension.

The storage moduli (G') and loss moduli (G") of the blend with different contents of CE are shown in Figure 6.11. The moduli of the neat blend showed strong frequency dependency, which indicated the characteristic of un-branched melts. The blends with CE have higher G' and G" at all frequencies compared to the neat blend. Also, G' and G" were became less shear sensitive after addition of CE, which showed the formation of a

strong branched structure. The blend with 0.5 wt % CE showed dominance of melt elasticity over the melt viscosity at frequency higher than ~100 rad/s, which represent the formation of branched structure in blend by reaction with epoxy moieties of CE. However, further addition of 2.0 wt % CE did not show any improvement in G' and G".

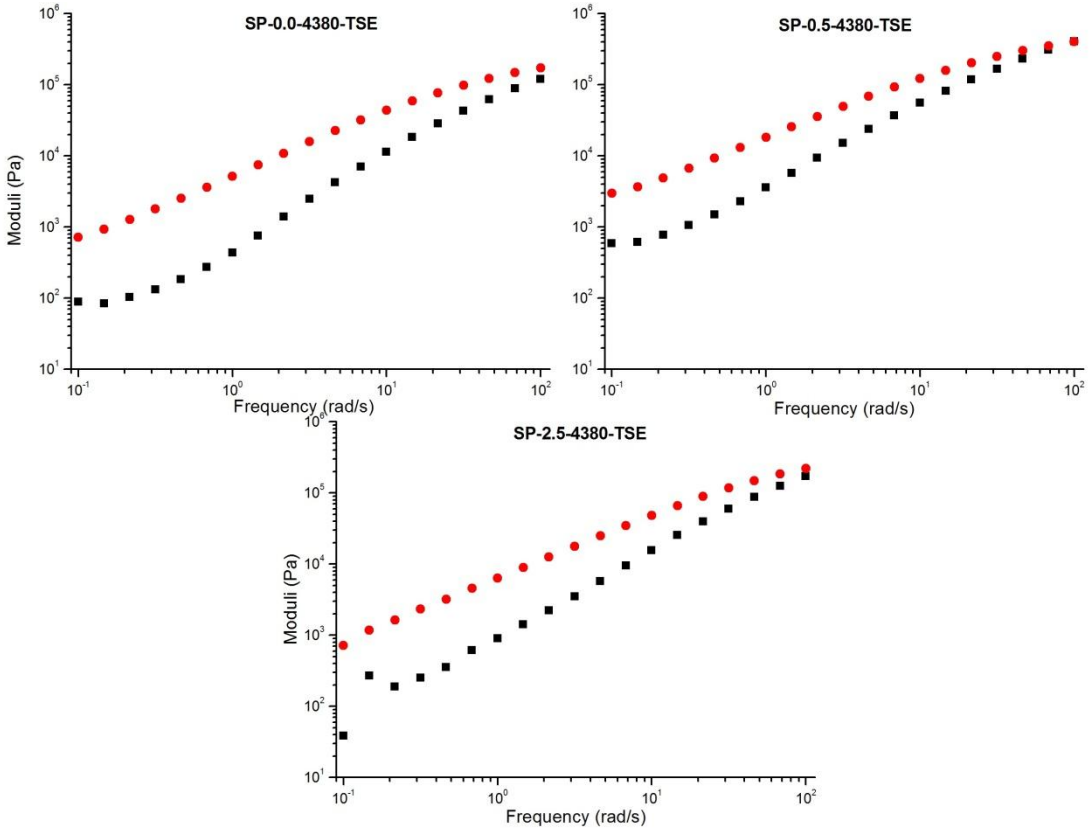

Figure 6.11 Frequency dependency of storage moduli G' (■) and loss moduli G" (●) of hydrolyzed starch/PLA blend with different contents of ADR 4380 CE at 170°C (Error for G' and G" : SP-0.0-4380-TSE = 4.1% RSD and 3.0% RSD , SP-0.5-4380-TSE = 6.6% RSD and 3.1% RSD, SP-2.5-4380-TSE = 5.5% RSD and 5.4% RSD)

6.2.2 HYDROLYZED SATRCH/PLA BLEND AND ADR 4370S

The effect of CE (ADR 4370S) addition on blend viscosity was evaluated on samples prepared in the TSE with different content of CE (Table 3.2).The effect of CE (ADR 4370S) contents on the complex viscosity (η*) as a function of frequency for the samples prepared in the TSE are presented in Figure 6.12. The addition of 0.5 wt % CE increased the η (0.1 rad/s) to 69 kPa.s, which was a tenfold increase compared to the neat blend. The viscosity continued to increase as CE content was increased to 2.0 wt % and η (0.1 rad/s) = 154 kPa.s. Equally important, the addition of 2.0 wt % CE in the blend exhibited more shear thinning behaviour compared to neat and blend with 0.5 wt % CE. This led to the η* being below that of the blend with 0.5 wt % CE for higher oscillation frequencies (about 15 rad/s). This significant change in viscosity was due to the reaction

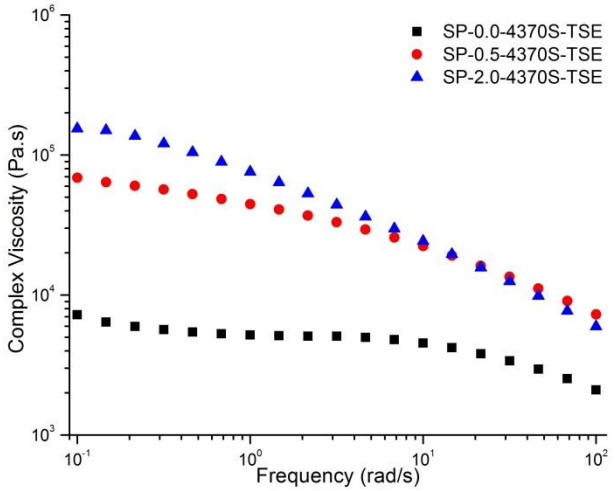

Figure 6.12 Frequency dependency of complex viscosity (η*) of hydrolyzed starch/PLA blend with different contents of ADR 4370S CE at 170°C
(Error for η*: SP-0.0-4370S-TSE = 2.9% RSD, SP-0.5-4370S-TSE = 8.5% RSD, SP-2.0-4370S-TSE = 70.3% RSD)

between reactive groups in blend with epoxy moieties of the CE.

The storage moduli (G') and loss moduli (G") of the blend with different content of CE are shown in Figure 6.13. The blend with CE showed higher G' and G" at all frequencies compared to neat blend, which revealing a branched or cross-linked structure formation. The dominance of melt elasticity over the viscous counterpart at oscillation frequency higher than 35 rad/s, reflected the formation of a rigid elastic structure in the

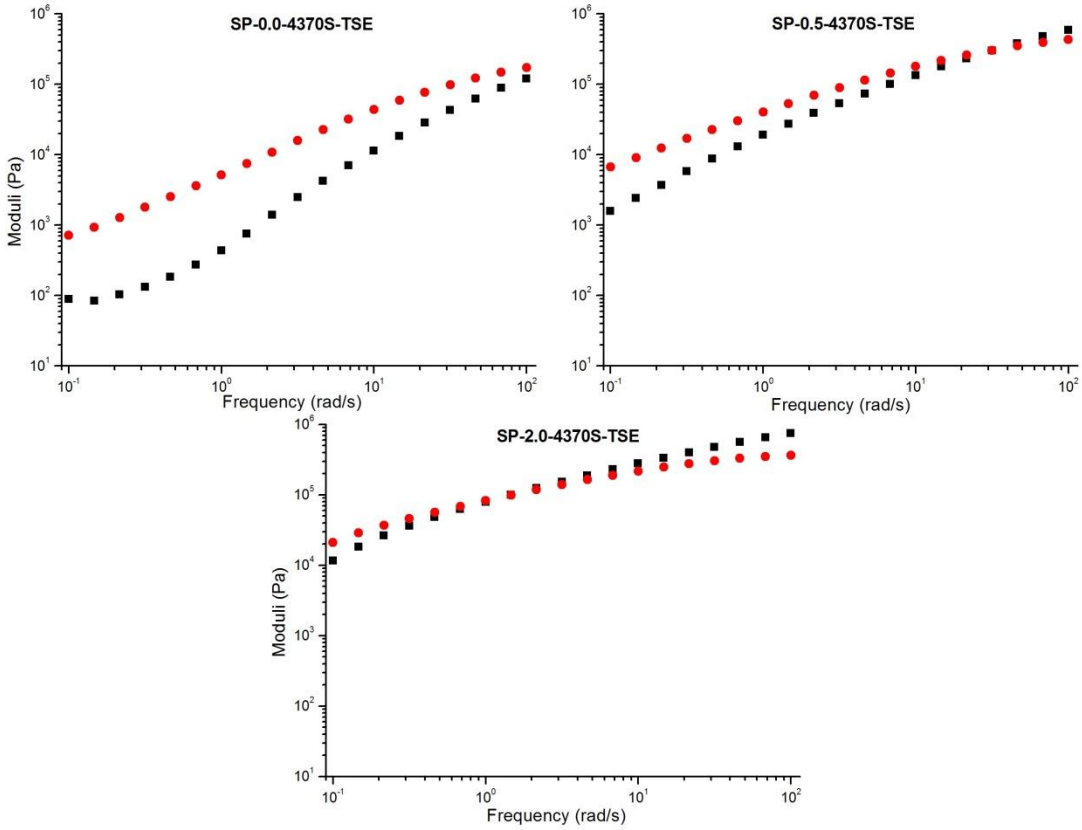

Figure 6.13 Frequency dependency of storage moduli G' (■) and loss moduli G" (●) of hydrolyzed starch/PLA blend with different contents of ADR 4370S CE at 170°C (Error for G' and G" : SP-0.0-4370S-TSE = 4.1 % RSD and 3.0% RSD, SP-0.5-4370S-TSE = 11.1% RSD and 7.9% RSD, SP-2.0-4370S-TSE = 10.1% RSD and 8.2% RSD)

blend. Further addition of CE to 2.0 wt %, the G' - G" cross-over pushed to lower oscillation frequency (~1.5 rad/s), which indicated the formation of a more rigid like structure in the blend due to presence of higher percentage of CE.

6.2.3 HYDROLYZED SATRCH/PLA BLEND AND DGEBA

The effect of CE (DGEBA) addition on blend viscosity was evaluated on samples prepared in the TSE with different content of CE (Table 3.2).The effect of CE (DGEBA) contents on the complex viscosity (η*) as a function of frequency for the samples prepared in the TSE are presented in Figure 6.14. The addition of CE did not improve the η* of the blend much as compared to other two previously investigated multifunctional epoxy CEs (Section 6.2.1 for ADR 4380 and Section 6.2.2 for ADR 4370S).

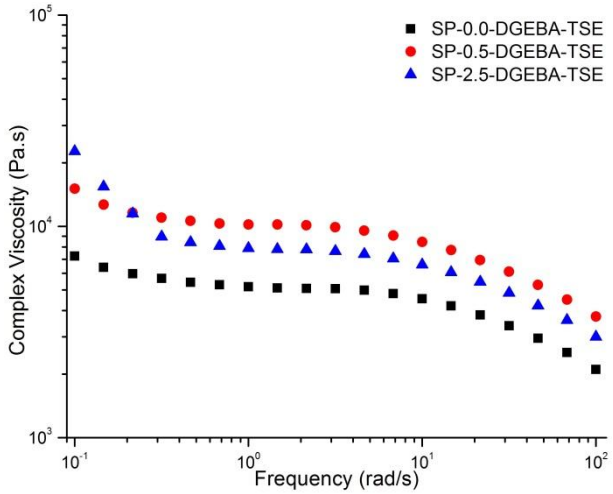

Figure 6.14 Frequency dependency of complex viscosity (η*) of hydrolyzed starch/PLA blend with different contents of DGEBA CE at 170°C
(Error for η*: SP-0.0-DGEBA-TSE = 2.9% RSD,
SP-0.5-DGEBA-TSE = 7.8% RSD, SP-2.0-DGEBA-TSE = 8.3% RSD)

The addition of 0.5 wt % CE in the blend increased the η (0.1 rad/s) to 11 kPa.s compared to the neat blend (7.2 kPa.s) and higher η* at all measures frequency range, suggesting the chain extension mechanism was prevalent in the blend with 0.5 wt % CE. The addition of 2.5 wt % CE increased the η* and remained low as compared to blend with 0.5 wt % CE. This showed a plasticization effect is dominant over chain extension in the modified blend. However, blend with CE showed almost the same shear thinning behaviour compared to neat blend at both levels of CE.

The storage moduli (G') and loss moduli (G") of the blend with different content of CE are shown in Figure 6.15. The addition of 0.5 wt % CE increased the G' and G" compared to neat blend. However, at 2.5 wt % of CE the values of G' and G" was less compared to the blend with 0.5 wt % CE, which showed plasticization effect was dominant over the chain extension in the blend.

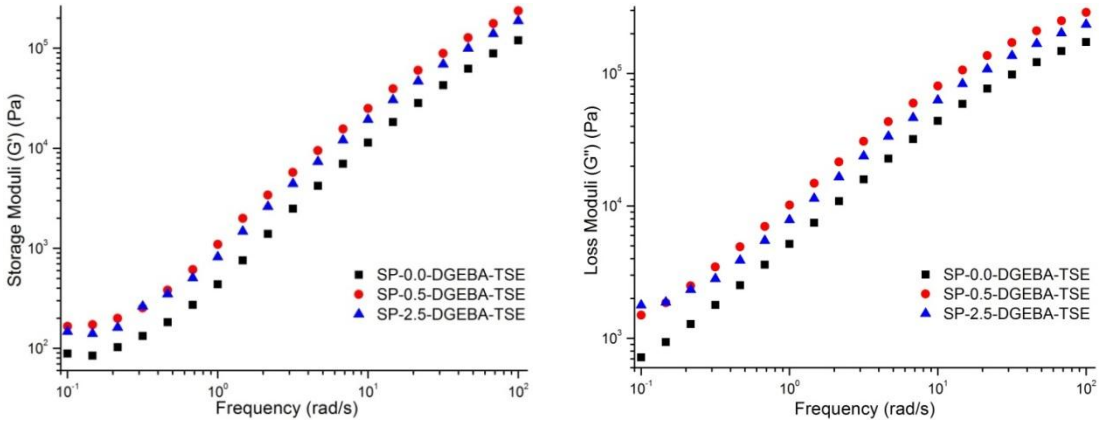

Figure 6.15 Frequency dependency of storage moduli (G') and loss moduli (G") of hydrolyzed starch/PLA blend with different contents of DGEBA CE at 170°C (Error for G' and G": SP-0.0-4380-TSE = 4.1% RSD and 3.0% RSD, SP-0.5-4380-TSE = 9.0% RSD and 7.7% RSD, SP-2.5-4380-TSE = 13.5% RSD and 14.8% RSD)

6.2.4 HYDROLYZED SATRCH/PLA BLEND AND PEG-DGE

The effect of CE (PEG-DGE) addition on blend viscosity was evaluated on samples prepared in the TSE with different content of CE (Table 3.2). The effect of CE (PEG-DGE) contents on the complex viscosity (η*) as a function of frequency for the samples prepared in the TSE are presented in Figure 6.16. The storage moduli (G') and loss moduli (G") of the blends with different contents of CE are shown in Figure 6.17. Almost the same behaviour for η*, G' and G" were observed compared blend with DGEBA CE (Section 6.2.3).

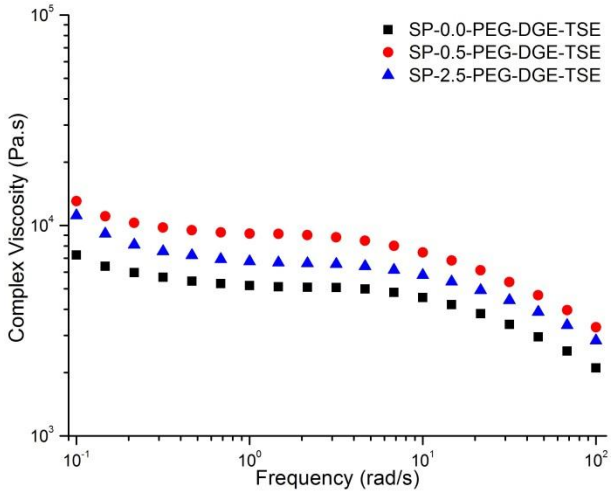

Figure 6.16 Frequency dependency of complex viscosity (η*) of hydrolyzed starch/PLA blend with different contents of PEG-DGE CE at 170°C
(Error for η*: SP-0.0-PEG-DGE-TSE = 2.9% RSD,
SP-0.5-PEG-DGE-TSE = 2.3% RSD, SP-2.0-PEG-DGE-TSE = 14.3% RSD)

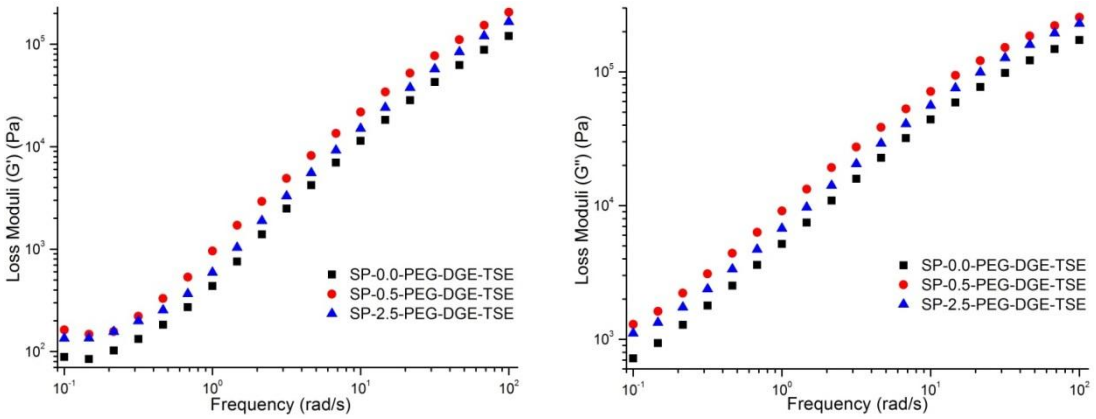

Figure 6.17 Frequency dependency of storage moduli (G') and loss moduli (G'') of hydrolyzed starch/PLA blend with different contents of PEG-DGE CE at 170°C (Error for G' and G'': SP-0.0-PEG-DGE-TSE = 4.1% RSD and 3.0% RSD, SP-0.5-PEG-DGE = 4.1% RSD and 2.2% RSD, SP-2.5-PEG-DGE-TSE = 15.3% RSD and 14.1% RSD)

CHAPTER: 7

RESULTS AND DISCUSSION –

FOAM CHARACTERIZATION

The foam morphologies reported in this chapter were not thought to closely represent the developed foam structure inside the vessel except for those materials exhibiting high melt strength. At the end of each test when the gas was decompressed, the foamed sample took approximately 2 minutes to be removed from the heated vessel before cooling could solidify the foamed structure. Also, since each sample was relatively thick, a temperature gradient existed as the material cooled which often results in a skin-core foam morphology being observed in the following micrographs.

7.1 FOAM CHARACTERIZATION OF SOLANYL® BLEND 30R

The micrographs shown in Figure 7.1 indicated the foamed samples had a closed-cell structure with thicker cell walls and elliptical cell size. Table 7.1 presents the effect of saturation pressure and saturation time on bulk foam density, weight average cell size, and average cell density for neat Solanyl® blend 30R.

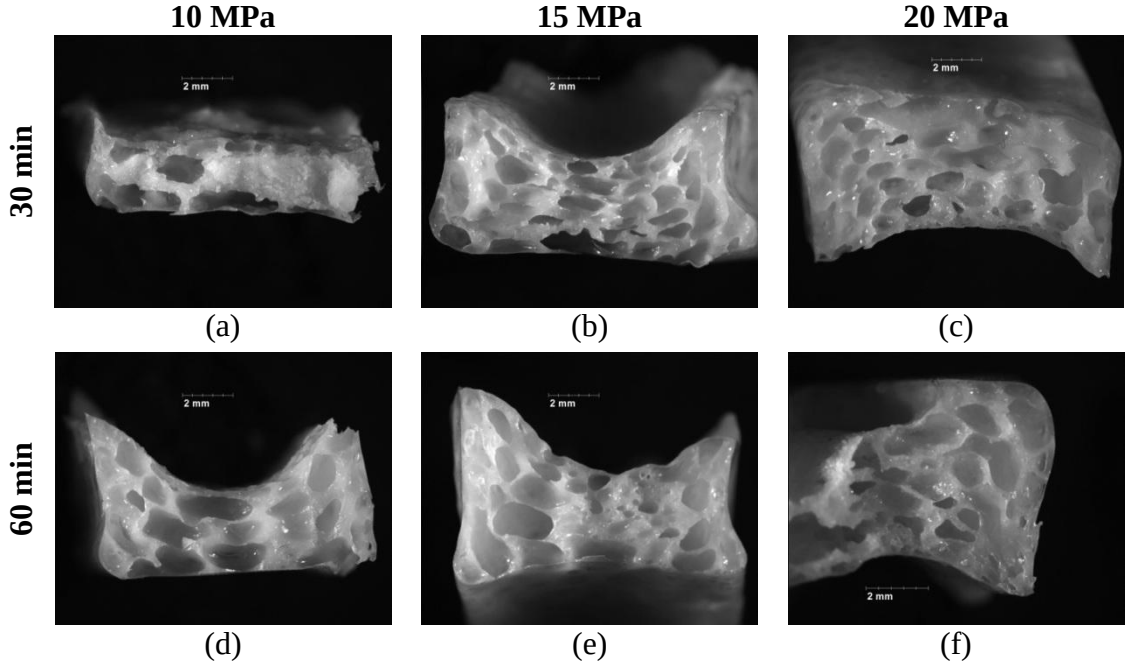

Figure 7.1 Optical micrographs of foamed neat Solanyl® blend 30R with different saturation pressures and saturation times at 170°C

At 10 MPa and 30 min saturation time, the bulk foam density of the neat blend without CE reduced to about half (0.761±0.12 g/cm^3) compared to an unfoamed sample (1.275±0.024 g/cm^3). At this low saturation pressure, the gas was not uniformly absorbed into the polymer matrix in 30 min. From a micrograph (Figure 7.1 (a)); it was observed that a small number of cells (301±130 cells/cm^3) with the weight average cell size of

Table 7.1 Effect of saturation pressures on bulk foam density, average cell size and average cell density of foamed neat Solanyl® blend 30R (SL-0.0-CE-Internal) at 30 min and 60 min saturation times

Saturation Pressure	Saturation Time	Bulk Foam Density	Weight Average Cell Size	Average Cell Density
(MPa)	min	(g/cm^3)	(mm)	(# Cells/cm^3)
10	30	0.761±0.12	0.992±0.369	301±130
15		0.561±0.04	0.714±0.263	1811±323
20		0.586±0.08	1.159±0.323	453±66
10	60	0.710±0.12	1.162±0.337	512±86
15		0.506±0.04	0.907±0.447	1205±442
20		0.482±0.03	0.965±0.490	1456±759

0.992±0.369 mm (Figure 7.2 (a)) were found around the periphery of the sample.

The low viscosity of the neat material offered insufficient stability to the foam morphology for the time lag between depressurization till when the part completely cooled. Coupled to this cooling effect, the relative low gas concentration present at this condition (assuming the gas concentration followed Henry`s law) would result in less cell growth and their collapse would occur more readily in the absence of adequate melt strength. Also, the earlier cooling of the skin increased its melt viscosity in a significantly short period of time to prevent cellular collapse unlike within the core.

As the gas pressure increased to 15 MPa and 20 MPa at 30 min saturation time, more gas molecules were available to be absorbed into the polymer matrix based on Henry's law and thus, a higher gas concentration in the polymer matrix should have resulted assuming that the solubility limit was not reached. With the higher gas

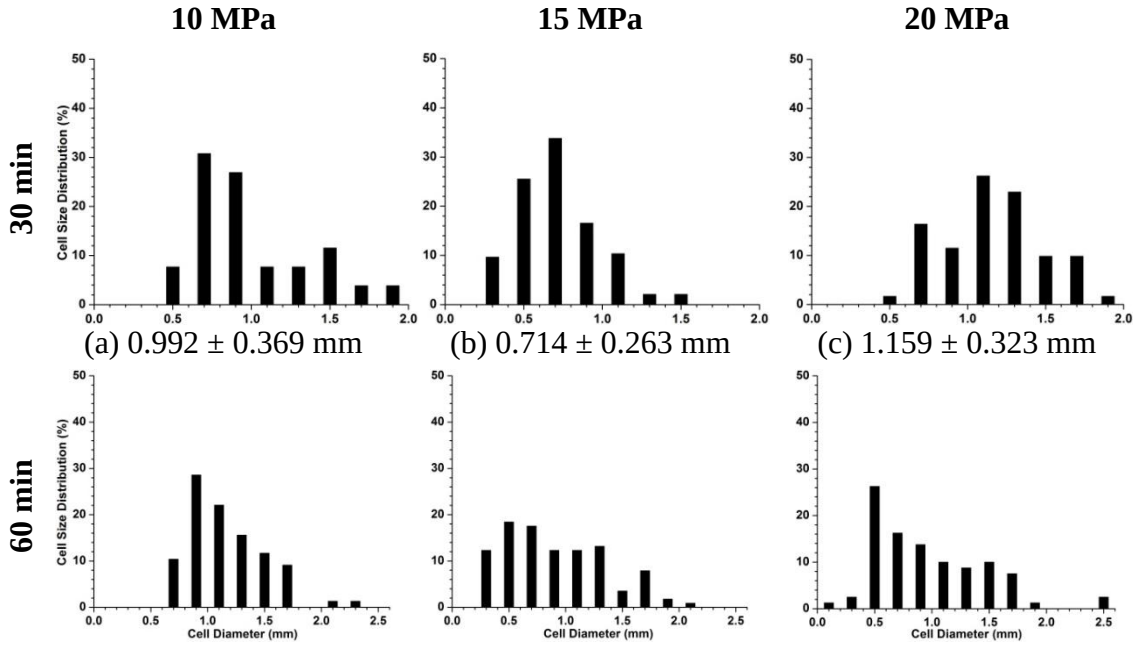

(a) 0.992 ± 0.369 mm (b) 0.714 ± 0.263 mm (c) 1.159 ± 0.323 mm

(d) 1.162 ± 0.337 mm (e) 0.907 ± 0.447 mm (f) 0.965 ± 0.490 mm

Figure 7.2 Cell size distributions (%) of foamed neat Solanyl® blend 30R with different saturation pressures and saturation times at 170°C
(The weight average cell diameter and standard deviation shown below each image)

concentration larger cells were found to have grown uniformly throughout the polymer matrix (Figure 7.1 (b), (c)). At 15 MPa, the weight average cell size was 0.714±0.263 mm (Figure 7.2 (b)) and the cell density was increased to 1811±323 cells/cm^3 (Table 7.1) for the 30 min saturation time. While at 20 MPa, the weight average cell size was increased to1.159±0.323 (Figure 7.2 (b)) mm and the cell density decreased to 453±66 cells/cm^3 (Table 7.1). Resulting from an increase in saturation pressure from 15 MPa to 20 MPa, cell coalescence was found, producing an increase in the weight average cell size and correspondingly a decrease in cell density. The cells in these samples were thought to still have shrunk in size from when the material was originally depressurized, as was

suspected to have occurred at 10 MPa, but due to the high gas concentration inside the foam at these two higher pressure conditions most cells were survived. The uniform and larger cells into the polymer matrix (seen by the micrographs in Figure 7.1 (b), (c) and from the size distribution plots in Figure 7.2 (b), (c) further decreased the bulk foam density to 0.561±0.04 g/cm^3 and 0.586±0.08 g/cm^3 for 15 MPa and 20 MPa, respectively.

Hao et al. (2008) also observed the reduction in the bulk foam density with increasing pressure and time for PLA/starch (60/40 weight ratio). In their work, the lowest bulk foam density of 0.35 g/cm^3 was obtained at 12 MPa and 60 min. For Hao et al., a further increased in pressure to 18 MPa, resulted in the bulk foam density increasing to 0.9 g/cm^3. As the chemistry of our tested blend distinctly differed from Hao et al., this outcome was not observed even at 20 MPa for our work. However, in our work the weight average cell size was considerable larger compared to Hao et al., who reported sizes of 15-50 μm.

Besides saturation pressure, the saturation time was also a decisive factor in the batch foaming process. As explained by Goel and Beckman (1994a and 1994b), the longer the saturation time, the greater the amount of gas which would be absorbed by the polymer matrix (up to the solubility limit of the polymer). By increasing the saturation time from 30 min to 60 min at 10 MPa, the gas concentration in the polymer matrix increased. As a result, larger cells were found uniformly across the cross-section of the sample (Figure 7.1 (d)), now being comparable to the higher pressure conditions since it is assumed that more gas was solubilized over the longer time period. The bulk foam

density was reduced to 0.710±0.12 g/cm^3 from 0.761±0.12 g/cm^3 in correspondence to the larger cell size (1.162±0.337 mm versus 0.992±0.369 mm) for 60 min versus 30 min (Table 7.1). With increasing saturation pressure for the 60 min duration, the bulk foam density was further reduced to 0.506±0.04 g/cm^3 and 0.482±0.03 g/cm^3 for 15 MPa and 20 MPa, respectively. At these high pressures, the cell density increased compared to the foamed sample at 10 MPa due to the corresponding larger pressure drop (since the depressurization time was fixed at 2 seconds in the experiments regardless of the saturation pressure used) and the weight average cell size decreased. However, between 15 MPa and 20 MPa, the average cell size (Figure 7.2 (e), (f)) and cell density showed little change (Table 7.1), which suggest the gas solubility limit had been reached and no gas solubilized into the polymer matrix above 15 MPa.

Below, the influence of the selected multi- and bi-functional chain extenders on the foam morphology is discussed. Unless otherwise stated, the influence of saturation pressure and saturation time noted in this section had the same effect on the bulk foam density, weight average cell density and average cell size.

7.1.1 MORPHOLOGY OF FOAMED SOLANYL® BLEND 30R AND ADR 4370S

The effect of CE content on the bulk foam density and the cell density of foamed Solanyl® blend 30R at different saturation pressures and 30 min saturation times at fixed temperature (170°C) are shown in Figure7.3.

From the micrograph (Figure 7.4 (a)), it was observed that the cells nucleated all the way to the core of the modified CE sample at 10 MPa and a 30 min saturation time,

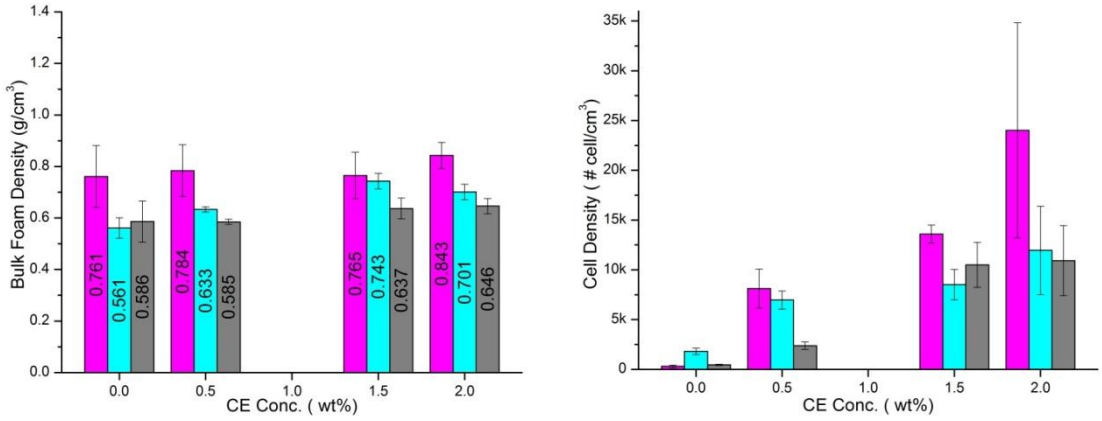

Figure 7.3 Effect of ADR 4370S CE concentration on the bulk foam density and cell density of foamed Solanyl® blend 30R for saturation pressure (■ 10 MPa, ■ 15 MPa, ■ 20 MPa) and 30 min saturation time

which was not observed in the neat foamed sample at this condition (Figure 7.1 (a)). The cell density increased (Figure 7.3) and the weight average cell size distribution shifted toward the smaller cell size (Figure 7.5 (a), (b), (c)) as CE content progressively increased to 2.0 wt % compared to the neat foamed samples. The weight average cell size decreased from 0.336 ± 0.145 mm (Figure 7.5 (a)), 0.251 ± 0.108 mm (Figure 7.5 (b)) to 0.220 ± 0.101 mm (Figure 7.5 (c)) for 0.5 wt %, 1.5 wt % to 2.0 wt % CE respectively. As explained by Di et al. (2005), the higher melt viscosity and elasticity offered greater resistance to cell expansion, which also restrained cell coalescence and cell rupture significantly. However, the increased melt viscosity of the modified blend would also reduce the diffusion rate of dissolved gas within the melt. Consequently, it required less energy to create new bubbles by nucleation than to inflate the existing bubbles by diffusion. As a result more cells were nucleated in modified blends. It was not possible to

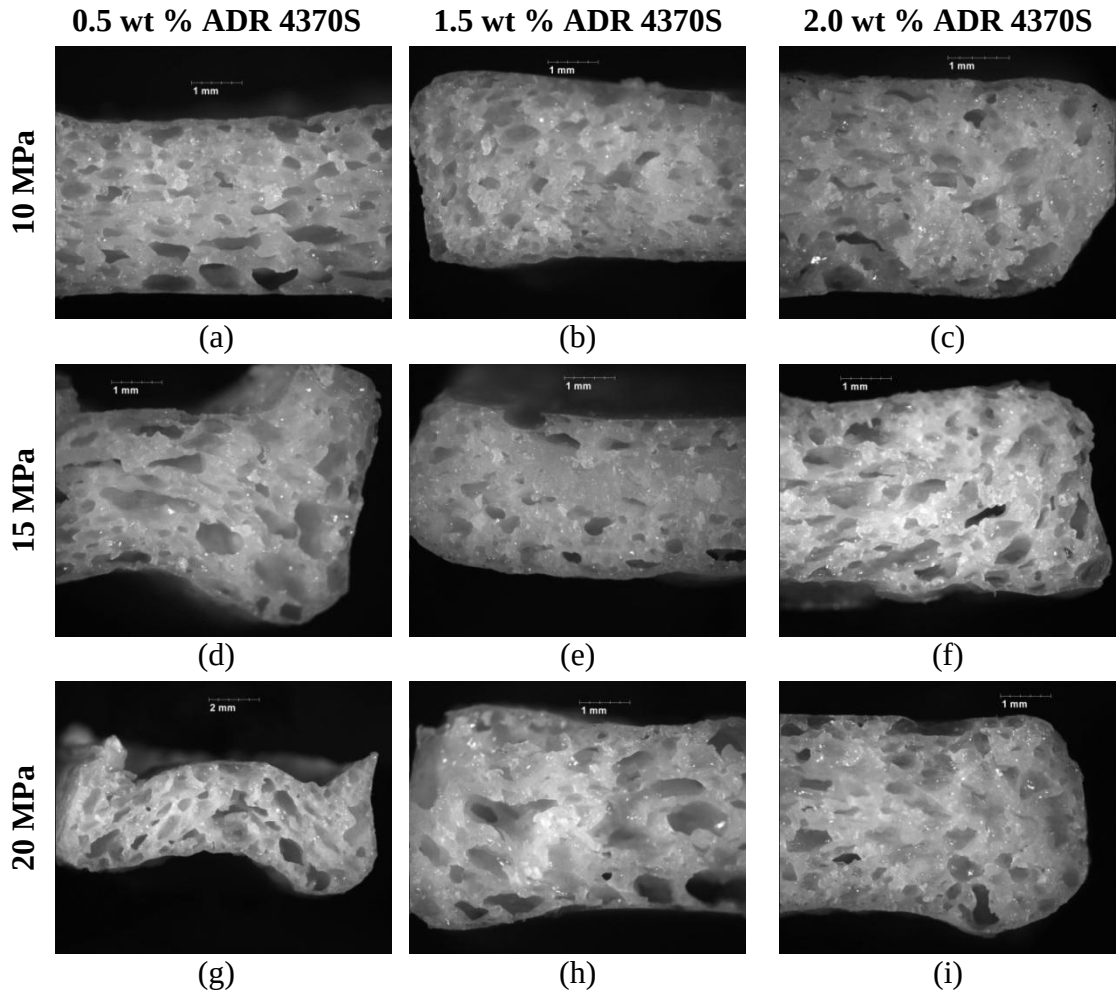

Figure 7.4 Optical micrographs of foamed Solanyl® blend 30R and ADR 4370S CE with different saturation pressures and 30 min saturation time at 170°C

determine if gas solubility was change by the ADR 4370S CE as the positive influence of rheology precluded that distinction. The same trends for the cell density (Figure 7.3) and the weight average cell size (Figure 7.5) were observed for the different levels of CE for 15 MPa and 20 MPa. At 30 min saturation time, the influence of the bulk foam density at

different levels of CEs was same as it was observed for the neat blend for 10 MPa, 15 MPa and 20 MPa (Figure 7.3).

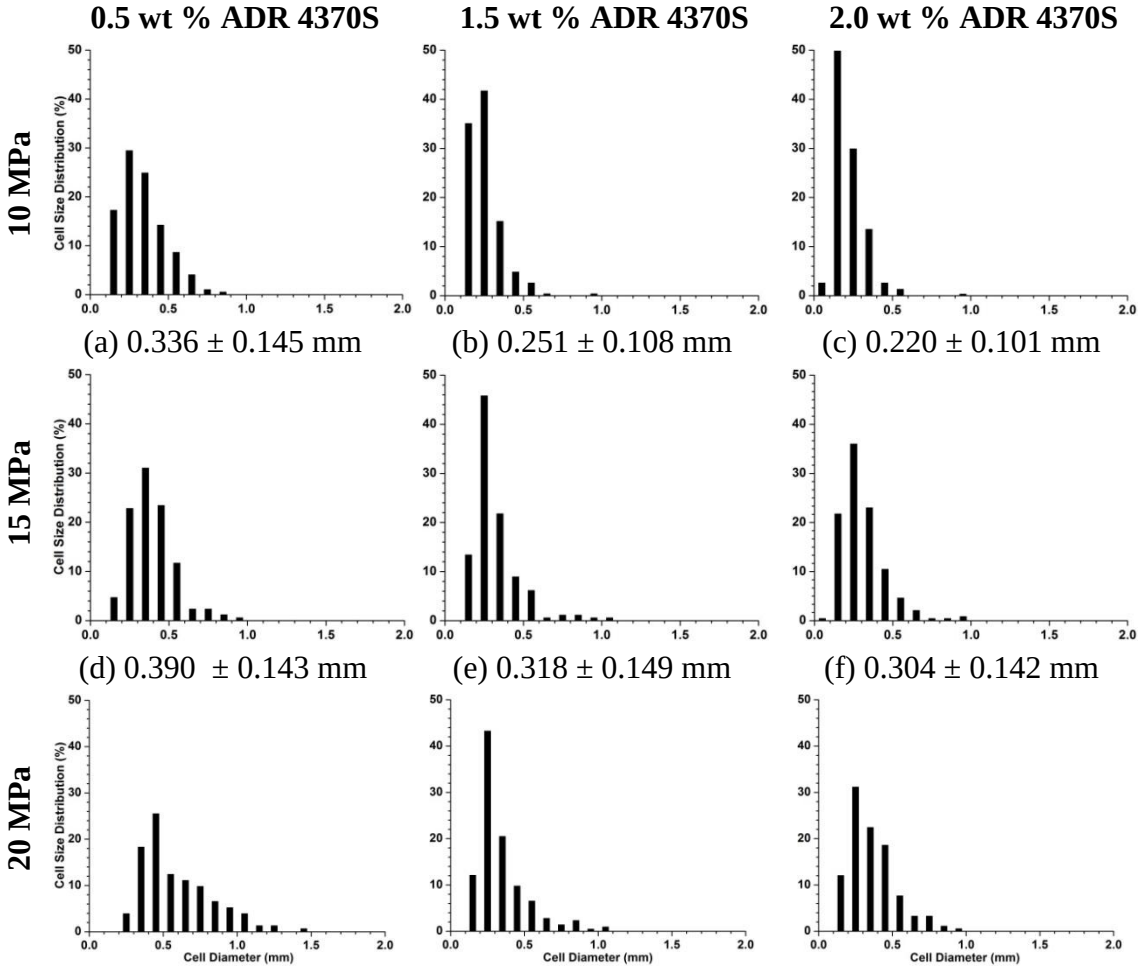

Figure 7.5 Cell size distributions (%) of foamed Solanyl® blend 30R and ADR 4370S CE with different saturation pressures and 30 min saturation time
(The weight average cell diameter and standard deviation shown below each image)

The effect of CE contents on the bulk foam density and the cell density of foamed Solanyl® blend 30R at different saturation pressures and 60 min saturation times at fixed

temperature (170°C) are shown in Figure 7.6. The optical micrographs for the 60 min saturation time were not presented due to the similar cell morphology between foamed samples with CE at 30 min and 60 min saturation time.

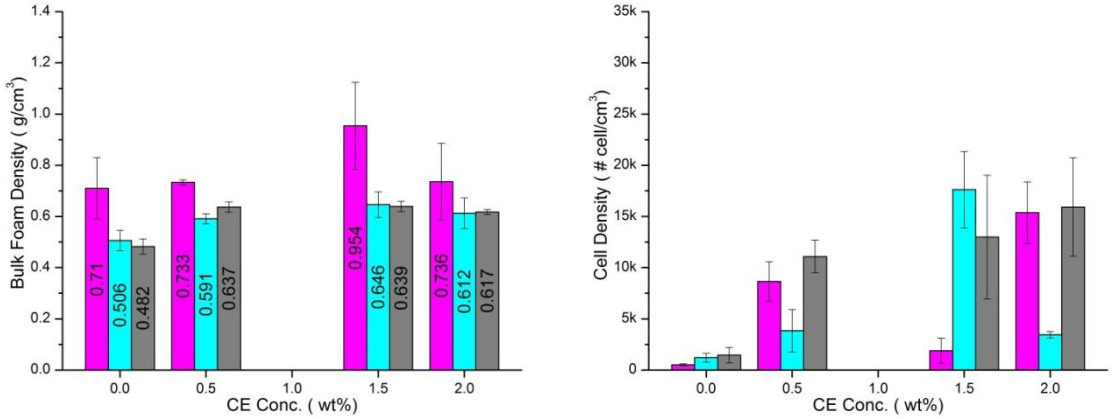

Figure 7.6 Effect of ADR 4370S CE concentration on the bulk foam density and cell density of foamed Solanyl® blend 30R for saturation pressure (■ 10 MPa, ■ 15 MPa, ■ 20 MPa) and 60 min saturation time

At 15 MPa and 20 MPa, the change in the weight average cell size was not consistent as CE contents increased from 0.5 wt % to 2.0 wt % for the 60 min saturation time (Figure 7.7 (d), (e), (f) for 15 MPa; Figure 7.7 (g), (h), (i) for 20 MPa). The weight average cell size remained relatively constant as saturation pressure increased from 10 MPa to 15 MPa (Figure 7.7 (d), (e), (f)). The same trend was also observed for the weight average cell size as saturation pressure increased from 15 MPa to 20 MPa (Figure 7.7 (g), (h), (i)). Also, the bulk foam density did not change significantly at each levels of CE when saturation pressure increased from 15 MPa to 20 MPa (Figure 7.6). This suggested that the gas solubility limit has been reached and no more gas was soluble in the polymer matrix beyond 15 MPa at 60 min saturation time. Once the gas solubility limit had been

reached in the polymer matrix, the maximum gas concentration into the polymer matrix caused the cell coalescence during the cell growth stage and it could randomly increases the weight average cell size at higher pressure (15 MPa and 20 MPa) and saturation time (60 min).

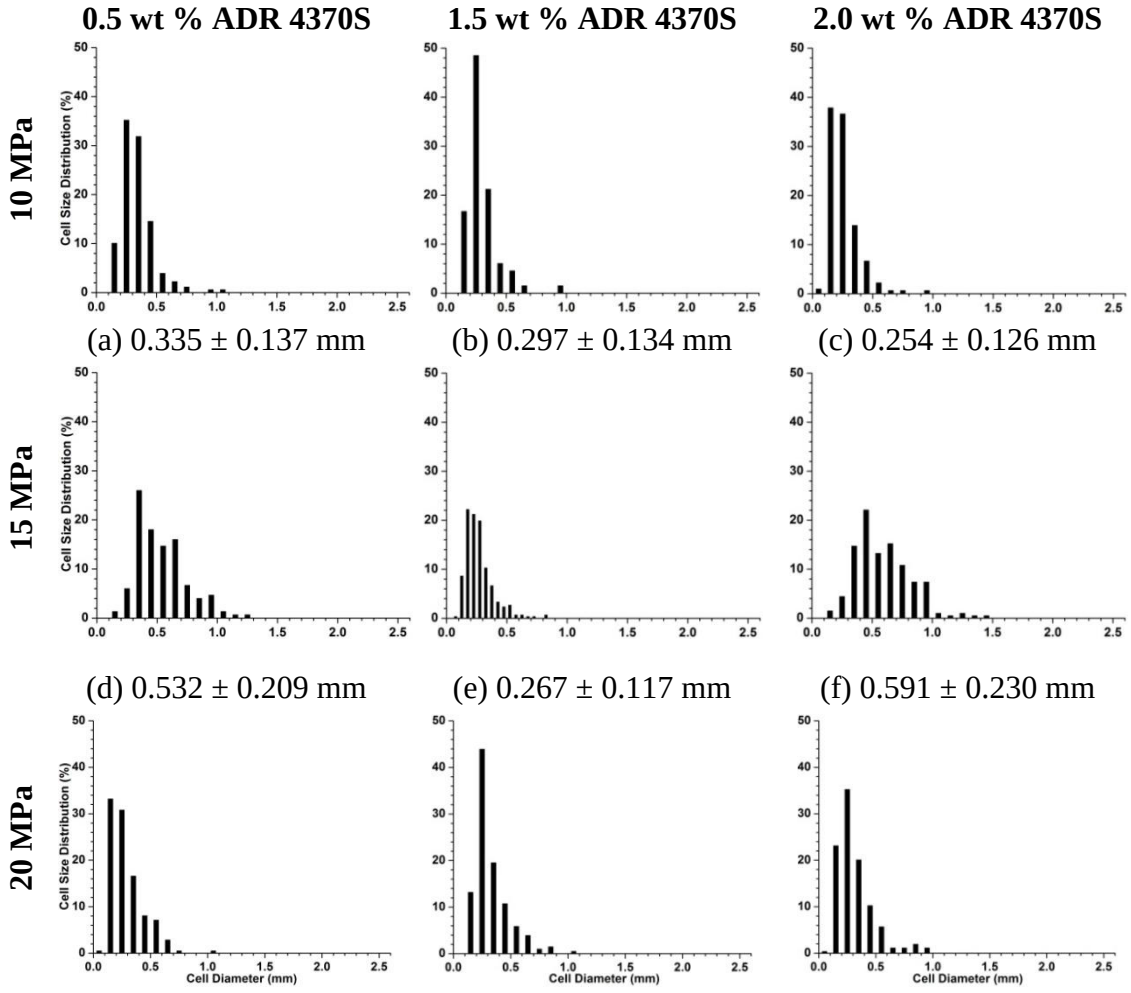

(a) 0.335 ± 0.137 mm (b) 0.297 ± 0.134 mm (c) 0.254 ± 0.126 mm

(d) 0.532 ± 0.209 mm (e) 0.267 ± 0.117 mm (f) 0.591 ± 0.230 mm

(g) 0.287 ± 0.149 mm (h) 0.329 ± 0.154 mm (i) 0.313 ± 0.163 mm

Figure 7.7 Cell size distributions (%) of foamed Solanyl® blend 30R and ADR 4370S CE with different saturation pressures and 60 min saturation time
(The weight average cell diameter and standard deviation shown below each image)

7.1.2 MORPHOLOGY OF FOAMED SOLANYL® BLEND 30R AND ADR 4380

The micrographs shown in Figure 7.8 (a) indicated that skin-core foam morphology was observed for the foamed samples at all levels of CE for 10 MPa saturation time only. The other optical micrographs of foamed samples at 15 MPa and 20 MPa with ADR 4380 CE were not presented in Figure 7.8 due to the same cell morphology between foamed samples with ADR 4380 and ADR 4370S (Figure 7.4) for 30 min saturation time.

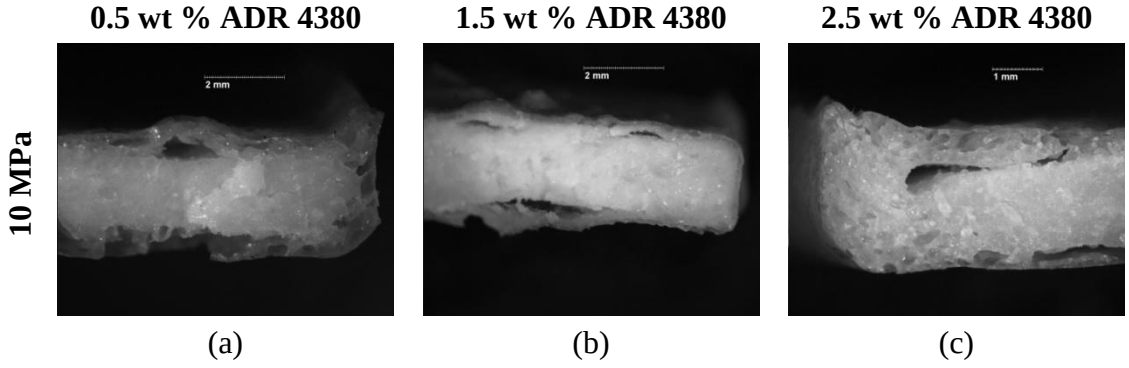

Figure 7.8 Optical micrographs of foamed Solanyl® blend 30R and ADR 4380 CE at 10 MPa saturation pressure and 30 min saturation time at 170°C

If we assumed that the gas solubility of the modified blend with ADR 4380 was low compared to the neat blend and the modified blend with ADR 4370S at the same pressure and saturation time. The observed micrographs of the foamed samples for the neat blend (Figure 7.1 (a)), the modified blend with ADR 4370S (Figure 7.4 (a)) and the modified blend with ADR 4380 (Figure 7.8 (a)) can be explained by Figure 7.9.

At 30 min saturation time and 10 MPa, no cells were observed across the cross-section of the foamed sample of the modified blend with ADR 4380 (Figure 7.8 (a)). The

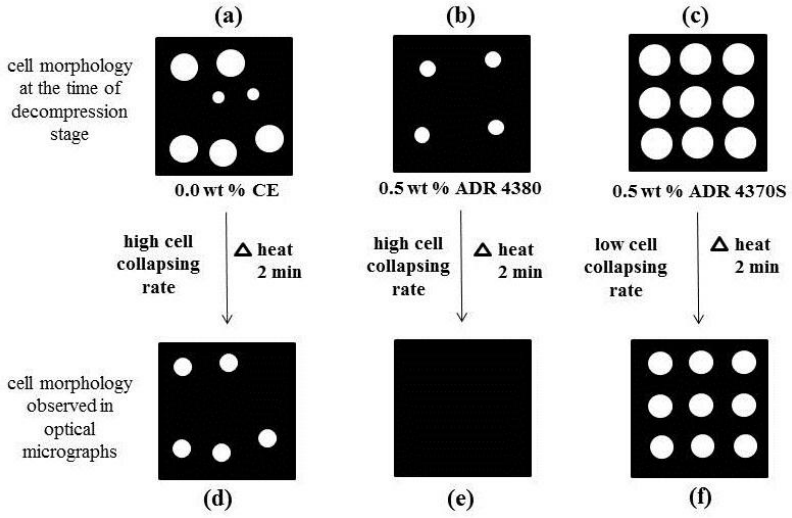

Figure 7.9 Cell morphology of blend with 0.0 wt % CE, 0.5 wt % ADR 4370S and 0.5 wt % ADR 4380 at the time of decompression and observed cell morphology in optical micrographs at same pressure and saturation time

less gas concentration in the modified blend with 0.5 wt % ADR 4380 would nucleate small and less numbers of cells in the polymer matrix during decompression (Figure 7.9 (b)). The high cell collapsing/shrinkage rate due to the insufficient melt strength of the modified blend (0.5 wt % ADR 4380) would result in smaller cells to collapse rapidly during 2 min time lag in the core as well as on the surface of the sample as a result no cells were observed in the foamed sample (Figure 7.8 (a) and Figure 7.9 (e)).

The skin-core cell morphology was observed in the foamed neat sample (Figure 7.1 (a)). Relative higher but non-uniform gas concentration in the neat blend compared to the modified blend with ADR 4380 nucleated the smaller cells at the core and the bigger cells at the surface during decompression (Figure 7.9 (a)). The relative low gas concentration in the smaller cells were collapsed in the core due to high cell collapsing

rate (low melt viscosity) of the neat blend, while the high gas concentration in the bigger cells were survived on the periphery during 2 min time lag. Also, earlier cooling of the skin could increase its melt strength in short period of time which could prevent the cells from being collapsed at the skin as a result the skin-core morphology was observed (Figure 7.1 (a) and Figure 7.9 (d)).

The higher gas concentration and high melt viscosity both were the contributing factors for the well-developed cell structure in the modified blend with 0.5 wt % ADR 4370S CE (Figure 7.4 (a)). The high gas concentration nucleated bigger and more cells uniformly across the polymer matrix during the decompression in the modified blend with ADR 4370S (Figure 7.9 (c)). The bigger cells had less chance to collapse due to its low cell collapsing rate (high melt viscosity) compared to the neat and modified blend (0.5 wt % ADR 4380) during 2 min time lag. Also, the cell structure was also survived during the cooling time frame due to rapid increased in the melt viscosity during cooling as a result the bigger cells were uniformly observed in the micrographs (Figure 7.4 (a) and Figure 7.9 (f)).

The cell morphology did not improve significantly for the modified blend with 1.5 wt % and 2.5 wt % ADR 4380 CE (Figure 7.8 (b), (c)), even the melt viscosity increased in the corresponding blends (Section 6.1.1) due to the low gas concentration in the polymer matrix at 10 MPa. Also, increased in saturation time to 60 min, the skin-core cell morphology was also observed for modified blends with 0.5 wt % and 1.5 wt % ADR 4380 CE (Figure 7.10 (a), (b)) at 10 MPa due to the low melt strength. But, the cell

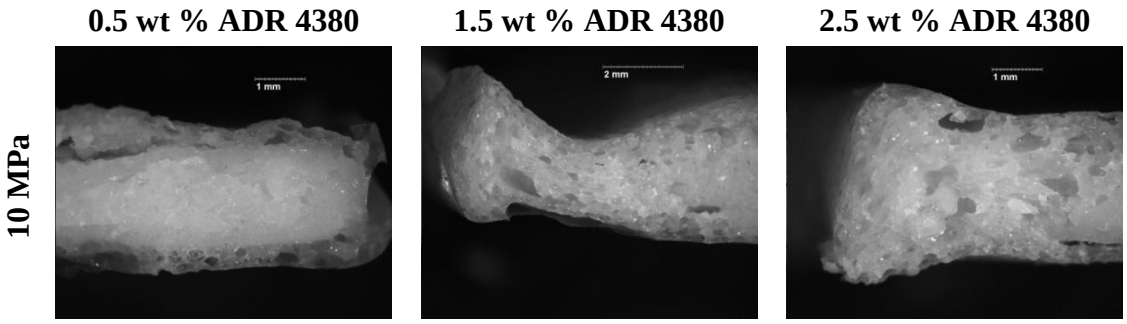

Figure 7.10 Optical micrographs of foamed Solanyl® blend 30R and ADR 4380 CE with 10 MPa saturation pressure and 60 min saturation time at 170°C

morphology of foamed sample with 2.5 wt % ADR 4380 CE was significantly improved due to the high gas concentration and the high melt viscosity (Figure 7.10 (c)). At 15 MPa and 20 MPa, the cell morphology significant improved at all levels of CE for 30 min and 60 min saturation time due to high gas concentration in the polymer matrix.

The weight average cell size of foamed samples with ADR 4380 CE smaller (Figure 7.11 and Figure 7.12) compared to foamed sample with ADR 4370S (Figure 7.5 and Figure 7.7) at all levels of CE for 15 MPa and 20 MPa saturation pressure. The reverse trend had been observed for the cell density at the same conditions (Figure 7.13 for ADR 4380, Figure 7.3 and Figure 7.6 for ADR 4370S). The difference in the average cell size and cell density between foamed sample with ADR 4370S and ADR 4380 CE at high pressure and saturation time can be explained by Figure 7.14.

At higher pressure (15 MPa and 20 MPa) and longer saturation time (60 min), the modified blend with ADR 4370S CE had reached its gas solubility limit in the polymer matrix (Section 7.1.1). The higher pressure drop created greater thermodynamic

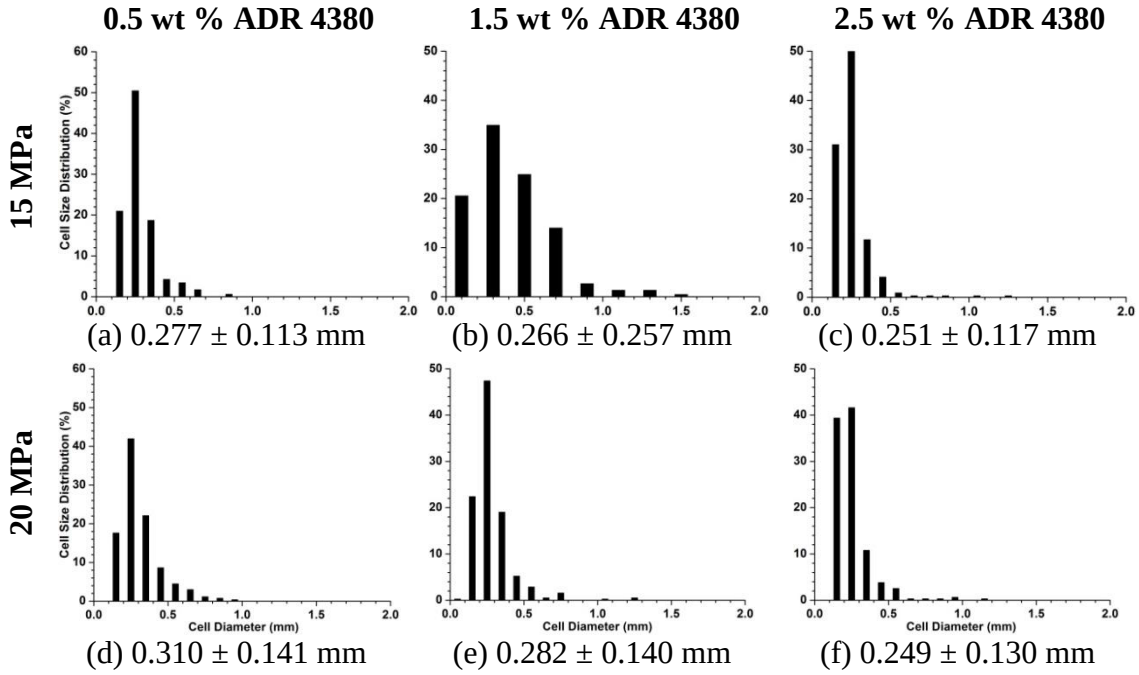

Figure 7.11 Cell size distributions (%) of foamed Solanyl® blend 30R and ADR 4380 CE with different saturation pressures and 30 min saturation time
(The weight average cell diameter and standard deviation shown below each image)

instability and more cells were nucleated during the decompression (Figure 7.14 (a)). But, the more gas concentration in the polymer matrix promoted the cell growth and the cell coalescence would occur. As a result, the weight average cell size was increased and the cell density decreased (Figure 7.14 (c)) in the foamed sample with ADR 4370S at high pressures and saturation times (Figure 7.5, Figure 7.7 for the weight average cell size and Figure 7.3, Figure 7.6 for cell density).

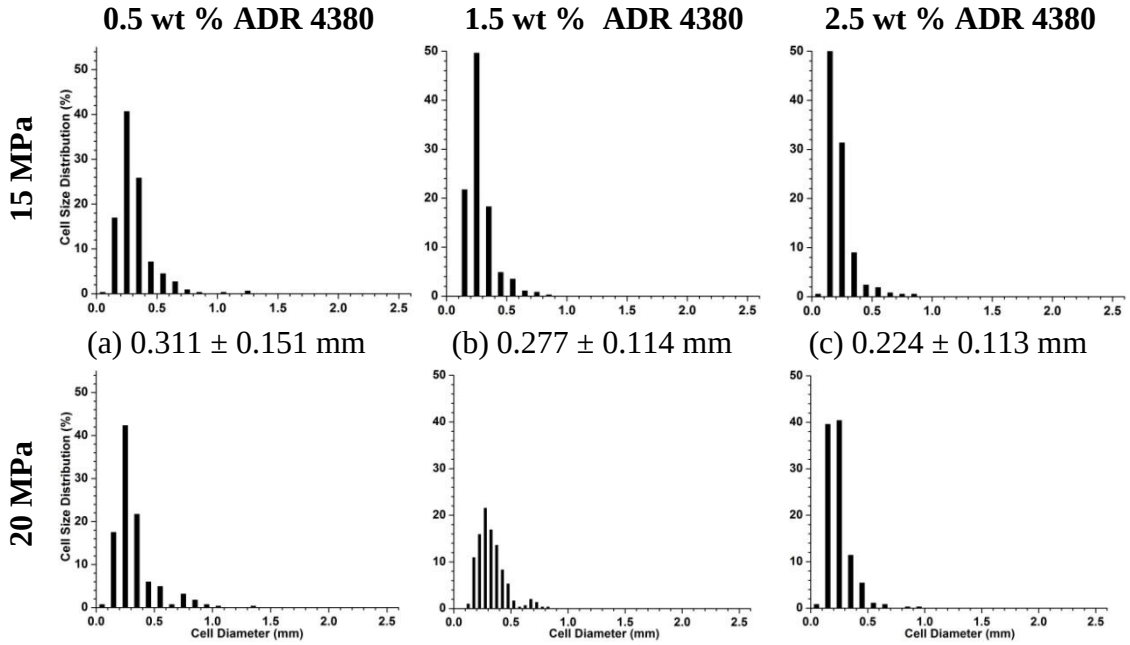

(a) 0.311 ± 0.151 mm (b) 0.277 ± 0.114 mm (c) 0.224 ± 0.113 mm

(d) 0.320 ± 0.177 mm (e) 0.325 ± 0.122 mm (f) 0.241± 0.110 mm

Figure 7.12 Cell size distributions (%) of foamed Solanyl® blend 30R and ADR 4380 CE with different saturation pressures and 60 min saturation time
(The weight average cell diameter and standard deviation shown below each image)

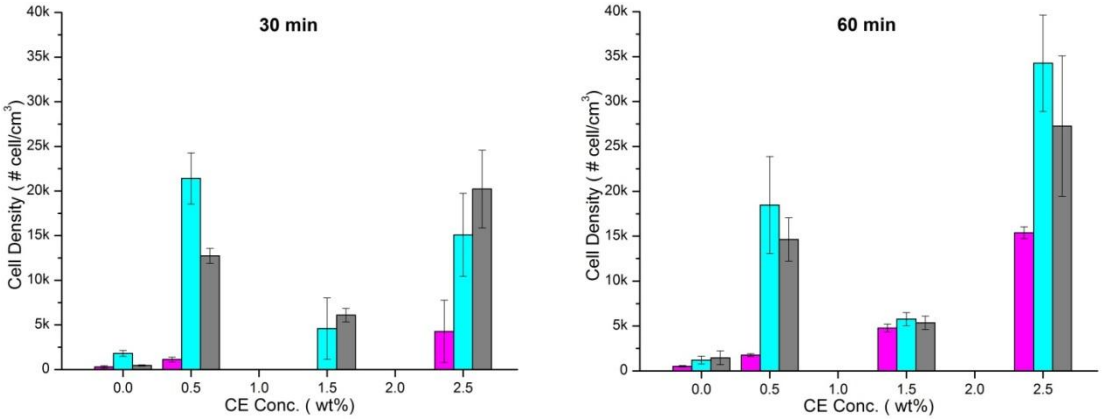

Figure 7.13 Effect of ADR 4380 CE concentration on the cell density of foamed Solanyl® blend 30R for saturation pressure (■ 10 MPa, ■ 15 MPa, ■ 20 MPa) and saturation times (30 min and 60 min)

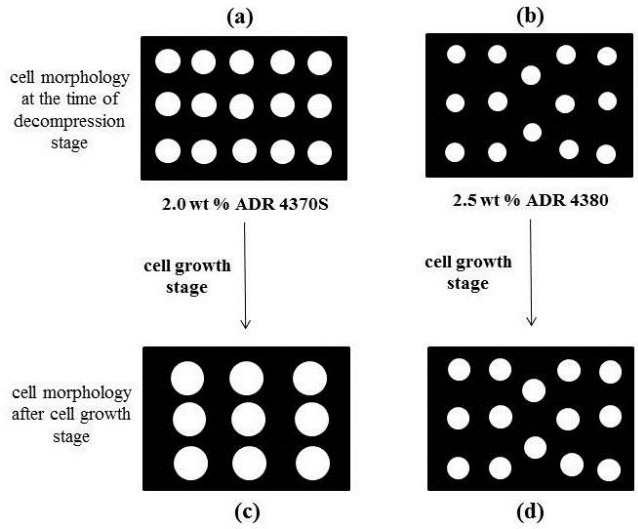

Figure 7.14 Cell morphology of the modified blend with 2.0 wt % ADR 4370S and 2.5 wt % ADR 4380 CE during cell growth stage at high pressure and high saturation time

For the modified blend with ADR 4380 CE, the polymer matrix did not fully saturated with gas at higher saturation pressure and times due to the low gas solubility of the modified blend. The relative less gas concentration in the polymer matrix would result in smaller cells (Figure 7.14 (b)) and less cell growth, which decreased the cell coalescence (Figure 7.14 (d)). As a result, the weight average cell size was decreased (Figure 7.11, Figure 7.12) and the cell density increased (Figure 7.13, Figure 7.14 (d)) in the foamed sample with ADR 4380 at high pressure and longer saturation time. However, at high saturation pressure and time, the cell shrinkage effect during the time lag in both modified blend with ADR 4370S and ADR 4380 CEs were less pronounced due to the relative higher gas concentration in the cells.

As the saturation pressure progressively increased from 10 MPa to 20 MPa, the bulk foam density was also progressively decreased for 30 min and 60 min saturation times (Figure 7.15), which also suggested that the gas solubility limit did not reach at this saturation times.

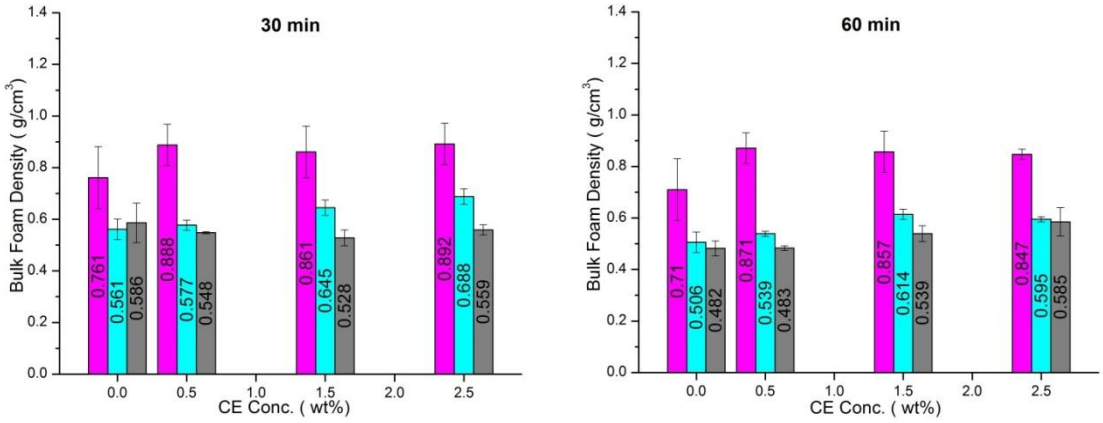

Figure 7.15 Effect of ADR 4380 CE concentration on the bulk form density of foamed Solanyl® blend 30R for different saturation pressure (■ 10 MPa, ■ 15 MPa, ■ 20 MPa) and saturation times (30 min and 60 min)

7.1.3 MORPHOLOGY OF FOAMED SOLANYL® BLEND 30R AND DGEBA

Figure 7.16 present the optical micrographs of foamed samples with CE at different saturation pressures and 30 min saturation times. The other micrographs of the foamed samples with DGEBA CE at 60 min saturation time did not present displaying similar cell morphology.

At 10 MPa, the same skin-core foam morphology was observed at all level of CE for 30 min saturation time (Figure 7.16 (a), (b), (c)) compared to the foamed samples of modified blend with ADR 4380 (Figure 7.8 (a), (b), (c)). The addition of CE (DGEBA) decreased the gas solubility in the modified blend compared to the modified blend with

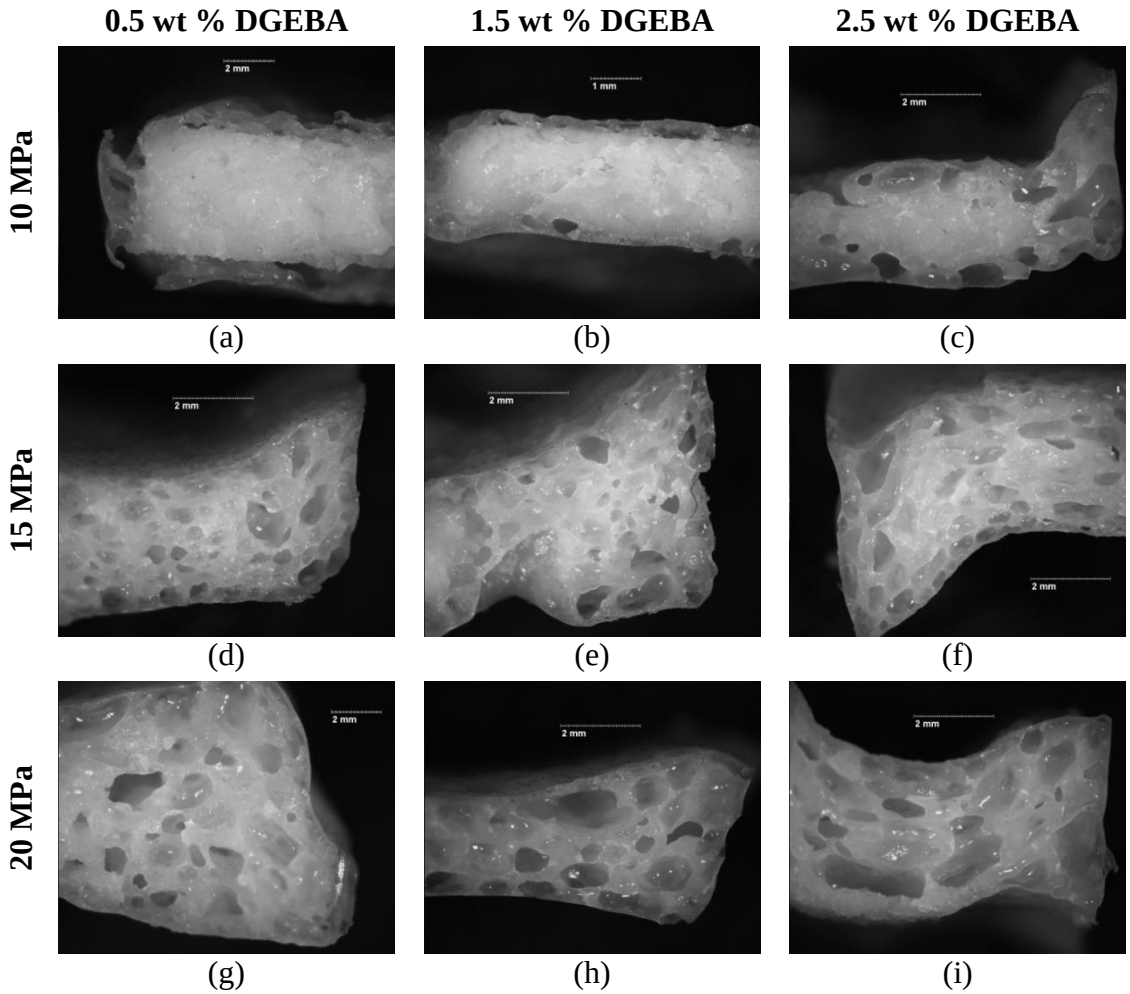

Figure 7.16 Optical micrographs of foamed Solanyl® blend 30R and DGEBA CE with different saturation pressures and 30 min saturation time at 170°C

ADR 4370S CE (Section 7.1.1). At 10 MPa, non-uniform gas concentration in the polymer matrix result in the skin-core foam morphology at different levels of CE (Figure 7.16 (a), (b), (c)). At 15 MPa and 20 MPa, the cell morphology of the modified blend was improved at all levels of CE due to the high gas concentration in the polymer matrix at 30 min and 60 min saturation time.

The weight average cell size was decreased (Figure 7.17 and Figure 7.18) and cell density increased compared to the foamed neat sample but did not show any particular trend as it was observed in ADR 4370S (Section 7.1.1) and ADR 4380 (Section 7.1.2) CEs at 30 min and 60 min saturation time. Our study on the rheology of the modified blend with DGEBA did not show any significant increase in the melt viscosity compared to other ADR 4370S and ADR 4380 CEs (Section 6.1.3). Also, the indirect measurement of intrinsic viscosity in section 5.2 indicated that the chain extension had been occurred between the reactive group in the blend and the bi-functional epoxy CE. However, such measurements were done in very dilute state in solvent, where no chains interaction

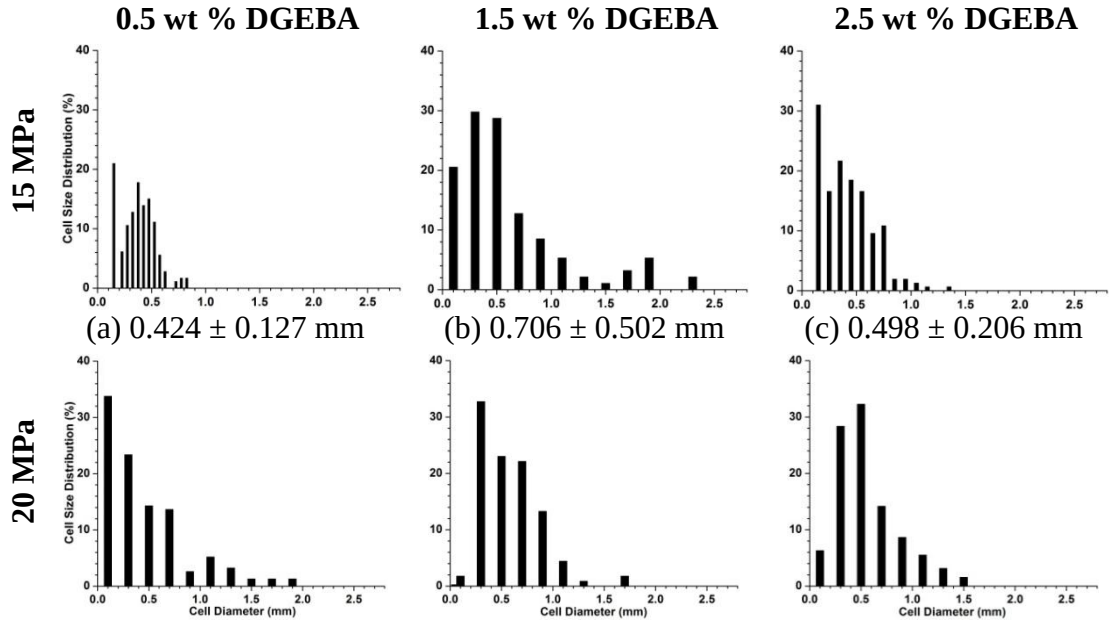

(a) 0.424 ± 0.127 mm (b) 0.706 ± 0.502 mm (c) 0.498 ± 0.206 mm

(c) 0.460 ± 0.410 mm (d) 0.580 ± 0.295 mm (e) 0.555 ± 0.306 mm

Figure 7.17 Cell size distributions (%) of foamed Solanyl® blend 30R and DGEBA CE with different saturation pressures and 30 min saturation time
(Average cell diameter and standard deviation shown below each image)

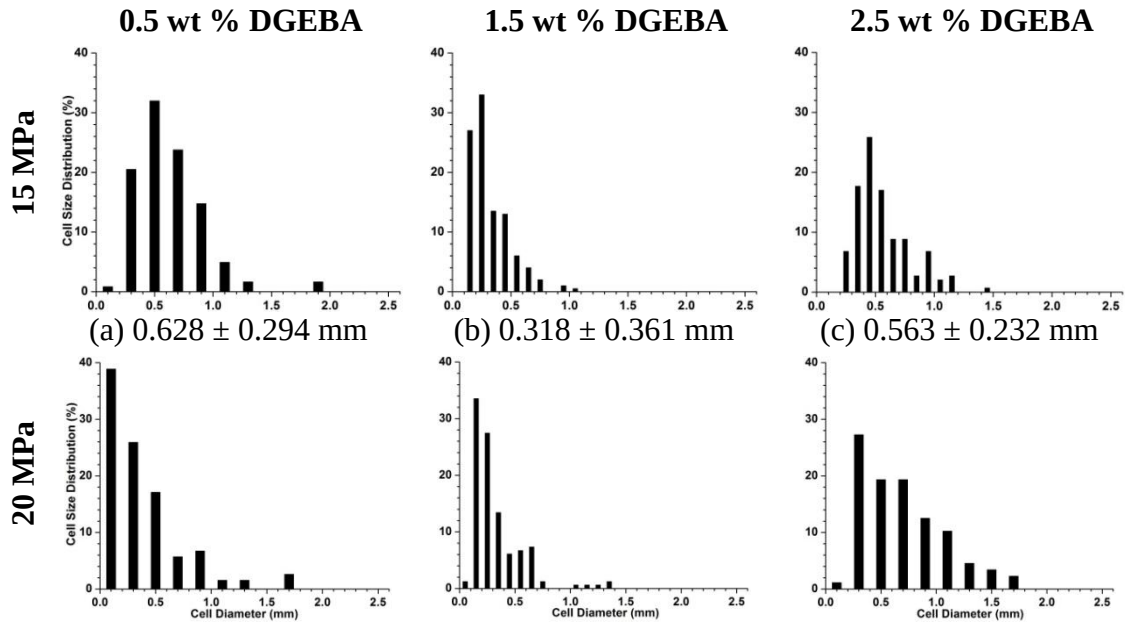

Figure 7.18 Cell size distributions (%) of foamed Solanyl® blend 30R and DGEBA CE with different saturation pressures and 60 min saturation time (Average cell diameter and standard deviation shown below each image)

was present. Our foaming experiments were done in the melt state and the strong intermolecular forces were obscured the effect of chain extension on the average cell size and cell density at different levels of CE. At high pressure and saturation time, the high gas concentration in the polymer matrix produced the bigger cells during depressurization, which more likely to survive during the 2 min time lag and cooling time frame. The bigger cells and high cell density reduced the bulk foam density at higher pressure (15 MPa and 20 MPa) and saturation time (30 min and 60 min) (Figure 7.19).

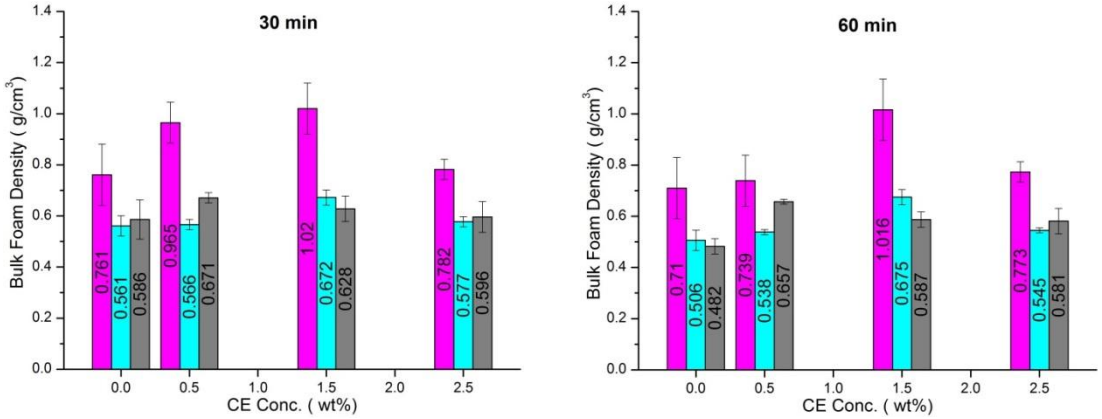

Figure 7.19 Effect of DGEBA CE concentration on the bulk foam density of foamed Solanyl® blend 30R for different saturation pressure (■ 10 MPa, ■ 15 MPa, ■ 20 MPa) and saturation times (30 min and 60 min)

7.1.4 MORPHOLOGY OF FOAMED SOLANYL® BLEND 30R AND PEG-DGE

Figure 7.20 presents the optical micrographs of foamed samples with CE at different saturation pressures and 30 min saturation times. The other micrographs of the foamed samples with DGEBA CE at 60 min saturation time were not presented displaying similar cell morphology.

At 10 MPa, the cell morphology of the modified blend was improved but some samples showed the skin-core foam morphology for 30 min and 60 min saturation time (Figure 7.20 (b)). This low-molecular weight CE (PEG-DGE) also did not show any significant change in the melt viscosity at all level of CE (Section 6.1.4). However, our work on intrinsic viscosity in section 5.2 indicated that the chain extension had been occurred between the reactive group in the blend and the bi-functional CE. At 15 MPa and 20 MPa, the effect of CE contents on the weight average cell size (Figure 7.21 and

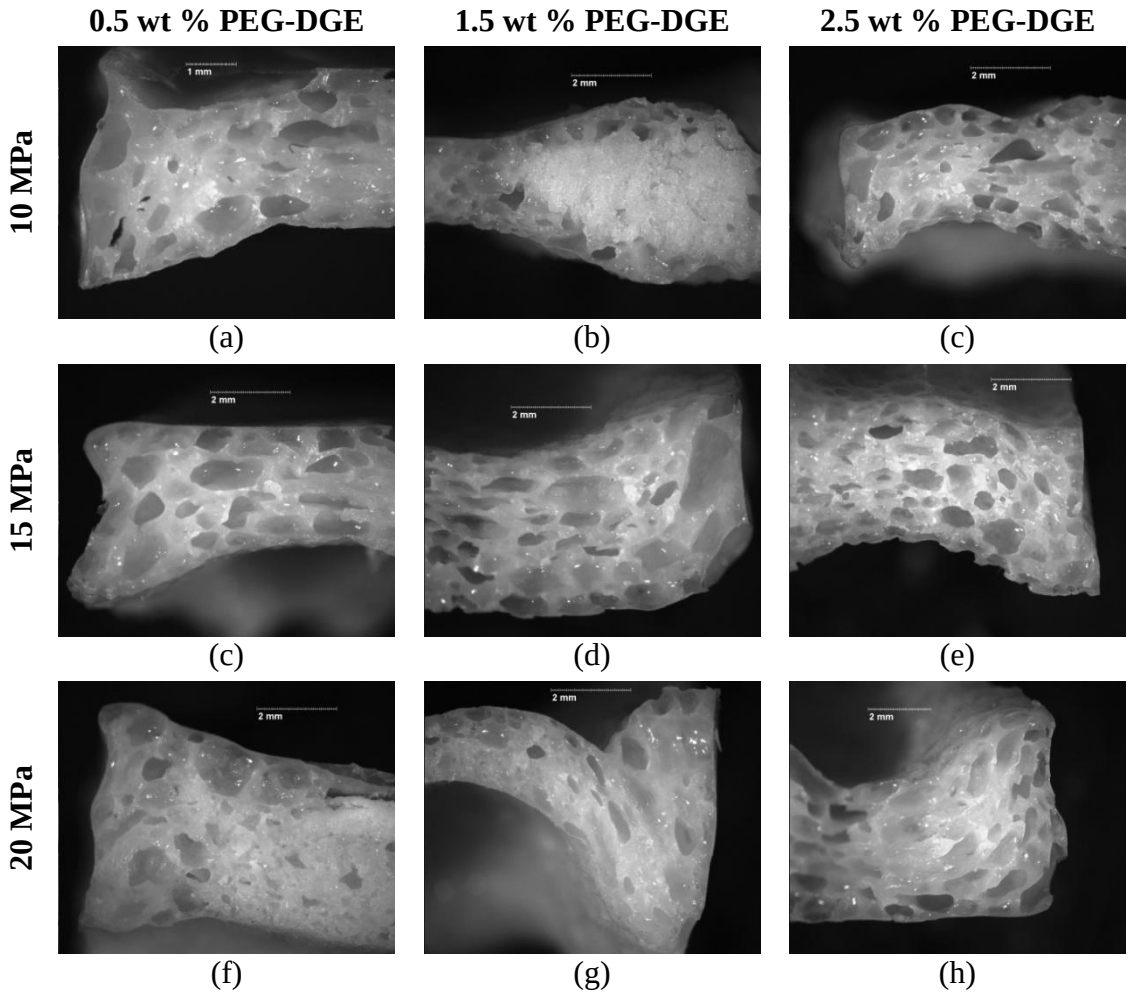

Figure 7.20 Optical micrographs of foamed Solanyl® blend 30R and PEG-DGE CE with different saturation pressures and 30 min saturation time at 170°C

Figure 7.22), cell density and bulk foam density (Figure 7.23) were same as it was observed in the previous bi-functional epoxy DGEBA CE (Section 7.1.3).

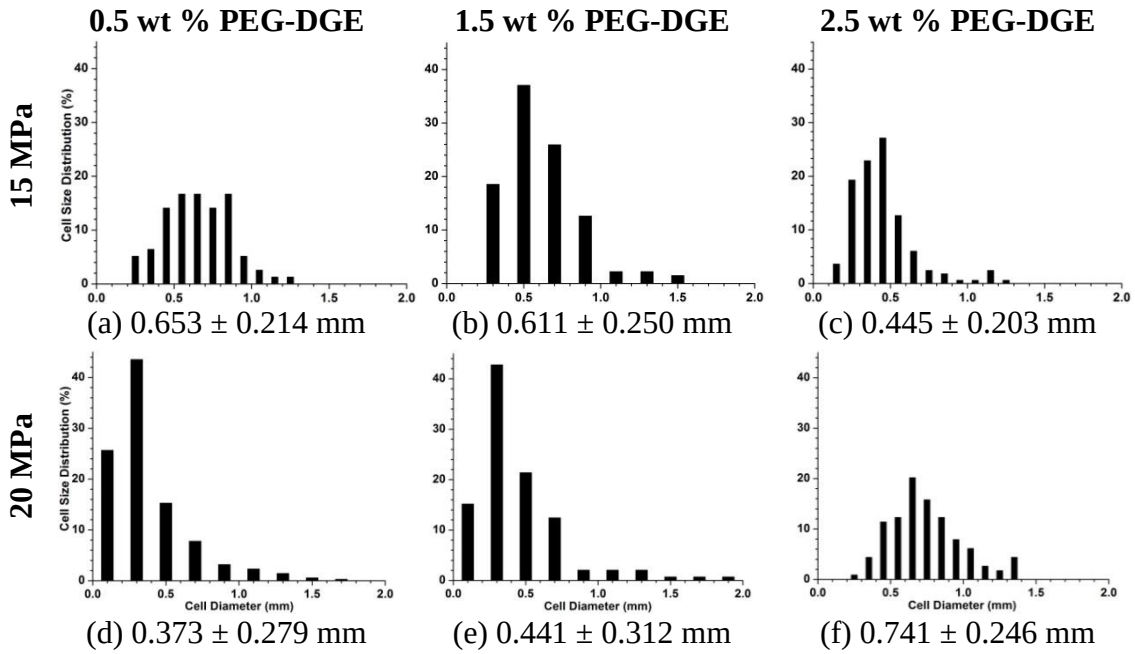

(a) 0.653 ± 0.214 mm (b) 0.611 ± 0.250 mm (c) 0.445 ± 0.203 mm

(d) 0.373 ± 0.279 mm (e) 0.441 ± 0.312 mm (f) 0.741 ± 0.246 mm

Figure 7.21 Cell size distribution(%) of foamed Solanyl® blend 30R and PEG-DGE CE with different saturation pressures and 30 min saturation time (The weight average cell diameter and standard deviation shown below each

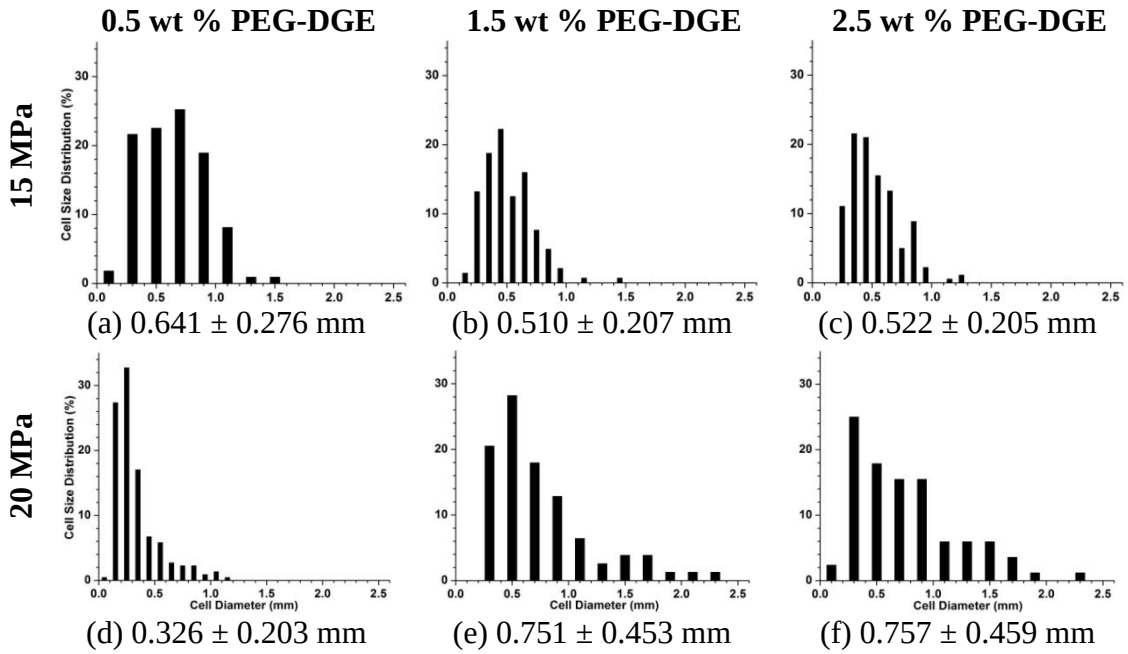

Figure 7.22 Cell size distribution (%) of foamed Solanyl® blend 30R and PEG-DGE CE with different saturation pressures and 60 min saturation time
(The weight average cell diameter and standard deviation shown below each image)

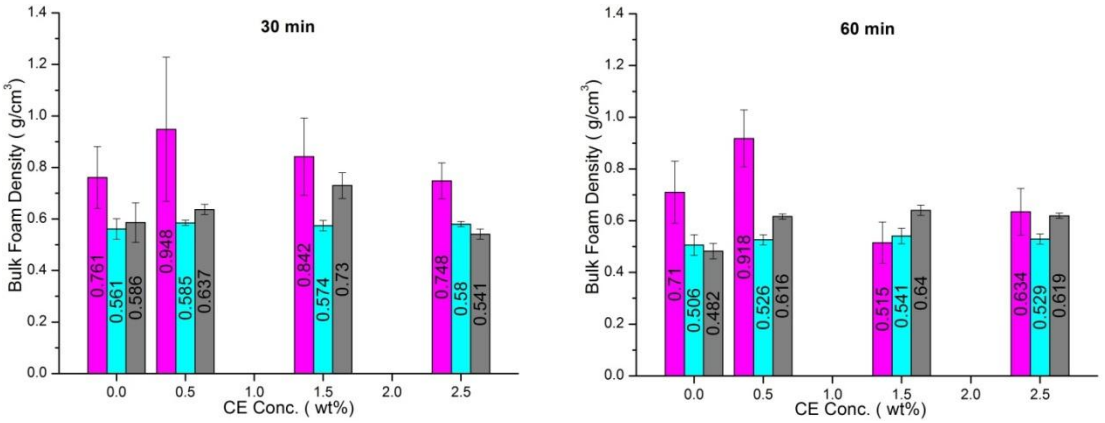

Figure 7.23 Effect of PEG-DGE CE concentration on the bulk density of foamed Solanyl® blend 30R for saturation pressure (■ 10 MPa, ■ 15 MPa, ■ 20 MPa) and saturation times (30 min and 60 min)

7.2 FOAM CHARACTERIZATION OF HYDROLYZED STARCH/PLA BLEND

The batch foaming trials of the neat and the modified hydrolyzed starch/PLA blends were attempted at the low saturation pressure (10 MPa) and time (30 min) but did not lead to a significant reduction in the bulk foam density compared to the unfoamed neat hydrolyzed starch /PLA blend (1.263±0.013 g/cm^3) and, therefore, no batch foaming trials were run with the neat and the modified hydrolyzed starch/PLA blends using either 10 MPa and 30 min saturation time. At low saturation pressure and time, the low gas concentration in the polymer matrix nucleated the smaller cells during depressurization. Also, inherently higher melt viscosity of the neat hydrolyzed starch/PLA blend significantly reduced the gas diffusion rate in the polymer matrix. As a result, the smaller cells were grown during cell growth period and cells were rapidly collapsed due to the low gas concentration in the cells during 2 min time lag. As a result, unfoamed structure was produced and the bulk foam density did not change significantly compared to the unfoamed neat hydrolyzed starch/PLA blend.

The micrographs shown in Figure 7.24 indicated that the foamed samples had a closed-cell structure with thicker cell walls and irregular shape. The high saturation pressures (15 MPa and 20 MPa) did not produced skin-core foam morphology structure as seen in the neat Solanyl® blend 30R due to the high melt viscosity and high gas concentration in the polymer matrix at those conditions. Table 7.2 presented the effect of saturation pressures (15 MPa and 20 MPa) on the bulk foam density, weight average cell size, and average cell density of the neat hydrolyzed starch/PLA blend.

15 MPa **20 MPa**

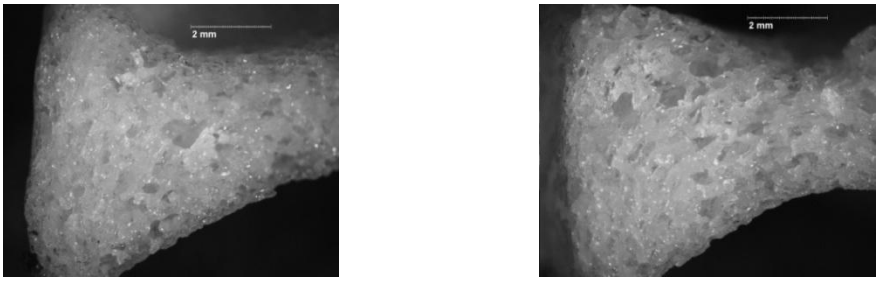

(a) (b)

Figure 7.24 Optical micrographs of foamed neat hydrolyzed starch/PLA (SP-0.0-CE-TSE) different saturation pressures and 60 min saturation time

Table 7.2 Effect of saturation pressures on the bulk foam density, weight average cell size and cell density of foamed neat hydrolyzed starch/PLA (SP-0.0-CE-TSE) at 60 min saturation time

Saturation Pressure	Bulk Foam Density	Weight Average Cell Size	Average Cell Density
(MPa)	(g/cm^3)	(mm)	(# $Cells/cm^3$)
15	0.590±0.02	0.315± 0.170	15179±5836
20	0.568±0.01	0.195± 0.095	24611±4623

At 15 MPa, the smaller cells (0.315± 0.170 mm) were found to have grown uniformly throughout the polymer matrix Figure 7.24 (a). However, the smaller cell size in the neat hydrolyzed starch/PLA blend compared to the neat foamed Solanyl® blend 30R (0.907 ± 0.447 mm and Figure 7.2 (e)) at same conditions was due to the lack of a low viscosity components (aliphatic-aromatic copolymer) now. The significantly high melt viscosity of the neat hydrolyzed starch/PLA blend offered greater resistance to cell growth and also reduced the gas diffusivity (Di et al., 2005). Consequently, the cell

density increased significantly (15179±5836 cells/cm^3) compared to the neat foamed Solanyl® blend 30R (1205±442 cells/cm^3) at the same conditions. The smaller cells size (seen by the micrographs in Figure 7.24 (a) and from the size distribution plots in Figure 7.25 (a)) and higher cell density into the polymer matrix consequently decreased the bulk foam density to 0.590±0.02 g/cm^3 at 15 MPa. However, with a further increase in the saturation pressure (20 MPa), the cell density increased (24611± 4623 cells/cm^3), but the average cell size decreased to 0.195± 0.095 mm. The high pressure promoted greater thermodynamic instability in the polymer matrix and high melt viscosity offered greater resistance to cell growth, which result in higher cell density and smaller weight average cell size (Di et al., 2005). The bulk foam density further reduced to 0.568±0.01 g/cm^3. However, the cell shrinkage effect during the 2 min time lag and cooling stage in the foamed neat hydrolyzed starch/PLA blend was less pronounced due to significantly higher melt strength of the neat hydrolyzed starch/PLA blend compared to neat Solanyl®

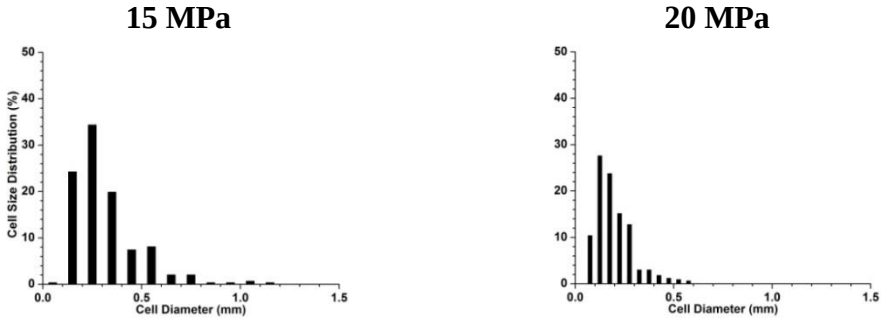

(a) 0.315± 0.168 mm (b) 0.195± 0.095 mm

Figure 7.25 Cell size distributions (%) of foamed neat hydrolyzed starch/PLA 7000D (SP-0.0-CE-TSE) different saturation pressures and 60 min saturation time (The weight average cell diameter and standard deviation shown below each image)

blend 30R and relative high gas concentration in the cells at high pressures and saturation time.

7.2.1 MORPHOLOGY OF FOAMED HYDROLYZED STARCH/PLA BLEND WITH ADR 4370S

The presence of CE did not improve the foamed samples cell morphology for the modified blends with ADR 4370S compared to the neat foamed blend at both level of saturation pressures. From the micrograph (Figure 7.26 (a)), it was observed that the smaller cells (0.192± 0.082 mm) were observed mostly at the skin of the modified blend and the core part remained unfoamed. However, this skin-core foam morphology was similar to what we observed in the modified Solanyl® blend 30R with ADR 4380 (Figure 7.8 and 7.10) in spite of the significant higher melt viscosity of the modified hydrolyzed starch/PLA blend with 0.5 wt % ADR 4370S CE (Section 6.2.2).

At 15 MPa, the gas was uniformly distributed into the modified blend with 0.5 wt % ADR 4370S CE. The significant higher melt viscosity of modified blend and higher pressure drop produced the smaller cells across the polymer matrix during the depressurization. As the gas diffusion rate would be very slow in the high viscosity polymer matrix, the cell would grow very slow during the cell growth stage. The smaller cells were more likely to collapse due to the low gas concentration during 2 min time lag. The smaller cells were also collapsed at the core due to the slow cooling rate of core when sample was removed from the vessel. As a result, the unfoamed core structure was observed in the micrograph (Figure 7.26 (a)). The smaller cells at the periphery would

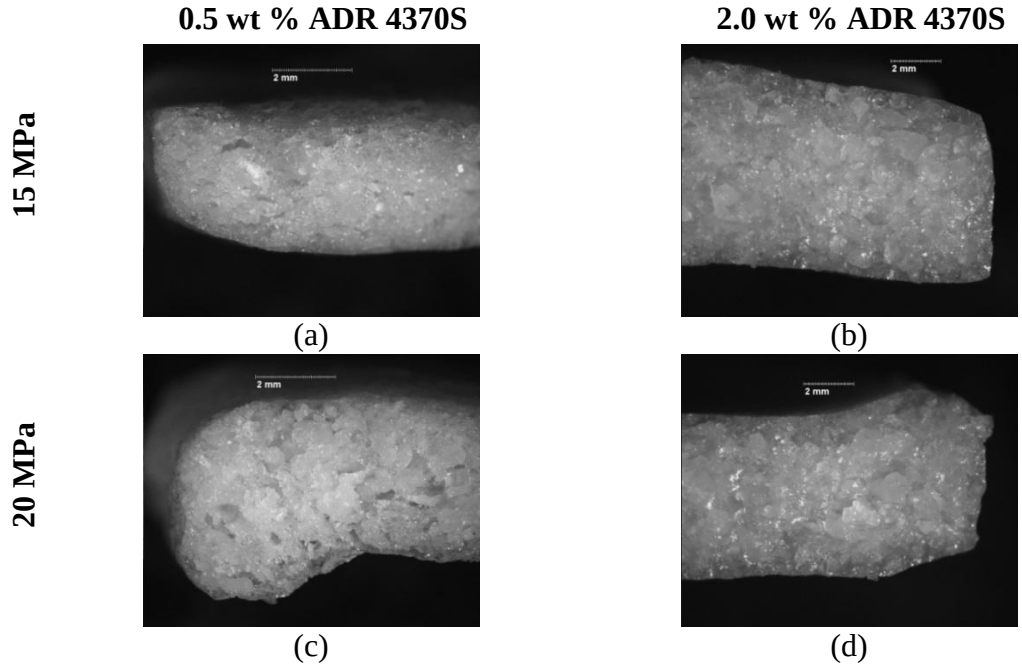

Figure 7.26 Optical micrographs of foamed hydrolyzed starch/PLA and ADR 4370S CE with different saturation pressures and 60 min saturation time

more likely to survive due to rapid cooling of the skin, when sample was removed from the vessel. As a result, skin-core cell morphology had been observed in the modified blend with 0.5 wt % ADR 4370S CE despite of higher melt viscosity of the modified blend. The smaller weight average cell size (0.192± 0.081 mm) at the periphery and more unfoamed core structure increased the bulk foam density of the modified hydrolyzed starch/PLA blend with 0.5 wt % CE to 0.783±0.03 g/cm^3 (Figure 7.28).

Addition of 2.0 wt % CE in hydrolyzed starch/PLA blend, the bigger cells (0.428±0.144mm) were observed at the skin and more unfoamed structure at the core (Figure 7.26 (b)) would result in further increased in the bulk foam density to 1.135±0.02 g/cm^3(Figure 7.28). At 20 MPa, the cell morphology of the modified blend did not

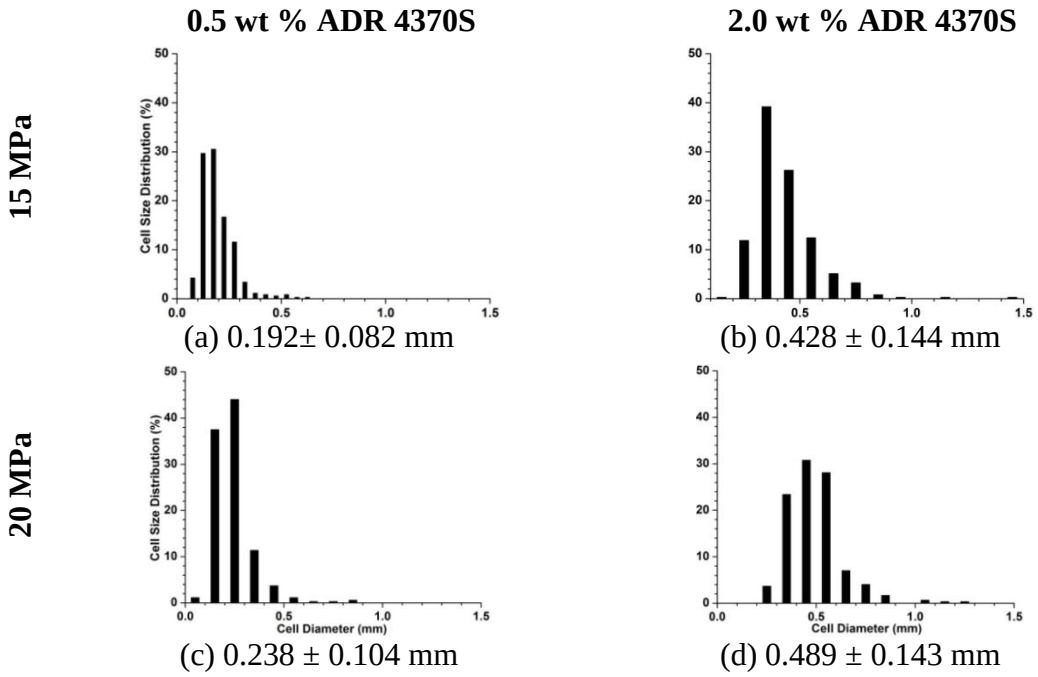

(a) 0.192± 0.082 mm (b) 0.428 ± 0.144 mm

(c) 0.238 ± 0.104 mm (d) 0.489 ± 0.143 mm

Figure 7.27 Cell size distributions (%) of foamed hydrolyzed starch/PLA and ADR 4370S CE with different saturation pressures and 60 min saturation time (The weight average cell diameter and standard deviation shown below each image)

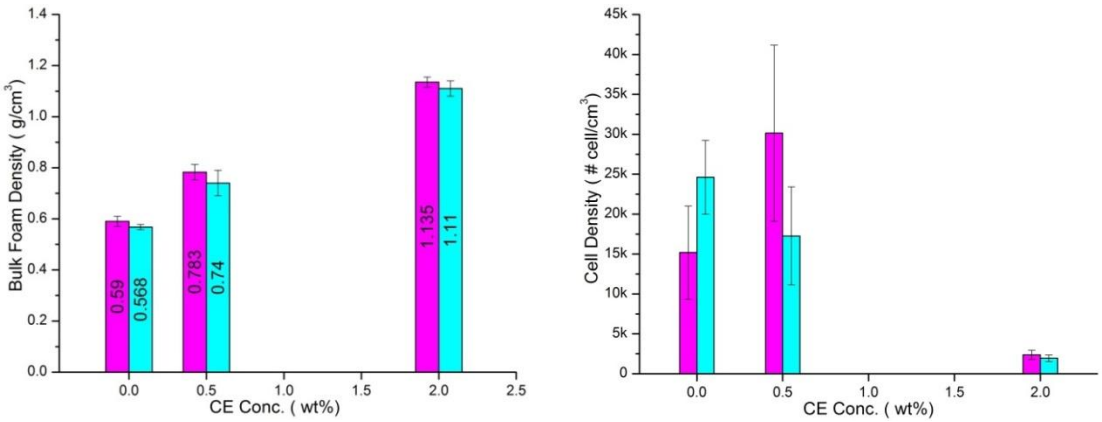

Figure 7.28 Effect of ADR 4370S CE concentration on the bulk foam density and cell density of foamed hydrolyzed starch/PLA for 60 min saturation time (■ 15 MPa and ■ 20 MPa)

change significantly (Figure 7.26 (c), (d)). The bulk foam density was increased at both levels of CE (Figure 7.28) due to more unfoamed core structure, while the weight average cell size increased due to high gas concentration in the polymer matrix at 20 MPa.

7.2.2 MORPHOLOGY OF FOAMED HYDROLYZED STARCH/PLA BLEND WITH ADR 4380

The micrographs shown in Figure 7.29 indicated that the addition of CE improved the cell morphology of the modified blend at all levels of CE compared to previously investigated ADR 4370S (Section 7.2.1). Our rheological study with modified hydrolyzed starch/PLA blend with CE showed that the addition of ADR 4380 CE did not increased the melt viscosity significantly compared to the modified hydrolyzed starch/PLA blend with ADR 4370S CE (Section 6.2.1 for ADR 4380 and Section 6.2.2 for ADR 4370S).

At 15 MPa, the smaller cells were produced during depressurization, but the higher gas diffusion rate (low melt viscosity) compared to the modified blend with ADR 4370S during cell growth stage result in the bigger cells, which would survived during 2 min time lag and cooling period at the core as well as the periphery of the foamed sample. The weight average cell size was decreased from 0.211 ± 0.093 mm (Figure 7.30 (a)) to 0.160 ± 0.064 mm (Figure 7.30 (b)) and cell density increased (Figure 7.31) as CE content increased from 0.5 wt % to 2.5 wt % CE at 10 MPa.

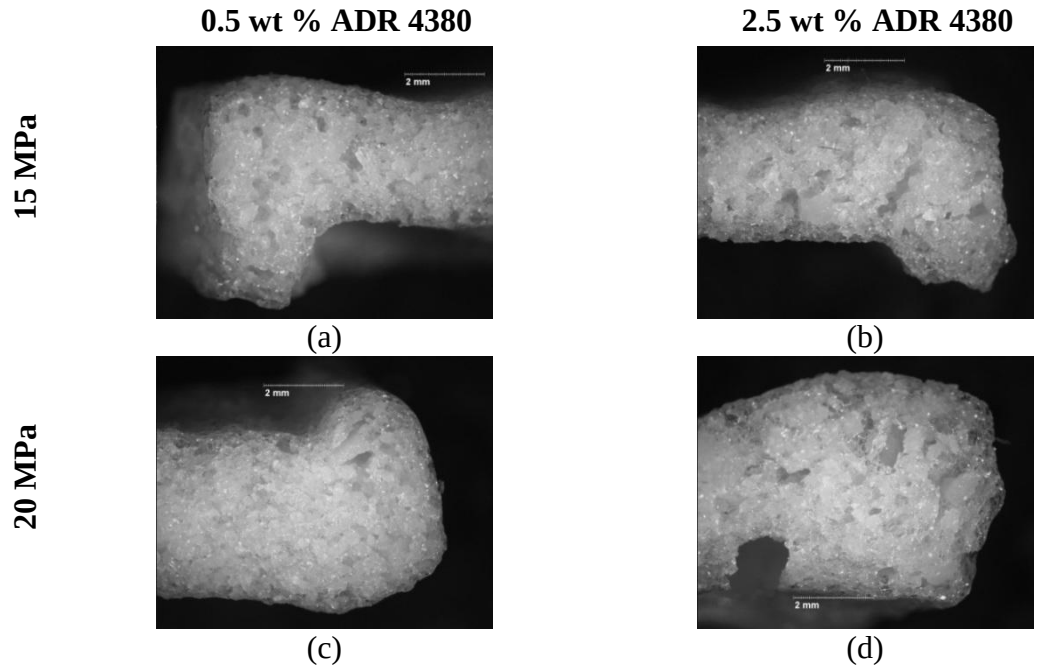

Figure 7.29 Optical micrographs of foamed hydrolyzed starch/PLA and ADR 4380 CE with different saturation pressures and 60 min saturation time

The same trend did not observed for the average cell size (Figure 7.30 (c), (d)) and cell density (Figure 7.31) at the 20 MPa due to the high gas concentration in the polymer matrix. However, the bulk foam density did not change significantly for the modified blends compared to the foamed neat blend at all levels of CE and both saturation pressures.

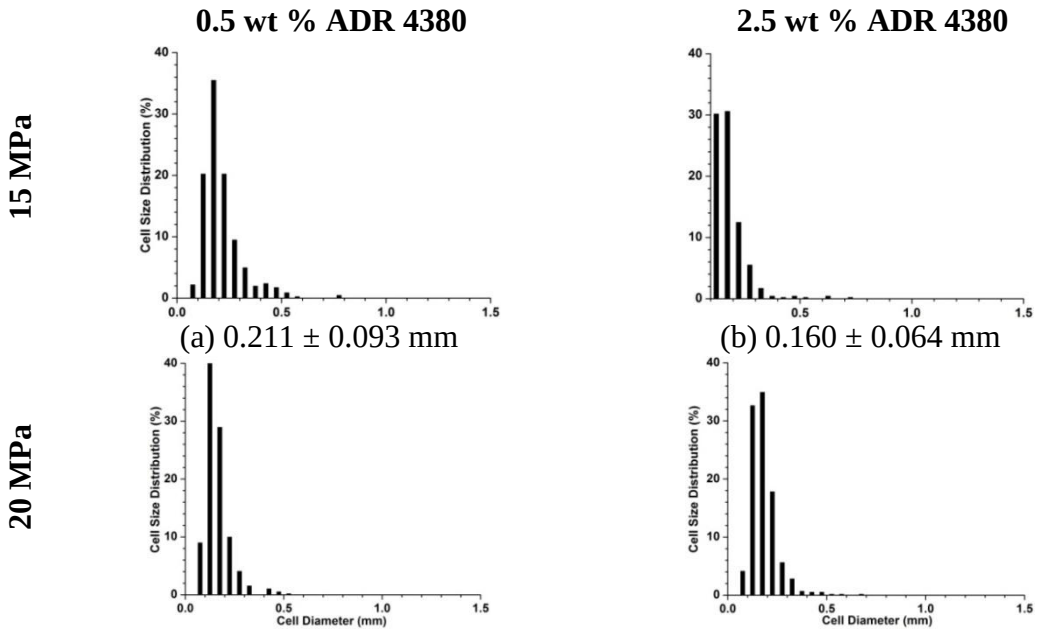

(a) 0.211 ± 0.093 mm (b) 0.160 ± 0.064 mm

(c) 0.163 ± 0.078 mm (d) 0.179 ± 0.069 mm

Figure 7.30 Cell size distributions (%) of foamed hydrolyzed starch/PLA and ADR 4380 CE with different saturation pressures and 60 min saturation time (The weight average cell diameter and standard deviation shown below each image)

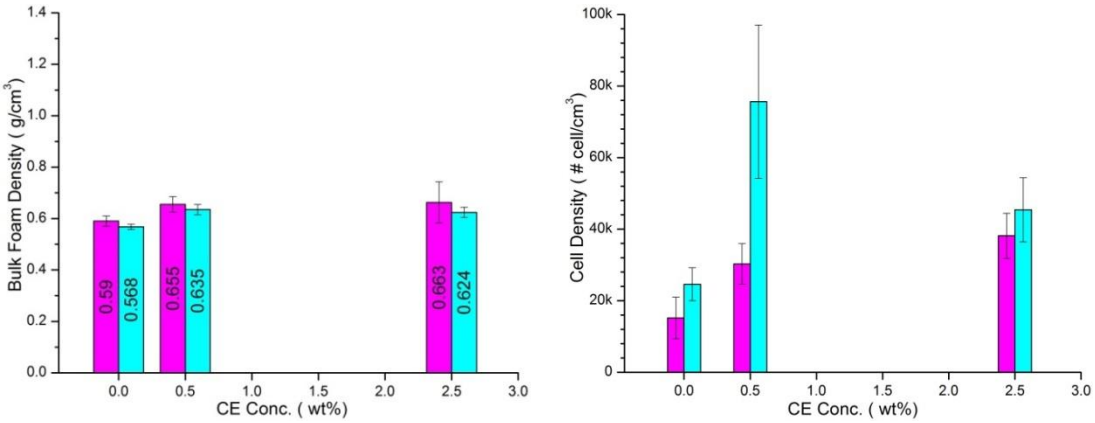

Figure 7.31 Effect of ADR 4380 CE concentration on the bulk foam density and cell density of foamed hydrolyzed starch/PLA for saturation pressure (■ 15 MPa, ■ 20 MPa) and 60 min saturation time

7.2.3 MORPHOLOGY OF FOAMED HYDROLYZED STARCH/PLA BLEND WITH DGEBA

The micrographs presented in Figure 7.32 showed the same cell morphology as it was observed in the previously investigated ADR 4380 CE at both levels of CE (Section 7.2.2) and the neat foamed samples (Section 7.2) for both saturation pressures. Our rheological study indicated that the addition of this low-molecular weight bi-functional CE did not increase the melt viscosity of modified blend significantly compared to the neat blend (Section 6.2.3). Addition of CE decreased the average cell size (Figure 7.33 (a), (b)) and increased the cell density (Figure 7.34) as CE content increased from 0.5 wt % to 2.5 wt % at 15 MPa compared to neat foamed samples. The cell shrinkage effect

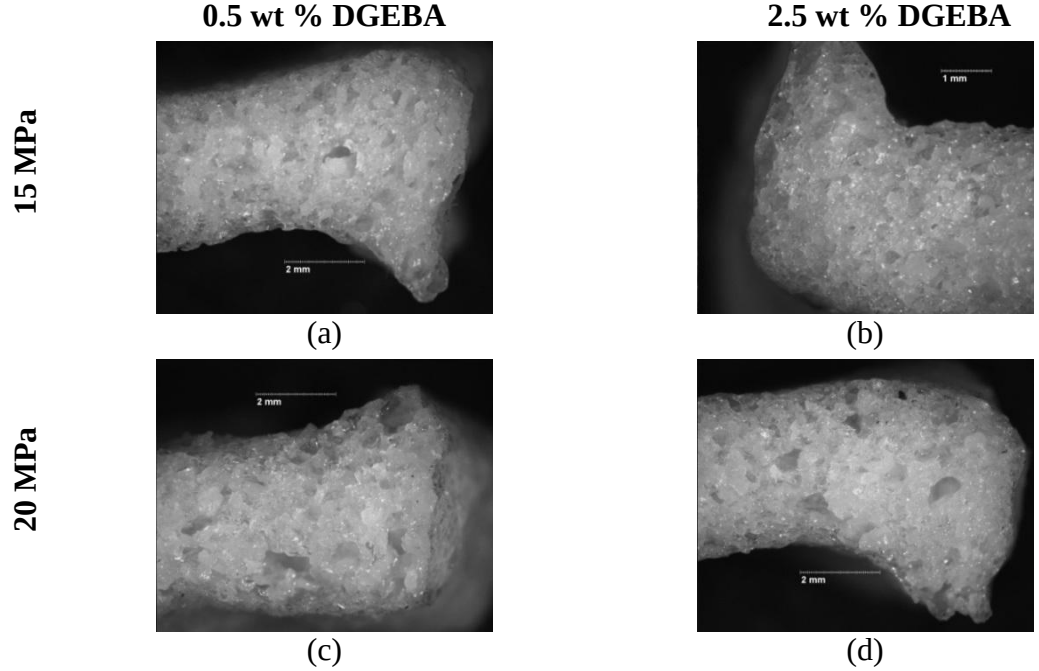

Figure 7.32 Optical micrographs of foamed hydrolyzed starch/PLA and DGEBA CE with different saturation pressures and 60 min saturation time

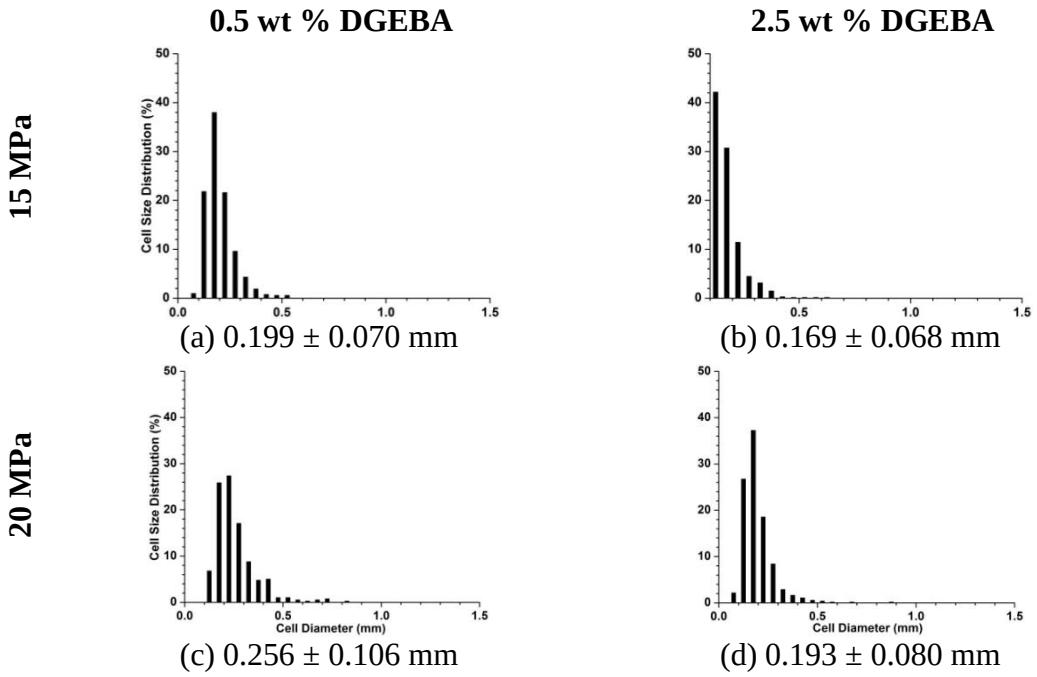

(a) 0.199 ± 0.070 mm (b) 0.169 ± 0.068 mm

(c) 0.256 ± 0.106 mm (d) 0.193 ± 0.080 mm

Figure 7.33 Cell size distributions (%) of foamed hydrolyzed starch/PLA and DGEBA CE with different saturation pressures and 60 min saturation time (The weight average cell diameter and standard deviation shown below each image)

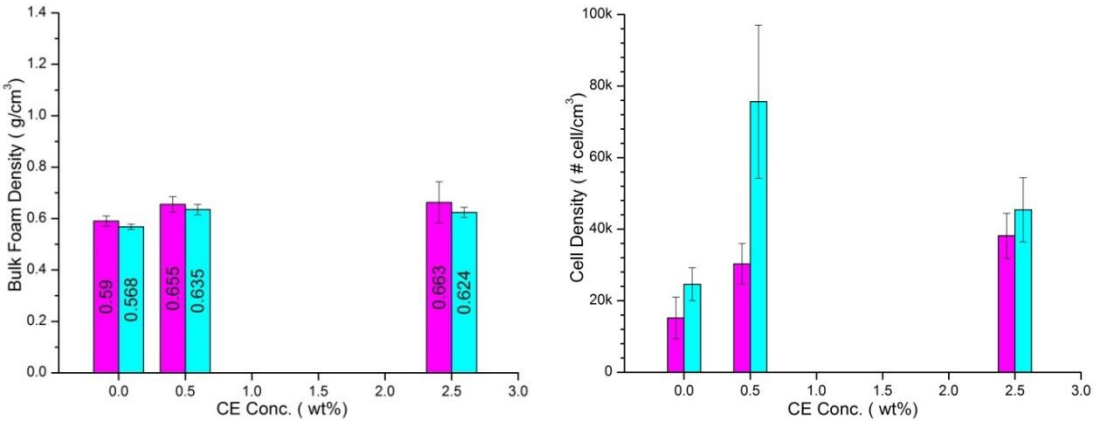

Figure 7.34 Effect of ADR 4380 CE concentration on the bulk foam density and cell density of foamed hydrolyzed starch/PLA for saturation pressure (■ 15 MPa, ■ 20 MPa) and 60 min saturation time

could be less pronounced in the modified blend due to relative higher gas concentration and bigger cells were produced during decompression. The same trend was also observed at 20 MPa for the average cell size (Figure 7.33 (c), (d)) and the cell density (Figure 7.34). The bulk foam density did not change significantly for the modified blends compared to the foamed neat blend at all levels of CE and both saturation pressures.

7.2.4 MORPHOLOGY OF FOAMED HYDROLYZED STARCH/PLA BLEND WITH PEG-DGE

The micrographs of foamed samples with PEG-DGE CE were not presented due to the similar cell morphology between the foamed samples with PEG-DGE and DGEBA CEs at 15 MPa and 20 MPa saturation pressure. Our rheological study indicated the identical melt viscosity behaviour between the modified blend with PEG-DGE and DGEBA (Section 6.2.4 for PEG-DGE and Section 6.2.3 for DGEBA) at all levels of CE.

At 15 MPa, the weight average cell size (Figure 7.35 (a) (b)) decreased and cell density (Figure 7.36) increased as CE level increased from 0.5 wt % to 2.5 wt % for the foamed samples of the modified blends. The cell shrinkage effect could be less pronounced in the modified blend due to relative higher gas concentration and bigger cell size produced during decompression. Increased in pressure to 20 MPa, the weight average cell size and the cell density did not make any significant difference as CE contents increased suggested the solubility limit has been reached in the polymer matrix. The bulk foam density did not change significantly for the modified blends compared to the foamed neat blend at all levels of CE and both saturation pressures.

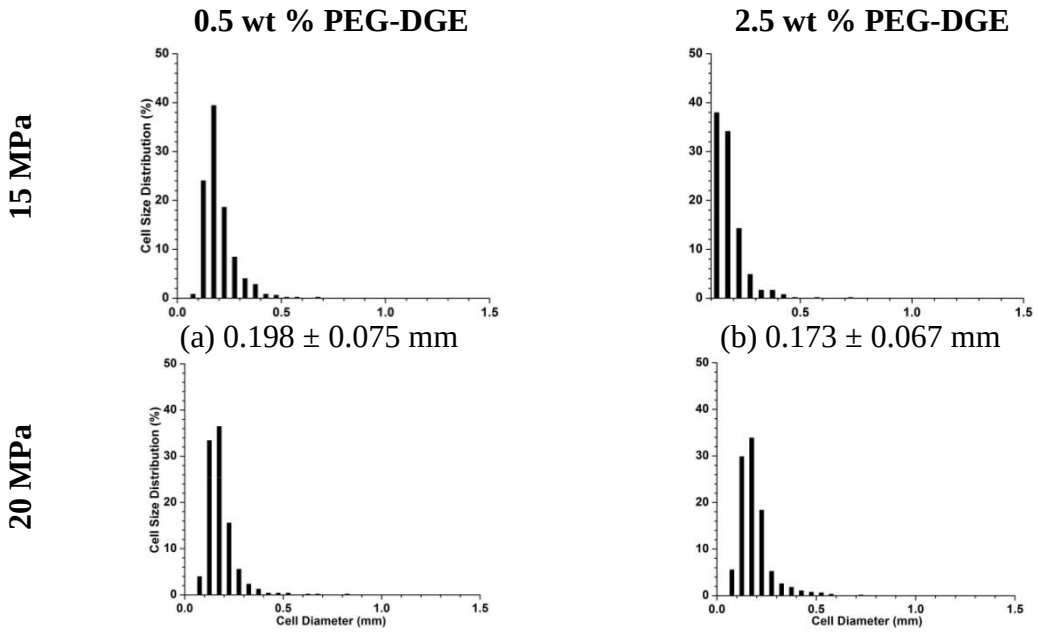

(a) 0.198 ± 0.075 mm (b) 0.173 ± 0.067 mm

(c) 0.180 ± 0.076 mm (d) 0.185 ± 0.080 mm

Figure 7.35 Cell size distributions (%) of foamed hydrolyzed starch/PLA and PEG-DGE CE with different saturation pressures and 60 min saturation time (The weight average cell diameter and standard deviation shown below each image)

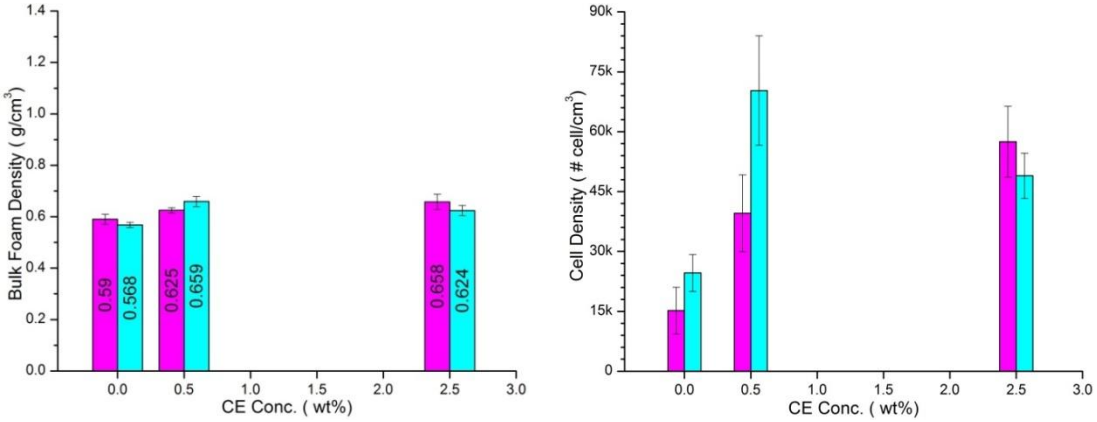

Figure 7.36 Effect of PEG-DGE CE concentration on the bulk foam density and cell density of foamed hydrolyzed starch/PLA for saturation pressure (■ 15 MPa, ■ 20 MPa) and 60 min saturation time

CHAPTER: 8

CONCLUSION AND FUTURE WORK

Two types of epoxy-styrene-acrylic oligomer chain extenders (Joncryl® ADR 4370S and Joncryl® ADR 4380) and two types of low-molecular weight epoxy chain extenders (DGEBA and PEG-DGE) were studied to increase the foamability of hydrolyzed starch based biopolymer blends. The effects of each chain extender on the thermal and rheological properties of the novel potato starch biopolymers (Solanyl® blend 30R and the hydrolyzed starch/PLA blend) were studied by using DSC and parallel plate rheometry, respectively. SEM and Intrinsic Viscosity techniques were employed to access the structural changes made to the modified blends with chain extenders. Finally, the foamability of the modified hydrolyzed starch/PLA blends and its corresponding

commercial biopolymer (Solanyl® blend 30R) based on the different chain extenders content was evaluated using a high-pressure batch foaming apparatus. The effect of the saturation pressure, saturation time and saturation temperature on the cell morphology of the foamed parts were evaluated.

8.1 CONCLUSION

It was found that the multi-functional epoxy-styrene-acrylic ADR 4370S was the most effective chain extender for increasing the shear viscosity and melt elasticity of both Solanyl® biopolymer blends (Solanyl® blend 30R and hydrolyzed starch/PLA blends) in comparison to neat blends and those modified with other low-molecular weight epoxy CEs (ADR 4380, DGEBA and PEG-DGE).

The increase in the shear viscosity and melt elasticity were attributed to the actual chain extension reaction which predominantly occurred in the PLA phase of either the modified Solanyl® blend 30R or the PLA/AAC phase of the modified hydrolyzed starch/PLA blend only. The chain extension also compensated for the molecular weight loss of PLA or PLA/AAC phase due to thermal hydrolysis detected in the results due to the presence of moisture; chain extension also decreased the crystallinity of the corresponding phases for both modified Solanyl® biopolymer blends. The starch phase made no detectable contribution toward the increase in the bulk shear viscosity of the modified blends and it suffered excessive degradation with loss of molecular weight during thermal processing.

The increased shear viscosity and melt elasticity of the modified Solanyl® blend 30R with multi-functional ADR 4370S chain extender improve the stability of foams generated during batch foaming process. It was concluded that the ADR 4370S was the effective chain extender for the production of Solanyl® blend 30R foams with the smaller cell size and higher cell density compared to the neat Solanyl® blend 30R blend at even 10 MPa saturation pressure and 30 min saturation time. Compared to neat Solanyl® blend 30R, the cell morphology of the neat hydrolyzed starch/PLA blend was significantly different, with smaller cell size and higher cell density at even higher saturation pressure (15 MPa and 20 MPa) and 60 min saturation time. These being due to inherently higher melt viscosity of the neat hydrolyzed starch/PLA blend. The use of higher epoxy functionality multi-functional ADR 4370S chain extender was not as effective in producing uniform cell morphology in hydrolyzed starch/PLA blend at those processing conditions due to the significant higher melt viscosity of modified blend, which reduced the gas diffusion rate during the batch foaming process.

The other chain extenders (ADR 4380, DGEBA and PEG-DGE) were not effective for increasing the melt viscosity of modified Solanyl® biopolymer blends (Solanyl® blend 30R and hydrolyzed starch/PLA blends). Intrinsic Viscosity measurement dictated the use of those chain extenders at higher concentration largely acted as a plasticizer for both Solanyl® biopolymer blends (Solanyl® blend 30R and hydrolyzed starch/PLA blends) and obscured any effects of the chain extension or branching that had occurred. The poor cell morphology of the modified Solanyl® blend

30R with other CEs (ADR 4380, DGEBA and PEG-DGE) at 10 MPa saturation pressure and 30 min saturation time were due to low gas concentration and high cell collapsing (low melt viscosity) phenomenon of the corresponding modified blends during foaming process. However, the higher saturation pressure (15 MPa and 20 MPa) and 60 min saturation time required in those modified blends for the uniform cell morphology across the polymer matrix. Due to the inherent high melt viscosity of the neat hydrolyzed starch/PLA blend, the moderate increased in shear viscosity and melt elasticity by using low-functionality epoxy CEs (ADR 4380, DGEBA and PEG-DGE) was sufficient for producing the uniform cell structure across polymer matrix at higher saturation pressure (15 MPa and 20 MPa) and 60 min saturation time during the batch foaming process.

The SEM analysis indicated that the addition of epoxy-styrene-acrylic multi-functional CE (ADR4370S) did not improve the blend's interface and did not sufficiently alter the blends morphology during dispersive mixing for both modified Solanyl® biopolymers (Solanyl® blend 30R and hydrolyzed starch/PLA blends).

8.2 FUTURE WORK

Since, the Solanyl® biopolymers are injection-molding grade resins, the possible future work from this research include the modification of Solanyl® biopolymers with chain extenders directly into the injection-molding machine. Also, producing foamed injection-molded parts of the modified Solanyl® biopolymers by using physical blowing agent (supercritical CO_2) or chemical blowing agent would be useful for the comparison

of its mechanical, water absorption and water vapour transmission properties with corresponding unfoamed injection-molded parts.

Solanyl® biopolymers are fully biodegradable and compostable resins, the biodegradability of the modified materials with chain extenders should be evaluated as well. In addition, as in our work we did not directly estimate the supercritical CO_2 solubility in the modified blend with chain extenders, the fundamental study on the supercritical CO_2 solubility of the modified polymer matrix should be conducted.

CHAPTER: 9

REFERENCES

http://www.greenerpackage.com/bioplastics/biodegradable_polymers_market_grow_13_through_2014

Aggarwal, P., Dollimore, D. (1998). A Thermal Analysis Investigation of Partially Hydrolyzed Starch, *Thermochimica Acta*, 319, 17-25

Auras, R., Harte, B., Selke, S. (2004). An Overview of Polylactides as Packaging Materials, *Macromolecular Bioscience*, 4, 835-864

Averous, L. H. (2004). Biodegradable Multiphase Systems based on Plasticized Starch: A review, *Journal of Macromolecular Science*, C44 (3), 231-274

Averous, L. H., Halley P. J. (2009). Biocomposites based on plasticized starch. Biofuels, Bioproducts, and Biorefining, 3,329 – 343

BASF, (2009). Product Information: Ecoflex® F BX 7011 – 22.1.2009 Biodegradable polyesters for compostable film, Version 2.1

Bastioli, C. (2005). Handbook of Biodegradable Polymers, Rapra Technology Limited, pp. 260

Bhatnagar, S., Hanna, M.A. (1995). Physical, Mechanical and Thermal Properties of Starch-Based Plastic Foams, Trans. ASAE, 38,567-571

Blanshard, J.M.V. (1987). Starch Granule Structure and Function: a physicochemical approach. In: Galliard, T., (Ed.), Starch: Properties and Potential, Wiley, Chichester, 16–54

Burt, D.J., Russell, P.L. (1983). Gelatinization of Low Water Content Wheat Starch-Water Mixtures, *Starch*, 35(10), 354-360

David, J., Vojtova, L., Bednarik, K., Kucerik, J., Vavrova, M., Jancar, J. (2010). Development of Novel Environmental Friendly Polyurethane Foams, *Environmental Chemistry Letters*, 8(4), 381-385

Dealy, J.M., Wissbrun, K.F. (1989). Melt Rheology and its Role in Plastic Processing: theory and application, Van Nostrand Reinhold, New York

Deenadayalan, E., Lele, A.K., Balasubramanian, M. (2009). Reactive Extrusion of Poly (L-lactic Acid) with Glycidol, *Journal of Applied Polymer Science*, 112, 1391-1398

Della Valle, G., Boche, Y., Colonna, P., Vergnes, B. (1995). The extrusion behaviour of potato starch, *Carbohydrate Polymer*, 28, 255-264

Di, Y., Iannace, S., Di Maio E., Nicolais, L. (2005). Reactively Modified Poly(lactic acid): Properties and Foam Processing, *Macromolecular Materials and Engineering*, 290, 1083-1090

Donovan, J.W. (1979). Phase Transitions of the Starch-Water System, *Biopolymers*, 18, 263-275

Drumright, R.E., Bruber, P.R., Henton, D.E. (2000). Polylactic Acid Technology, *Advanced Materials*, 12 (23), 1841-1846

Eliasson, A.C. (1980). Effect of Water Content on the Gelatinization of Wheat Starch, *Starch*, 32(8), 270-272

Fang, Q., Hanna, M.A. (2000). Functional Properties of Polylactic acid Starch-Based Loose-fill Packaging Foams. *Cereal Chemistry*, 77(6), 779-783

Fang, Q., Hanna, M.A. (2001). Preparation and Characterization of Biodegradable Copolyester-Starch Based Foams, 78, 115-122

Fujimoto, Y., Ray, S.S., Okamoto, M., Ogami, A., Yamada, K., Ueda, K. (2003). Well-Controlled Biodegradable Nanocomposites Foams: From Microcellular to Nanocellular, *Macromolecular Rapid Communications*, 24,457-461

Garlotta, D. (2001). A Literature Review of Poly (Lactic Acid), *Journal of Polymers and the Environment*, 9, 63-84

Glenn, G.M., Irving, D.W. (1995). Starch-Based Microcellular Foams, 72(2), 155-161

Glenn, G.M., Klamczynski, A.K., Holtman, K.M., Shey, J., Chiou, B., Berrios, J., Wood, D., Orts, W.J., Imam, S.H. (2007). Heat Expanded Starch-Based Compositions, *Journal of Agriculture Food Chemistry*, 55, 3936-3843

Goel, S.K., Beckman, E.J. (1994a). Generation of Microcellular Polymeric Foams Using Supercritical Carbon Dioxide. I: Effect of Pressure and Temperature on Nucleation, *Polymer Engineering and Science*, 34(14), 1137-1147

Goel, S.K., Beckman, E.J. (1994b). Generation of Microcellular Polymeric Foams Using Supercritical Carbon Dioxide. I: Cell Growth and Skin Formation, *Polymer Engineering and Science*, 34(14), 1148-1156

Guan, J., Hanna, M.A. (2005). Selected Morphological and Functional Properties of Extruded Acetylated Starch-Polylactic Acid Foams, *Industrial & Engineering Chemistry Research*, 44, 3106-3115

Hao, A., Geng, Y., Xu, Q., Lu, Z., Yu, L. (2008). Study of Different Effects on Foaming Process of Biodegradable PLA/Starch Composites in Supercritical/Compressed Carbon Dioxide, *Journal of Applied Polymer Science*, 109, 2679–2686

Haralabakopoulos, A.A., Tsiourvas, D., Paleos, C.M. (1998). Chain Extension of Poly(ethylene terephthalate) by Reactive Blending Using Diepoxides, *Journal of Applied Polymer Science*, 71, 2121-2127

Harper, J., (1989). Food extruders and their applications. In: Mercier, C., Linko, P.,Harper, J. (Eds.), Extrusion Cooking. *American Association of Cereal Chemists*, St. Paul, pp. 1–15

Hermansson, A., Svegmark, K. (1996). Developments in the Understanding of Starch Functionality, *Trends in Food Science & Technology*, 7, 345-353

Huda, M.S., Drzal, L.T., Misra, M., Mohanty, A.K. (2006). Wood –Fiber-Reinforced Poly (lactic acid) Composites: Evaluation of the Physicomechanical and Morphology Properties, *Journal of Applied Polymer Science*, 102, 4856-4869

Huneault M.A., Li H. (2007). Morphology and Properties of Compatibilized Polylactide/Thermoplastic Starch Blends, *Polymer*, 48,270-280

Jacobsen, S., Fritz, H.G. (1999). Plasticizing Polylactide – The Effects of Different Plasticizers on the Mechanical Properties, *Polymer Engineering and Science*, 39(7), 1303-1310

Jang, W.J., Shin, B.Y., Lee, T.J., Narayan, R. (2007). Thermal Properties and Morphology of Biodegradable PLA/Starch Compatibilized Blends, *Journal of Industrial and Engineering Chemistry*, 13(3), 457-464

Jiang, L., Wolcott, M.P., Zhang, J. (2006). Study of biodegradable Polylactide/Poly (butylenes adiapate-co-terephthalate) blends, Biomacromolecules, 71, 19-207

Ke, T., Sun, X. (2000). Physical Properties of Poly (lactic acid) and Starch Composites with Various Blending Ratios, *Cereal Chemistry*, 77(6), 761-768

Ke, T., Sun, X. (2003). Melting Behaviour and Crystallization Kinetics of Starch and Poly (lactic acid) Composites, *Journal of Applied Polymer Science*, 89, 1203-1210

Klempner, D., Sendijarevic, V. (2004). Handbook of Polymeric Foams and Foam Technology, Second Edition, Hancer, Munich

Kramschuster, A., Pilla, S., Gong, S., Chandra, A., Turng, L. (2007). Injection Molded Solid and Microcellular Polylactide Compounded With Recycled Paper Shopping Bag Fibers. *International Polymer Processing*, 22(5), 436-445

Labrecque, L.V., Kumar, R.A., Dave, V., Gross, R.A., McCarthy, S.P. (1997). Citrate Ester as Plasticizers for Poly (lactic acid), *Journal of Applied Polymer Science*, 66, 1507-1513

Lee, M.W., Ho, S.Y., Lim, K.P., Ng, T.T, Juay, Y.K. (2008a). Development of Biocomposites with Improved Mechanical Properties, *SIMTech Technical Reports*, 9(3), 115-118

Lee, S.T., Kareko, L., Jun, J. (2008b). Study of Thermoplastic PLA Foam Extrusion, *Journal of Cellular Plastics*, 44, 293-305

Lee, S.T. (2000). Foam Extrusion: Principles and Practice, Technomic Publications, Lancaster, Basel

Li, H., Huneault, M.A. (2007). Effect of Nucleation and Plasticization on the Crystallization of Poly (lactic acid), *Polymer*, 48, 6855-6866

Li, H., Huneault, M.A. (2011). Effect of Chain extension on the Properties of PLA/TPS Blends, *Journal of Applied Polymer Science*, 122(1), 34-141

Liao, H., Wu, C. (2009). Preparation and Characterization of Ternary Blends Composed of Polylactide, Poly(ε-caprolactone) and Starch, *Material Science and Engineering*, A-515, 207-214

Lim, L.T., Aurus, R., Rubino, M. (2008). Processing Technology for Poly (lactic acid), *Progress in Polymer Science*, 33, 820-852

Lim, M.H., Wu, H., Reid, D.S. (2000). The Effect of Starch Gelatinization and Solute Concentrations on T_g' of Starch Model System, *Journal of the Science of Food and Agriculture*, 80, 1757-1762

Liu, Q. (2002). A Study of Enzymatic Hydrolysis of Starch in Potato Pulp, *Journal of Food Science*, 67(6): 2113-2117

Liu, Q. (2005). Food Carbohydrates: Chemistry, Properties and Applications, Chapter 7, 309-406

Martin, O., Averous, L. (2001). Poly (lactic acid): Plasticization and Properties of Biodegradable Multiphase Systems, *Polymer*, 42, 6209-6219

Martini, J.E., Suh, N.P., Waldman, F.A. (1984). Microcellular Closed Cell Foams and their Method of Manufacturing, US Patent No. 4,473,665

Matuana, L.M. (2008). Solid State Microcellular Foamed Poly (lactic acid): Morphology and Property Characterization, *Bioresource Technology*, 99, 3643-3650

Matuana, L.M., Faruk, O., Diaz, C.A. (2009). Cell Morphology of Extrusion Foamed Poly (lactic acid) using Endothermic Chemical Foaming Agent, *Bioresource Technology*, 100, 5947-5954

Mihai, M., Huneault M.A., Favis B.D., Li, H. (2007). Extrusion foaming of Semi-Crystalline PLA and PLA/Thermoplastic Starch Blends, Macromolecular Bioscience, 7, 907-920

Mihai, M., Huneault, A.A., Favis, B.D. (2010). Rheology and Extrusion Foaming of Chain-Branched Poly(lactic acid), *Polymer Engineering and Science*, 50(3), 629-642

Mohanty, A. K.., Misra, M., Hinrichsen G. (2000). Biofibres, Biodegradable Polymers and Biocomposites: An overview, *Macromolecular Materials and Engineering*, 276/277, 1-24

Muller, R.J., Witt, U., Rantze, E., Deckwer, W.D. (1998). Architecture of biodegradable copolyesters containing aromatic constituents, *Polymer Degradation and Stability*, 59, 203-208

Nampoothiri, K. M., Nair, N.R., John, R.P. (2010). An Overview of the recent Developments in Polylactide (PLA) Research, *Bioresources Technology*, 101, 8493-8501

Ning, W., Jiugao, Y., Xiaofei, M. (2008). Preparation and Characterization of Compatible Thermoplastic Dry Starch/Poly (lactic acid), Polymer Composites, 29(5), 551-559

Oliveira, C.I.R., Cunha, F.R., Andrade, C.T. (2010). Evaluation of biodegradability of different blends of polystyrene and starch buried in soil, *Macromolecules Symposia*, 290(1), 115-120

Park, J.W., Im, S.S., Kim, S.H., Kim, Y.H. (2000). Biodegradable Polymer Blends of Poly (lactic acid) and Gelatinized Starch, *Polymer Engineering and Science*,40(12), 2539-2550

Pilla, S., Gong, S., O'Neill, E., Rowell, R.M., Krzysik, A.M. (2008). Polylactide-Pine Wood Flour Composites, *Polymer Engineering and Science*, 48(3), 578-587

Pilla, S., Kim, S.G., Auer, G.K., Gong, S., Park, C.B. (2009). Microcellular Extrusion-Foaming of Polylactide with Chain-Extenders, *Polymer Engineering and Science*, 49(8), 1654-1660

Poutanen, K., Forssell, P. (1996). Modification of Starch Properties with Plasticizers, *Trends in Polymer Science*, 4 (4), 128-132

Pushpadass, H.A., Babu, G.S., Weber, R.W., Hanna, M.A. (2008). Extrusion of Starch-based Loose-fill Packaging Foams: Effect of Temperature, Moisture and Talc on Physical Properties, *Packaging Technology and Science*, 21,171-183

Qu, D., Wang, S.S. (1994). Kinetics of the Formations of Gelatinized and Melted Starch at Extrusion Cooking Condition, *Starch*, 46 (6), 225-229

Reignier, J., Gendron, R., Champagne, M.F. (2007). Extrusion Foaming of Poly (lactic acid) Blown with CO_2: Toward 100% Green Material, 26(2), 83-115

Ren X. (2003). Biodegradable plastics: a solution or a challenge?, *Journal of Cleaner Production*, 11, 27-40

Sarazin, P., Li G., Orts, W.J., Favis, B.D. (2008). Binary and Ternary Blends of Polylactide, Polycaprolactone and Thermoplastic Starch, *Polymer*, 49: 599-609

Shah, P.B., Bandopadhyay, S., Bellare, J.R. (1995). Environmentally Degradable Starch Filled Low Density Polyethylene, 47 (2), 165-173

Shin B.Y., Jang S.H., Kim B.S. (2011). Thermal, Morphological and Mechanical Properties of Biobased and Biodegradable Blends of Poly(lactic acid) and Chemically Modified Thermoplastic Starch, *Polymer Engineering and Science*, 51(5), 826-834

Shogren, R.L., Lawton, J.W., Tiefenbacher, K.F. (2002). Baked Starch Foams: Starch Modifications and Additives Improve Process Parameters, Structure and Properties, *Industrial Crops and Products*, 16, 69-79

Steinbuchel, A. (1995). Use of Biosynthetic, Biodegradable Thermoplastics and Elastomers from Renewable Resources: The Pros and Cons, *Journal of Macromolecular Science (Part A)*, 32 (4), 653 – 660

Sungsanit, K., Kao, N., Bhattacharya, S.N., Pivsaart, S. (2010). Physical and Rheological Properties of Plasticized Linear and Branched PLA, *Korea-Australia Rheology Journal*, 22(3), 187-195

Swinkels, J.J.M., Veendam, (1985). Composition and Properties of Commercial Native Starches, Starch, 37 (1), 1-5

Tharanathan, R.N. (2005). Starch - Value addition by Modification, *Critical Reviews in Food Science and Nutrition*, 45 (5), 371-384

Thorne J.L., (1996). Thermoplastic Foams, Sherwood Publishers, Ohio

Thorne, J.L. (2002). Rotational Molding v. the Mechanics of Foaming. Proceedings of SPE/ANTEC.

Thuwall, M., Boldizar, A., Rigdahl M. (2006). Extrusion Processing of High Amylose Potato Starch Material, *Carbohydrate Polymers*, 65(4), 441-446

van Soest J.J.G., Vliegenthart, J.F.G. (1997). Crystallinity in starch plastics: consequences for material properties, *Trends in Biotechnology*, 15(6), 208-213

Villalobos, M., Awojulu, A., Greeley, T., Turco, G., Deeter, G. (2006). Oligomeric Chain Extenders for Economic Reprocessing and Recycling of Condensation Plastics, *Energy*, 31, 3227-3234

Waldman, F.A. (1982). The processing of microcellular foam, S.M.Thesis, Department of Mechanical Engineering, Massachusetts Institute of Technology, Cambridge, MA

Wang, H., Sun, X., Seib, P. (2001). Strengthening Blends of Poly (lactic acid) and Starch with Methylenediphenyl Diisocyanate, *Journal of Applied Polymer Science*, 82, 1761-1767

Wang, L.K., Hung, Y., Lo, H.H., Yapijakis, C. (2006). Waste treatment in the food processing industries, Chapter 6: Potato Wastewater Treatment, CRC Press, Florida

Wang, W., Flores, R.A., Huang, C.T. (1995). Physical Properties of Two Biological Cushioning Materials from Wheat and Corn Starches, *Cereal Chemistry*, 72(1), 38-41

Wang, X., Kumar, V., Li, W. (2007). Low Density Sub-Critical CO_2 –Blown Solid-State PLA Foams, *Cellular Polymers*, 26(1), 11-35

Whittam M.A., Noel T.R., Ring S.G., (1990). Melting behaviour of A- and B- type crystalline starch, Int. J. Biol. Macromol., Vol. 12:359-362

Willett, J.L., Shogren, R.L. (2002). Processing and Properties of Extruded Starch/Polymer Foams, 43, 5935-5947

Witt, U., Einig, T., Yamamoto, M., Kleeberg, I., Deckwer, W.D., Muller, R.J. (2001). Biodegradation of aliphatic-aromatic copolyesters: evaluation of the final biodegradability and exotoxicological impact of degradation intermediates, *Chemosphere*, 44(2), 289-299

Xie, F., Liu, H., Chen, P., Xue, T., Chen, L., Yu, L., Corrigan, P. (2006). Starch Gelatinization Under Shearless and Shear Conditions, *International Journal of Food Engineering*, 2(5), 1-29

Yamamoto, M., Witt, U., Skupin, G., Beimborn, D., Muller, R.J. (2002). "Biodegradable Aliphetic-Aromatic Polyesters: Ecoflex®" Chapter 11 in Doi Y, A.Steinbuchel (Ed.) "Biopolymers", Vol. 4, Wiley-VCH Verlag GmbH, Weinheim, Germany, p.299

Yuan, H., Liu, Q., Hrymak, A., Thompson, M., Ren, J. (2010). Thermoplastic Potato Starch Blends and Bioplastic Films, ANTEC

Yuan X., Mak A.F.T., Kwok K.W., Yung K.O., Yao K. (2001). Characterization of Poly (L-lactic acid) Fibers Produced by Melt Spinning, *Journal of Applied Polymer Science*, 81, 251-260

Zhang J., Sun X. (2004). Mechanical and Thermal Properties of Poly (lactic acid)/Starch blends with Dioctyl Maleate, *Journal of Applied Polymer Science*, 94,1697-1704

Zhang, J., Sun, X. (2007a). Biodegradable Foams of Poly (lactic acid)/Starch. I. Extrusion Condition and Cellular Size Distribution, *Journal of Applied Polymer Science*, 106, 857-862

Zhang, J., Sun, X. (2007b). Biodegradable Foams of Poly (lactic acid)/Starch. II. Cellular Structure and Water Resistance, *Journal of Applied Polymer Science*, 106, 3058-3062

Zhang, N., Wang, Q., Ren, J., Wang, L. (2009). Preparation and Properties of Biodegradable Poly (Lactic acid)/Poly(butylene adipate-co-terephthalate) Blend with Glycidyl Methacrylate as Reactive Processing Agent, *Journal of Materials Science (January 2009)*, 44 (1), 250-256

Van Soest J.J.G., Vliegenthart J.F.G. (1997). Crystallinity in Starch Plastics: Consequences for Material Properties, TIBTECH, 15, 208-213

APPENDIX A

EXPERIMENTAL DATA FROM PARALLEL PLATE RHEOMETRY

Table A1. Frequency, Complex Viscosity(η*), Storage Moduli (G') and loss (G") Moduli data of Solanyl® blend 30R after processed in the Internal Mixer (Haake) at 170°C and Strain 5%

Freq. (rad/s)	η* (Pa.s)	G' (Pa)	G" (Pa)
0.10	1198.31 ± 43.83	13.83 ± 15.11	118.37 ± 5.21
0.15	1145.12 ± 65.64	33.20 ± 5.24	164.74 ± 8.79
0.22	938.84 ± 102.55	25.75 ± 8.41	200.42 ± 23.14
0.32	894.96 ± 40.37	45.13 ± 2.16	279.37 ± 13.11
0.46	831.90 ± 38.68	58.68 ± 3.92	381.64 ± 17.77
0.68	787.55 ± 40.09	79.28 ± 1.62	530.65 ± 27.41
1.00	751.21 ± 36.73	107.32 ± 4.91	743.50 ± 36.42
1.47	720.22 ± 36.94	151.01 ± 7.57	1046.30 ± 53.69
2.15	692.45 ± 35.15	219.82 ± 11.18	1475.55 ± 75.00
3.16	665.16 ± 33.31	328.67 ± 18.52	2077.59 ± 103.78
4.64	637.62 ± 31.88	496.64 ± 27.42	2917.58 ± 145.44
6.81	610.23 ± 30.75	744.39 ± 42.96	4090.23 ± 205.13
10.00	585.94 ± 29.21	1115.67 ± 68.26	5752.13 ± 284.90
14.68	569.44 ± 28.90	1682.95 ± 107.39	8186.97 ± 411.13
21.54	556.03 ± 29.64	2794.79 ± 168.33	11716.63 ± 617.00
31.62	539.59 ± 29.11	3601.46 ± 236.91	16678.87 ± 890.54
46.42	520.93 ± 27.62	5209.83 ± 343.04	23611.23 ± 1237.09
68.13	498.20 ± 25.52	7716.72 ± 531.35	33021.73 ± 1661.61
100.00	468.09 ± 23.31	11706.27 ± 824.92	45321.10 ± 2194.34

Table A2. Frequency, Complex Viscosity(η*), Storage Moduli (G') and loss (G") Moduli data of Solanyl® blend 30R modified with 0.5 wt % ADR 4370S after processed in the Internal Mixer (Haake) at 170°C and Strain 4%

Freq. (rad/s)	η* (Pa.s)	G' (Pa)	G" (Pa)
0.10	7517.50 ± 339.03	130.12 ± 34.67	739.87 ± 33.50
0.15	6829.26 ± 360.37	200.28 ± 39.19	981.48 ± 57.73
0.22	6176.29 ± 370.36	279.14 ± 13.09	1300.93 ± 81.26
0.32	5711.89 ± 379.57	420.47 ± 24.95	1756.64 ± 117.45
0.46	5333.20 ± 319.74	608.30 ± 28.17	2399.54 ± 146.00
0.68	4996.00 ± 291.02	899.47 ± 49.27	3282.71 ± 192.80
1.00	4652.35 ± 275.91	1326.27 ± 85.53	4459.29 ± 262.64
1.47	4341.58 ± 253.12	1984.10 ± 126.59	6055.81 ± 349.66
2.15	4030.81 ± 237.48	2927.05 ± 202.08	8175.91 ± 470.49
3.16	3753.87 ± 213.48	4367.79 ± 275.54	11037.87 ± 619.24
4.64	3469.99 ± 200.97	6293.03 ± 412.12	14825.97 ± 838.41
6.81	3192.85 ± 181.55	8953.45 ± 569.03	19824.47 ± 1100.22
10.00	2909.97 ± 161.54	12489.83 ±771.71	26283.00 ± 1421.89
14.68	2627.91 ± 142.98	17226.17 ± 1044.24	34512.00 ± 1824.36
21.54	2351.98 ± 124.66	23558.30 ± 1894.29	44862.17 ± 2298.59
31.62	2083.42 ± 108.78	32018.57 ± 2516.02	57579.73 ± 2882.34
46.42	1827.46 ± 93.30	43283.57 ± 2516.02	72948.17 ± 3543.11
68.13	1591.06 ± 79.30	58251.60 ± 3313.09	91414.43 ± 4297.45
100.00	1367.08 ± 66.73	77572.40 ± 4330.56	112570.00 ± 5125.18

Table A3. Frequency, Complex Viscosity(η*), Storage Moduli (G') and loss (G") Moduli data of Solanyl® blend 30R modified with 1.5 wt % ADR 4370S after processed in the Internal Mixer (Haake) at 170°C and Strain 4%

Freq. (rad/s)	η* (Pa.s)	G' (Pa)	G" (Pa)
0.10	18751.93 ± 606.06	458.89 ± 18.02	1818.00 ± 66.02
0.15	17198.80 ± 343.11	666.58 ± 38.35	2434.68 ± 48.00
0.22	15769.53 ± 286.67	985.77 ± 40.81	3251.22 ± 52.78
0.32	14568.60 ± 327.51	1482.70 ± 48.06	4361.86 ± 93.46
0.46	13421.50 ± 377.53	2199.87 ± 52.89	5828.35 ± 118.42
0.68	12273.37 ± 241.20	3207.23 ± 75.23	7722.18 ± 148.51
1.00	11198.50 ± 206.46	4647.40 ± 100.11	10188.58 ± 182.74
1.47	10231.97 ± 162.01	6700.22 ± 115.52	13441.00 ± 208.41
2.15	9283.10 ± 139.18	9448.90 ± 157.52	17627.00 ± 256.69
3.16	8332.27 ± 113.07	13024.63 ± 211.45	22904.70 ± 292.20
4.64	7411.63 ± 96.99	17703.73 ± 284.25	29496.63 ± 356.82
6.81	6529.86 ± 81.09	23760.60 ± 374.83	37610.63 ± 419.41
10.00	5702.82 ± 68.13	31572.63 ± 482.31	47490.73 ± 501.59
14.68	4935.25 ± 54.31	41591.63 ± 596.09	59309.37 ± 560.10
21.54	4231.52 ± 46.94	54356.70 ± 768.48	73187.80 ± 693.72
31.62	3600.53 ± 38.71	70504.27 ± 959.47	89403.27 ± 805.56
46.42	3038.02 ± 31.22	90764.03 ± 1175.22	107916.67 ± 908.42
68.13	2542.54 ± 25.18	115883.33 ± 1426.78	128750.00 ± 1028.98
100.00	2105.72 ± 20.29	146456.67 ± 1732.78	151300.00 ± 1158.06

Table A4. Frequency, Complex Viscosity(η*), Storage Moduli (G') and loss (G") Moduli data of Solanyl® blend 30R modified with 2.0 wt % ADR 4370S after processed in the Internal Mixer (Haake) at 170°C and Strain 2%

Freq. (rad/s)	η* (Pa.s)	G' (Pa)	G" (Pa)
0.10	18426 ± 867.47	451.62 ± 44.32	1786.37 ± 78.54
0.15	16757.03 ± 597.04	653.93 ± 39.94	2371.03 ± 79.96
0.22	15453.97 ± 535.98	946.25 ± 21.42	3192.14 ± 114.16
0.32	14352.97 ± 422.98	1429.30 ± 42.76	4307.88 ± 126.73
0.46	13168.80 ± 370.20	2156.04 ± 58.83	5719.53 ± 161.71
0.68	11991.00 ± 336.69	3169.27 ± 98.10	7529.56 ± 207.81
1.00	10829.37 ± 296.78	4571.16 ± 131.10	9817.30 ± 267.78
1.47	9729.87 ± 270.10	6499.87 ± 181.16	12716.57 ± 354.91
2.15	8710.46 ± 256.82	9173.03 ± 306.76	16371.33 ± 463.18
3.16	7775.79 ± 227.49	12758.30 ± 400.49	21020.30 ± 600.06
4.64	6935.83 ± 192.15	17563.83 ± 471.25	26979.97 ± 757.72
6.81	6142.16 ± 161.21	23750.30 ± 592.84	34453.10 ± 927.20
10.00	5387.82 ± 134.60	31565.90 ± 701.80	43662.87 ± 1155.25
14.68	4682.06 ± 112.83	41477.27 ± 904.44	54795.03 ± 1394.12
21.54	4037.37 ± 93.06	54037.87 ± 1128.00	68160.60 ± 1665.22
31.62	3451.84 ± 77.26	69846.50 ± 1450.86	83884.93 ± 1971.78
46.42	2925.07 ± 64.34	89637.07 ± 1860.44	101972.80 ± 2341.52
68.13	2453.31 ± 52.98	114103.33 ± 2325.22	122133.33 ± 2766.45
100.00	2039.29 ± 44.19	144233.33 ± 2985.07	144166.67 ± 3265.90

Table A5. Frequency, Complex Viscosity(η*), Storage Moduli (G') and loss (G") Moduli data of Solanyl® blend 30R modified with 0.5 wt % ADR 4380 after processed in the Internal Mixer (Haake) at 170°C and Strain 4%

Freq. (rad/s)	η* (Pa.s)	G' (Pa)	G" (Pa)
0.10	1022.66 ± 98.69	39.25 ± 19.58	93.35 ± 4.27
0.15	1278.18 ± 122.96	47.59 ± 33.14	178.83 ± 25.66
0.22	1169.70 ± 75.27	35.58 ± 5.53	249.39 ± 17.22
0.32	975.54 ± 26.76	58.28 ± 19.63	302.57 ± 5.10
0.46	945.54 ± 26.76	86.89 ± 11.15	430.07 ± 17.01
0.68	888.81 ± 16.97	98.95 ± 9.47	597.33 ± 13.06
1.00	842.57 ± 25.44	144.98 ± 9.33	829.95 ± 26.41
1.47	804.81 ± 27.36	196.49 ± 3.19	1164.84 ± 40.19
2.15	768.55 ± 29.96	281.06 ± 8.32	1631.75 ± 64.47
3.16	736.01 ± 27.91	406.99 ± 13.52	2291.59 ± 87.50
4.64	704.19 ± 25.58	601.74 ± 18.81	3212.68 ± 117.27
6.81	671.63 ± 24.01	883.23 ± 25.21	4489.68 ± 161.76
10.00	640.85 ± 23.30	1295.70 ± 23.93	6276.08 ± 233.07
14.68	614.23 ± 23.08	1911.75 ± 38.23	8810.49 ± 340.56
21.54	593.64 ± 24.97	2857.21 ± 65.97	12466.20 ± 538.51
31.62	573.97 ± 25.89	4274.17 ± 106.84	17639.83 ± 816.91
46.42	552.52 ± 25.67	6349.90 ± 207.93	24847.00 ± 1180.30
68.13	526.84 ± 25.01	9463.16 ± 378.15	34623.20 ± 1669.29
100.00	493.13 ± 23.57	14214.40 ± 647.42	47219.40 ± 2275.14

Table A6. Frequency, Complex Viscosity(η*), Storage Moduli (G') and loss (G") Moduli data of Solanyl® blend 30R modified with 1.5 wt % ADR 4380 after processed in the Internal Mixer (Haake) at 170°C and Strain 6%

Freq. (rad/s)	η* (Pa.s)	G' (Pa)	G" (Pa)
0.10	2212.82 ± 79.89	41.42 ± 3.42	217.35 ± 8.26
0.15	1934.33 ± 250.00	61.27 ± 2.29	277.14 ± 37.68
0.22	1731.36 ± 118.98	76.50 ± 7.05	365.07 ± 24.77
0.32	1687.81 ± 88.45	96.55 ± 5.02	524.92 ± 27.74
0.46	1574.75 ± 98.21	128.00 ± 4.22	719.62 ± 45.12
0.68	1493.21 ± 96.40	177.38 ± 8.92	1001.72 ± 85.87
1.00	1435.33 ± 87.54	263.65 ± 16.51	1410.91 ± 85.98
1.47	1372.34 ± 85.48	377.55 ± 15.65	1978.61 ± 124.75
2.15	1310.61 ± 80.60	561.54 ± 25.72	2767.21 ± 171.97
3.16	1247.75 ± 16.64	841.57 ± 44.40	3854.92 ± 238.41
4.64	1187.35 ± 17.21	1260.86 ± 78.80	5365.00 ± 335.39
6.81	1134.60 ± 71.94	1878.15 ± 128.91	7498.29 ± 473.12
10.00	1087.94 ± 70.38	2774.63 ± 212.57	10519.61 ± 671.84
14.68	1040.59 ± 66.86	4048.32 ± 315.29	14727.37 ± 932.16
21.54	989.13 ± 61.63	5877.20 ± 461.31	20483.37 ± 1252.11
31.62	931.15 ± 56.02	8565.99 ± 664.58	28171.47 ± 1655.11
46.42	866.38 ± 49.99	12612.23 ± 963.57	38183.90 ± 2132.92
68.13	796.09 ± 44.70	18660.53 ± 1398.33	50924.77 ± 2741.33
100.00	717.67 ± 38.18	27367.00 ± 1949.56	66342.27 ± 3340.94

Table A7. Frequency, Complex Viscosity(η*), Storage Moduli (G') and loss (G") Moduli data of Solanyl® blend 30R modified with 2.5 wt % ADR 4380 after processed in the Internal Mixer (Haake) at 170°C and Strain 6%

Freq. (rad/s)	η* (Pa.s)	G' (Pa)	G" (Pa)
0.10	4047.46 ± 92.21	45.78 ± 1.90	402.14 ± 9.47
0.15	3655.30 ± 155.15	75.91 ± 3.22	531.12 ± 22.82
0.22	3539.38 ± 104.58	108.62 ± 7.68	754.73 ± 22.66
0.32	3348.28 ± 123.34	169.47 ± 9.00	1045.14 ± 39.35
0.46	3203.07 ± 112.40	252.49 ± 5.12	1465.14 ± 52.06
0.68	3077.01 ± 112.58	383.99 ± 14.15	2060.87 ± 75.40
1.00	2950.10 ± 118.52	592.25 ± 28.08	2890.03 ± 115.35
1.47	2823.15 ± 112.85	914.26 ± 36.81	4041.70 ± 161.52
2.15	2714.78 ± 128.93	1448.70 ± 89.95	5666.54 ± 263.67
3.16	2594.07 ± 116.04	2210.57 ± 13.09	7899.71 ± 349.49
4.64	2469.80 ± 105.50	3300.40 ± 147.34	10978.37 ± 467.47
6.81	2334.33 ± 95.15	4818.12 ± 206.12	15156.17 ± 616.06
10.00	2187.63 ± 84.07	6960.64 ± 294.58	20739.33 ± 790.16
14.68	2033.83 ± 73.54	10034.07 ± 414.39	28115.50 ± 1001.26
21.54	1872.51 ± 64.67	14480.60 ± 592.11	37653.30 ± 1270.46
31.62	1702.89 ± 56.64	20875.27 ± 833.42	49638.83 ± 1599.72
46.42	1532.53 ± 49.48	30017.83 ± 1159.32	64489.67 ± 2003.44
68.13	1361.03 ± 43.18	42774.47 ± 1608.99	82270.23 ± 2791.04
100.00	1186.72 ± 37.11	59831.80 ± 2170.47	102783.33 ± 3043.57

Table A8. Frequency, Complex Viscosity(η*), Storage Moduli (G') and loss (G") Moduli data of Solanyl® blend 30R modified with 0.5 wt % DGEBA after processed in the Internal Mixer (Haake) at 170°C and Strain 3%

Freq. (rad/s)	η* (Pa.s)	G' (Pa)	G" (Pa)
0.10	1192.77 ± 233.95	27.63 ± 7.52	115.71 ± 24.54
0.15	955.61 ± 136.48	40.07 ± 15.52	134.09 ± 17.07
0.22	739.70 ± 30.85	55.78 ± 4.84	149.16 ± 8.66
0.32	641.88 ± 66.51	64.96 ± 6.81	192.26 ± 20.53
0.46	608.18 ± 19.35	80.75 ± 12.82	270.24 ± 11.17
0.68	552.25 ± 20.08	91.56 ± 5.25	364.89 ± 14.51
1.00	517.89 ± 23.90	116.01 ± 7.42	504.71 ± 23.33
1.47	488.95 ± 20.20	150.49 ± 7.16	701.71 ± 29.13
2.15	464.90 ± 18.50	198.03 ± 10.25	981.81 ± 38.74
3.16	442.81 ± 16.72	266.58 ± 12.99	1374.67 ± 51.72
4.64	421.22 ± 15.10	367.14 ± 15.70	1920.32 ± 68.63
6.81	400.67 ± 13.83	506.33 ± 15.77	2682.35 ± 93.13
10.00	381.47 ± 12.97	693.43 ± 15.29	3751.11 ± 129.21
14.68	364.69 ± 12.70	957.59 ± 15.64	5266.50 ± 186.71
21.54	350.28 ± 12.80	1338.82 ± 24.31	7426.84 ± 275.98
31.62	339.13 ± 13.63	1652.76 ± 60.56	10545.70 ± 427.31
46.42	334.56 ± 14.90	3083.27 ± 130.83	15219.23 ± 679.51
68.13	329.45 ± 14.73	4918.89 ± 191.98	21899.23 ± 985.29
100.00	320.26 ± 13.84	7711.47 ± 276.66	31083.60 ± 1358.98

Table A9. Frequency, Complex Viscosity(η*), Storage Moduli (G') and loss (G") Moduli data of Solanyl® blend 30R modified with 1.5 wt % DGEBA after processed in the Internal Mixer (Haake) at 170°C and Strain 3%

Freq. (rad/s)	η* (Pa.s)	G' (Pa)	G" (Pa)
0.10	1372.77 ± 122.52	58.17 ± 37.01	118.44 ± 30.52
0.15	852.18 ± 136.44	24.62 ± 13.16	122.12 ± 20.47
0.22	623.35 ± 72.97	40.45 ± 7.10	128.03 ± 14.45
0.32	551.21 ± 77.83	54.00 ± 10.86	134.93 ± 29.76
0.46	535.63 ± 12.93	65.61 ± 1.80	239.81 ± 5.76
0.68	485.58 ± 10.83	75.34 ± 1.60	322.12 ± 7.60
1.00	447.83 ± 17.10	96.25 ± 3.99	437.37 ± 16.71
1.47	427.30 ± 12.33	123.00 ± 4.70	615.01 ± 17.52
2.15	408.25 ± 11.91	165.60 ± 8.62	863.80 ± 24.48
3.16	389.37 ± 11.02	225.11 ± 10.98	1210.54 ± 33.46
4.64	371.18 ± 10.32	313.69 ± 12.73	1694.08 ± 46.54
6.81	352.87 ± 10.19	437.88 ± 14.21	2363.86 ± 68.04
10.00	335.87 ± 9.91	604.21 ± 19.22	3303.88 ± 97.30
14.68	320.72 ± 9.75	827.62 ± 27.17	4634.26 ± 140.57
21.54	307.88 ± 9.61	1143.16 ± 37.37	6533.81 ± 203.85
31.62	297.59 ± 9.72	1635.34 ± 59.58	9267.54 ± 301.70
46.42	292.99 ± 10.83	2547.77 ± 116.74	13301.53 ± 489.83
68.13	289.59 ± 11.37	4088.02 ± 179.51	19301.53 ± 754.17
100.00	283.39 ± 11.50	6491.58 ± 242.28	27585.23 ± 1124.54

Table A10. Frequency, Complex Viscosity(η*), Storage Moduli (G') and loss (G") Moduli data of Solanyl® blend 30R modified with 2.5 wt % DGEBA after processed in the Internal Mixer (Haake) at 170°C and Strain 3%

Freq. (rad/s)	η* (Pa.s)	G' (Pa)	G" (Pa)
0.10	773.43 ± 294.97	13.64 ± 11.22	74.32 ± 33.94
0.15	787.71 ± 164.30	8.86 ± 15.33	114.47 ± 24.99
0.22	779.91 ± 22.40	19.59 ± 3.23	166.87 ± 4.48
0.32	740.24 ± 15.71	32.35 ± 8.64	231.74 ± 4.25
0.46	656.28 ± 32.60	36.84 ± 7.90	302.28 ± 16.10
0.68	645.19 ± 19.13	62.66 ± 5.99	435.03 ± 13.89
1.00	625.56 ± 15.64	76.93 ± 2.49	620.81 ± 16.04
1.47	599.37 ± 19.15	113.81 ± 2.12	872.36 ± 28.18
2.15	580.22 ± 18.68	174.84 ± 4.70	1237.75 ± 40.50
3.16	558.60 ± 18.63	269.22 ± 4.49	1745.80 ± 59.35
4.64	533.86 ± 18.63	408.89 ± 9.08	2444.00 ± 87.03
6.81	508.77 ± 17.66	614.02 ± 20.04	3411.37 ± 118.74
10.00	485.60 ± 15.57	900.65 ± 34.86	4771.75 ± 152.09
14.68	463.70 ± 14.12	1292.43 ± 62.65	6682.36 ± 199.33
21.54	446.86 ± 11.67	1889.08 ± 93.21	9440.17 ± 237.99
31.62	435.84 ± 11.03	2864.08 ± 93.21	13481.37 ± 322.21
46.42	426.67 ± 10.99	4420.18 ± 277.05	19304.10 ± 461.38
68.13	414.72 ± 10.40	6833.92 ± 423.62	27414.47 ± 630.72
100.00	397.24 ± 9.76	10594.60 ± 600.70	38283.70 ± 858.06

Table A11. Frequency, Complex Viscosity(η*), Storage Moduli (G') and loss (G") Moduli data of Solanyl® blend 30R modified with 0.5 wt % PEG-DGE after processed in the Internal Mixer (Haake) at 170°C and Strain 6%

Freq. (rad/s)	η* (Pa.s)	G' (Pa)	G" (Pa)
0.10	1425.23 ± 290.82	10.75 ± 17.66	414.22 ± 30.24
0.15	1319.40 ± 121.88	46.54 ± 13.02	187.22 ± 18.36
0.22	1111.06 ± 154.93	47.07 ± 3.83	234.65 ± 33.67
0.32	1054.14 ± 103.07	51.25 ± 5.34	329.28 ± 33.68
0.46	976.84 ± 86.81	65.59 ± 5.31	448.59 ± 40.71
0.68	925.46 ± 94.74	97.21 ± 5.13	622.92 ± 65.05
1.00	871.07 ± 92.95	129.76 ± 9.01	861.34± 92.67
1.47	834.19 ± 90.60	183.26 ± 17.41	1210.64 ± 131.86
2.15	801.31 ± 88.89	267.53 ± 26.10	1705.50 ± 189.74
3.16	768.28 ± 86.02	403.91 ± 46.17	2395.71 ± 268.06
4.64	734.85 ± 81.12	613.18 ± 76.02	3355.29 ± 377.55
6.81	700.85 ± 81.12	922.99 ± 121.71	4684.79 ± 539.34
10.00	670.46 ± 79.65	1374.33 ± 184.16	6562.18 ± 775.38
14.68	646.91 ± 76.60	2037.42 ± 258.94	9274.13 ± 1094.38
21.54	624.45 ± 72.63	2957.96 ± 366.87	13124.20 ± 1521.46
31.62	600.45 ± 68.24	4255.62 ± 532.64	18504.77 ± 2091.72
46.42	573.62 ± 63.29	6194.04 ± 818.11	25894.23 ± 2824.56
68.13	542.23 ± 57.98	9246.26 ± 1292.14	35764.90 ± 3745.37
100.00	503.20 ± 52.32	14016.27 ± 2015.82	48325.90 ± 4861.52

Table A12. Frequency, Complex Viscosity(η*), Storage Moduli (G') and loss (G") Moduli data of Solanyl® blend 30R modified with 1.5 wt % PEG-DGE after processed in the Internal Mixer (Haake) at 170°C and Strain 3%

Freq. (rad/s)	η* (Pa.s)	G' (Pa)	G" (Pa)
0.10	1502.86 ± 62.17	31.40 ± 2.69	146.94 ± 6.55
0.15	1343.32 ± 34.22	41.86 ± 18.37	192.06 ± 6.76
0.22	1187.63 ± 54.45	55.91 ± 3.85	249.68 ± 11.16
0.32	1054.39 ± 49.04	69.64 ± 3.66	326.03 ± 16.27
0.46	976.97 ± 57.56	92.16 ± 1.97	443.97 ± 27.59
0.68	896.97 ± 48.33	124.86 ± 3.55	598.10 ± 33.07
1.00	844.53 ± 48.76	168.31 ± 4.52	827.58 ± 48.85
1.47	796.81 ± 47.87	224.60 ± 6.16	1147.78 ± 70.41
2.15	758.02 ± 46.71	309.14 ± 15.00	1603.57 99.60±
3.16	722.55 ± 45.23	437.39 ± 28.77	2242.66 ± 140.11
4.64	685.90 ± 42.08	631.01 ± 40.87	3120.52 ± 191.00
6.81	650.69 ± 39.33	911.97 ± 56.78	4338.29 ± 261.84
10.00	616.70 ± 38.27	1302.96 ± 82.75	6027.80 373.62±
14.68	587.30 ± 38.95	1876.26 ± 130.35	8413.73 ± 556.73
21.54	565.69 ± 41.50	2780.08 ± 233.27	11866.07 ± 863.63
31.62	550.44 ± 43.31	4170.13 ± 336.67	16899.50 ± 1327.75
46.42	534.78 ± 39.08	6277.35 ± 371.85	24015.13 ± 1777.79
68.13	514.37 ± 35.53	9438.11 ± 538.24	33748.77 ± 2363.09
100.00	486.16 ± 31.38	14211.77 ± 860.28	46492.07 ± 3018.25

Table A13. Frequency, Complex Viscosity(η*), Storage Moduli (G') and loss (G") Moduli data of Solanyl® blend 30R modified with 2.5 wt % PEG-DGE after processed in the Internal Mixer (Haake) at 170°C and Strain 3%

Freq. (rad/s)	η* (Pa.s)	G' (Pa)	G" (Pa)
0.10	1256.90 ± 68.31	19.31 ± 12.09	123.72 ± 8.89
0.15	987.64 ± 76.06	15.79 ± 1.69	144.09 ± 11.34
0.22	981.68 ± 56.36	22.90 ± 7.75	210.15 ± 12.43
0.32	906.20 ± 56.68	32.52 ± 1.84	284.70 ± 18.26
0.46	895.57 ± 83.11	58.02 ± 8.74	411.58 ± 38.20
0.68	816.12 ± 28.47	76.96 ± 4.94	550.66 ± 19.07
1.00	781.12 ± 28.47	106.81 ± 4.72	773.78 ± 34.67
1.47	756.70 ± 35.21	156.80 ± 4.55	1099.54 ± 51.82
2.15	729.15 ± 36.52	242.28 ± 2.57	1552.08 ± 79.62
3.16	698.54 ± 35.59	371.63 ± 6.77	2177.47 ± 113.13
4.64	666.31 ± 35.22	559.60 ± 19.66	3041.66 ± 162.69
6.81	633.59 ± 34.59	833.79 ± 41.66	4235.31 ± 231.96
10.00	601.55 ± 33.60	1211.27 ± 86.36	5892.32 ± 325.26
14.68	574.81 ± 32.49	1754.86 ± 152.29	8252.42 ± 455.50
21.54	557.07 ± 32.98	2650.16 ± 280.48	11705.07 ± 665.74
31.62	543.43 ± 30.57	4059.83 ± 364.16	16697.87 ± 906.78
46.42	527.43 ± 27.39	6201.32 ± 459.82	23682.33 ± 1193.91
68.13	506.28 ± 24.67	9511.42 ± 613.14	33155.20 ± 1572.41
100.00	477.51 ± 21.69	14592.80 ± 830.24	45466.10 ± 2012.18

Table A14. Frequency, Complex Viscosity(η*), Storage Moduli (G') and loss (G") Moduli data of neat hydrolyzed starch/PLA blend after processed in the TSE at 170°C and Strain 5%

Freq. (rad/s)	η* (Pa.s)	G' (Pa)	G" (Pa)
0.10	7236.33 ± 217.93	88.73 ± 15.76	718.08 ± 20.65
0.15	6408.97 ± 127.64	84.47 ± 5.87	936.90 ± 18.37
0.22	5966.68 ± 128.67	102.60 ±1.71	1281.38 ± 27.92
0.32	5668.96 ± 148.02	132.69 ± 3.40	1787.77 ± 46.70
0.46	5442.33 ± 157.75	182.47 ± 14.10	2519.49 ± 72.78
0.68	5294.59 ± 149.57	271.59 ± 13.69	3596.91 ± 101.42
1.00	5182.41 ± 148.99	437.48 ± 21.37	5163.90 ± 148.11
1.47	5113.10 ± 140.87	757.21 ± 16.27	7466.70 ± 206.19
2.15	5090.52 ± 129.19	1393.11 ± 28.62	10878.33 ± 278.15
3.16	5078.88 ± 129.75	2484.22 ± 57.54	15867.50 ± 408.93
4.64	4987.35 ± 131.07	4214.49 ± 113.90	22762.27 ± 604.04
6.81	4804.47 ± 131.16	6992.19 ± 200.57	31976.60 ± 890.78
10.00	4542.68 ± 127.08	11400.60 ± 331.05	43972.07 ± 1272.38
14.68	4205.30 ± 121.39	18235.10 ± 514.75	58968.60 ± 1796.16
21.54	3813.42 ± 115.23	28356.57 ± 766.76	77105.40 ± 2521.37
31.62	3385.01 ± 108.09	42732.30 ± 1097.64	98137.17 ± 3494.53
46.42	2952.21 ± 99.67	62452.97 ± 1097.64	121960.00 ± 4741.43
68.13	2528.01 ± 91.11	88415.37 ± 2163.87	147790.00 ± 6325.01
100.00	2104.86 ± 80.69	120103.33 ± 3072.87	172840.00 ± 8098.97

Table A15. Frequency, Complex Viscosity(η*), Storage Moduli (G') and loss (G") Moduli data of neat hydrolyzed starch/PLA blend modified with 0.5 wt % ADR 4370S after processed in the TSE at 170°C and Strain 1%

Freq. (rad/s)	η* (Pa.s)	G' (Pa)	G" (Pa)
0.10	68853.20 ± 7446.37	1581.58 ± 424.87	6697.68 ± 667.00
0.15	64005.30 ± 6289.88	2412.21 ± 263.57	9079.38 ± 89015
0.22	60225.37 ± 5098.17	3713.95 ± 435.80	12431.83 ± 1016.50
0.32	56682.53 ± 5165.92	5827.70 ± 722.67	16949.93 ± 1479.61
0.46	52673.30 ± 5150.07	8778.89 ± 1179.34	22816.53 ± 2108.44
0.68	48535.00 ± 4667.38	13014.10 ± 1748.90	30394.60 ± 2710.74
1.00	44582.50 ± 4489.29	19042.03 ± 2581.52	40306.83 ± 3746.03
1.47	40784.17 ± 4045.34	27468.77 ± 3457.74	53184.40 ± 4898.13
2.15	36945.03 ± 3497.46	38739.33 ± 4405.20	69528.77 ± 6171.73
3.16	33116.93 ± 2962.01	53762.73 ± 5672.90	89867.73 ± 7521.73
4.64	29375.23 ± 2484.02	73711.37 ± 7244.76	114703.33 ± 9052.19
6.81	25776.90 ± 2082.50	100068.43 ± 9262.42	144310.00 ± 10847.87
10.00	22344.37 ± 1723.20	134216.67 ± 11810.17	178633.33 ± 12683.78
14.68	19155.87 ± 1418.40	178053.33 ± 15005.97	217600.00 ± 14627.19
21.54	16179.23 ± 1156.29	232716.67 ± 18656.00	259500.00 ± 16739.14
31.62	13519.40 ± 934.76	300346.67 ± 23171.70	304233.33 ± 18670.05
46.42	11146.53 ± 590.88	381516.67 ± 28348.75	349446.67 ± 20446.46
68.13	9068.91 ± 590.88	477233.33 ± 34229.01	392403.33 ± 21764.66
100.00	7279.34 ± 464.41	587696.67 ± 40992.17	429503.33 ± 22636.47

Table A16. Frequency, Complex Viscosity(η*), Storage Moduli (G') and loss (G") Moduli data of neat hydrolyzed starch/PLA blend modified with 2.0 wt% ADR 4370S after processed in the TSE at 170°C and Strain 1%

Freq. (rad/s)	η* (Pa.s)	G' (Pa)	G" (Pa)
0.10	154375.30 ± 118587.53	11591.17 ± 1901.43	21052.93 ± 2417.44
0.15	149838.00 ± 115839.98	18285.07 ± 2492.24	28688.63 ± 2975.85
0.22	136755.23 ± 105585.17	26420.40 ± 3355.57	36848.13 ± 3510.15
0.32	120759.63 ± 92583.75	36298.20 ± 4092.72	45794.70 ± 4248.99
0.46	104568.20 ± 79539.25	48091.77 ± 5271.98	56288.43 ± 5209.59
0.68	89613.60 ± 67586.47	62384.73 ± 6555.87	68586.97 ± 6248.93
1.00	75878.43 ± 56669.74	79365.80 ± 8090.53	82684.40 ± 7181.92
1.47	63757.05 ± 47094.19	99654.60 ±9710.66	99118.90 ± 8287.58
2.15	53173.63 ± 38796.11	124030.00 ± 11628.81	117886.67 ± 9608.17
3.16	44107.76 ± 31727.67	153220.00 ± 14008.17	139436.67 ± 11079.11
4.64	36347.86 ± 25694.98	187960.00 ± 16861.76	163360.00 ± 12760.48
6.81	29798.71 ± 20676.05	229330.00 ± 20160.37	189633.33 ± 14285.47
10.00	24244.04 ± 16488.68	278110.00 ± 24182.80	217593.33 ± 16268.76
14.68	19594.76 ± 13048.83	334980.00 ± 28771.47	246746.67 ± 18203.08
21.54	15718.89 ± 10227.24	400516.67 ± 34209.39	275946.67 ± 19835.24
31.62	12506.58 ± 7933.58	474503.33 ± 40127.39	304103.33 ± 21350.75
46.42	9863.47 ± 6085.19	557000.00 ± 46764.86	329383.33 ± 22482.53
68.13	7713.90 ± 4618.19	647556.67 ± 54006.08	350670.00 ± 23195.91
100.00	5976.37 ± 3461.81	745823.33 ± 62370.27	364183.33 ± 22789.25

Table A17. Frequency, Complex Viscosity(η*), Storage Moduli (G') and loss (G") Moduli data of neat hydrolyzed starch/PLA blend modified with 0.5 wt % ADR 4380 after processed in the TSE at 170°C and Strain 1%

Freq. (rad/s)	η* (Pa.s)	G' (Pa)	G" (Pa)
0.10	30420.10 ± 1173.84	588.96 ± 144.75	2982.40 ± 105.57
0.15	25411.87 ± 789.26	609.02 ± 92.85	3679.01 ± 1210.05
0.22	22838.87 ± 1422.99	769.19 ± 147.51	4858.92 ± 293.50
0.32	21544.90 ± 857.73	1065.44 ± 42.10	6728.92 ± 280.95
0.46	20401.03 ± 992.24	1489.56 ± 113.93	9351.36 ± 448.36
0.68	19524.20 ± 794.13	2288.85 ± 119.49	13103.27 ± 528.39
1.00	18654.60 ± 801.32	3568.36 ± 237.83	18310.03 ± 770.14
1.47	17885.23 ± 666.43	5714.05 ± 255.34	25622.47 ± 945.39
2.15	17154.43 ± 604.78	9321.06 ± 462.73	35763.10 ± 1230.21
3.16	16418.33 ± 476.75	15046.20 ± 524.42	49691.17 ± 1421.02
4.64	15628.27 ± 408.67	23888.60 ± 869.37	68493.33 ± 1710.24
6.81	14628.27 ± 408.67	36841.80 ± 1463.63	92738.10 ± 2113.35
10.00	13494.13 ± 338.72	55529.47 ± 2173.90	122983.33 ± 2741.54
14.68	12217.43 ± 300.48	82145.43 ± 2998.77	159400.00 ± 3447.96
21.54	10870.23 ± 256.34	118610.00 ± 4076.26	201930.00 ± 4092.77
31.62	9505.19 ± 216.79	167340.00 ± 5367.14	249686.67 ± 4730.67
46.42	8158.97 ± 175.18	230133.33 ± 6767.14	300750.00 ± 5209.54
68.13	6898.77 ± 139.34	309343.33 ± 8412.28	353846.67 ± 5530.59
100.00	5727.58 ± 110.52	405433.33 ± 10226.72	404553.33 ± 5829.31

Table A18. Frequency, Complex Viscosity(η*), Storage Moduli (G') and loss (G") Moduli data of neat hydrolyzed starch/PLA blend modified with 2.5 wt% ADR 4380 after processed in the TSE at 170°C and Strain 1%

Freq. (rad/s)	η* (Pa.s)	G' (Pa)	G" (Pa)
0.10	7178.10 ± 984.23	38.62 ± 106.46	712.34 ± 104.95
0.15	8278.64 ± 1001.28	268.09 ± 178.93	1175.12 ± 192.79
0.22	7663.71 ± 528.15	188.80 ± 316	1640.23 ± 114.90
0.32	7435.69 ± 186.78	250.96 ± 16.13	2337.93 ± 57.67
0.46	6942.89 ± 217.77	353.01 ± 34.44	3203.17 ± 97.90
0.68	6773.77 ± 183.24	614.34 ± 22.07	4573.84 ± 122.99
1.00	6439.08 ± 267.06	902.16 ± 27.18	6375.57 ± 265.88
1.47	6180.42 ± 258.96	1404.49 ± 44.60	8962.23 ± 377.74
2.15	5948.45 ± 252.74	2212.68 ± 53.44	12623.05 ± 543.41
3.16	5720.35 ± 259.49	3496.19 ± 335.23	17748.20 ± 803.56
4.64	5492.85 ± 263.71	5699.65 ± 335.23	24850.25 ± 1178.96
6.81	5275.14 ± 267.53	9442.64 ± 589.78	34676.35 ± 1728.52
10.00	5067.80 ± 272.23	15614.35 ± 1130.88	48212.05 ± 2495.31
14.68	4836.80 ± 263.12	25387.65 ± 1849.30	66298.40 ± 3427.49
21.54	4529.00 ± 238.51	39623.10 ± 2764.65	89165.40 ± 4394.67
31.62	4148.93 ± 207.30	59777.95 ± 4112.	116790.00 ± 5260.87
46.42	3718.29 ± 169.83	87582.45 ± 5669.51	148705.00 ± 5805.35
68.13	3260.07 ± 127.75	124415.00 ± 7332.70	183975.00 ± 5550.79
100.00	2795.55 ± 84.53	171365.00 ± 8449.93	220850.00 ± 4143.65

Table A19. Frequency, Complex Viscosity(η*), Storage Moduli (G') and loss (G") Moduli data of neat hydrolyzed starch/PLA blend modified with 0.5 wt % DGEBA after processed in the TSE at 170°C and Strain 4%

Freq. (rad/s)	η* (Pa.s)	G' (Pa)	G" (Pa)
0.10	15082.17 ±	166.25 ± 16.33	1499.02 ± 126.74
0.15	12690.10 ± 938.48	172.78 ± 12.83	1854.60 ± 137.43
0.22	11604.17 ± 883.23	199.70 ± 11.59	2492.05 ± 190.01
0.32	10993.73 ± 868.09	253.41 ± 25.74	3467.26 ± 273.56
0.46	10636.02 ± 880.15	382.70 ± 46.18	4921.94 ± 406.19
0.68	10332.60 ± 868.51	613.07 ± 69.62	7012.75 ± 587.87
1.00	10221.64 ± 875.39	1094.19 ± 129.73	10162.86 ± 866.46
1.47	10207.32 ± 871.70	1993.72 ± 212.67	14849.00 ± 1262.45
2.15	10129.73 ± 846.93	3412.30 ± 331.01	21555.33 ± 1795.40
3.16	9909.49 ± 815.82	5730.98 ± 552.14	30807.93 ± 2522.74
4.64	9548.96 ± 769.95	9488.31 ± 880.21	43294.50 ± 3468.90
6.81	9050.97 ± 709.81	15557.83 ± 1383.83	59668.07 ± 4644.20
10.00	8432.58 ± 647.27	25064.67 ± 2168.62	80513.63 ± 6118.24
14.68	7720.68 ± 576.80	39364.93 ± 3297.44	106268.80 ± 7832.66
21.54	6931.44 ± 503.80	60089.77 ± 4809.07	136706.67 ± 9777.13
31.62	6170.00 ± 432.44	88764.77 ± 6826.10	171506.67 ± 11923.23
46.42	5288.38 ± 362.25	127196.67 ± 9346.03	209933.33 ± 14083.71
68.13	4500.81 ± 300.96	176746.67 ± 12531.63	250563.33 ± 16372.40
100.00	3741.94 ± 244.19	237003.00 ± 16317.23	289660.00 ± 18365.59

Table A20. Frequency, Complex Viscosity(η*), Storage Moduli (G') and loss (G") Moduli data of neat hydrolyzed starch/PLA blend modified with 2.5 wt % DGEBA after processed in the TSE at 170°C and Strain 4%

Freq. (rad/s)	η* (Pa.s)	G' (Pa)	G" (Pa)
0.10	11246.07 ± 736.41	147.40 ± 8.78	1780.35 ± 1116.61
0.15	9357.03 ± 608.36	140.50 ± 12.83	1875.12 ± 839.39
0.22	8667.73 ± 656.81	161.97 ± 18.83	2330.34 ± 752.56
0.32	8081.83 ± 573.78	263.02 ± 111.26	2817.88 ± 407.79
0.46	8400.38 ± 953.78	348.31 ± 102.57	3883.15 ± 435.70
0.68	8077.73 ± 834.05	504.65 ± 108.23	5479.88 ± 561.20
1.00	7897.19 ± 777.63	819.21 ± 147.71	7854.36 ± 7676.02
1.47	7811.13 ± 748.62	1473.50 ± 217.11	11369.87 ± 1080.48
2.15	7773.11 ± 718.20	2617.61 ± 307.94	16540.73 ± 1517.91
3.16	7644.73 ± 686.54	4425.18 ± 483.84	23766.13 ± 2118.46
4.64	7397.45 ± 646.36	7352.27 ± 766.77	33539.30 ± 2904.24
6.81	7040.44 ± 598.08	12043.53 ± 1212.29	46428.97 ± 3901.14
10.00	6596.13 ± 543.08	19397.73 ± 1881.93	63043.80 ± 5108.30
14.68	6061.73 ± 484.71	30519.47 ± 2861.93	83574.57 ± 6539.93
21.54	5468.77 ± 422.62	46686.07 ± 4201.57	108175.30 ± 8125.82
31.62	4841.58 ± 362.87	69272.63 ± 5984.99	136533.33 ± 9867.33
46.42	4213.80 ± 307.12	99720.23 ± 8253.23	168253.33 ± 11741.22
68.13	3602.20 ± 253.81	139246.67 ± 11052.52	202080.00 ± 13481.07
100.00	3006.88 ± 204.69	187540.00 ± 14256.50	235026.67 ± 14946.98

Table A21. Frequency, Complex Viscosity(η*), Storage Moduli (G') and loss (G") Moduli data of neat hydrolyzed starch/PLA blend modified with 0.5 wt % PEG-DGE after processed in the TSE at 170°C and Strain 5%

Freq. (rad/s)	η* (Pa.s)	G' (Pa)	G" (Pa)
0.10	13052.93 ± 168.88	162.67 ± 13.76	1295.06 ± 18.35
0.15	11064.47 ± 368.73	147.76 ± 8.36	1617.28 ± 54.86
0.22	10302.77 ± 276.25	157.16 ± 16.33	2214.03 ± 60.71
0.32	9790.91 ± 228.15	221.16 ± 13.58	3088.21 ± 73.28
0.46	9489.16 ± 243.14	330.15 ± 6.59	4392.09 ± 112.69
0.68	9270.85 ± 271.94	533.96 ± 23.63	6293.54 ± 183.99
1.00	9153.02 ± 265.30	960.93 ± 31.85	9102.44 ± 263.42
1.47	9116.20 ± 259.51	1710.84 ± 52.37	13270.90 ± 377.54
2.15	9014.81 ± 237.08	2921.78 ± 84.35	19200.77 ± 504.51
3.16	8799.28 ± 214.43	4911.98 ± 157.06	27388.77 ± 661.23
4.64	8462.89 ± 195.25	8184.03 ± 267.78	38419.17 ± 869.54
6.81	8012.21 ± 177.37	13464.87 ± 442.41	52899.67 ± 1134.35
10.00	7456.25 ± 158.30	21738.93 ± 714.92	71322.80 ± 1437.63
14.68	6823.99 ± 139.83	34224.27 ± 1092.39	94133.37 ± 1788.89
21.54	6119.60 ± 121.23	52248.60 ± 1600.95	121043.33 ± 2158.62
31.62	5386.43 ± 103.31	77225.30 ± 2247.73	151816.67 ± 2833.40
46.42	4657.99 ± 85.48	110606.67 ± 3026.79	185766.67 ± 2833.40
68.13	3959.34 ± 69.90	153636.67 ± 3932.94	221716.67 ± 3114.63
100.00	3284.55 ± 56.78	205680.00 ± 5013.17	256067.67 ± 3328.46

Table A22. Frequency, Complex Viscosity(η*), Storage Moduli (G') and loss (G") Moduli data of neat hydrolyzed starch/PLA blend modified with 2.5 wt % PEG-DGE after processed in the TSE at 170°C and Strain 4%

Freq. (rad/s)	η* (Pa.s)	G' (Pa)	G" (Pa)
0.10	11172.78 ±	134.73 ± 6.73	1108.92 ± 183.93
0.15	9141.18 ± 1428.79	135.23 ± 14.23	1334.90 ± 209.35
0.22	8099.46 ± 1165.30	153.56 ± 31.70	1737.91 ± 249.41
0.32	7540.46 ± 1114.62	199.00 ± 36.88	2376.17 ± 350.65
0.46	7217.90 ± 1022.60	254.09 ± 18.59	3340.55 ± 474.90
0.68	6917.87 ± 981.82	366.39 ± 50.71	4698.83 ± 667.03
1.00	6762.81 ± 968.20	593.64 ± 105.86	6736.67 ± 962.75
1.47	6656.12 ± 966.98	1035.75 ± 194.72	9714.68 ± 1406.88
2.15	6611.08 ± 962.52	1889.75 ± 194.72	14117.07 ± 2047.56
3.16	6551.61 ± 953.04	3300.65 ± 569.59	20453.23 ± 2961.19
4.64	6395.39 ± 925.32	5558.82 ± 962.77	29159.33 ± 4189.49
6.81	6144.66 ± 925.32	9215.89 ± 1567.74	40835.47 ± 5809.27
10.00	5813.58 ± 825.20	15061.63 ± 2518.55	56149.67 ± 7870.99
14.68	5403.09 ± 753.92	24153.40 ± 3975.62	75536.70 ± 10352.55
21.54	4928.40 ± 678.32	37718.47 ± 6059.46	99250.33 ± 16643.43
31.62	4412.69 ± 595.58	57217.03 ± 8945.88	127263.33 ± 16643.43
46.42	3884.03 ± 541.94	84224.63 ± 12798.70	15986.67 ± 20298.80
68.13	3359.03 ± 436.20	120286.67 ± 17786.32	194670.00 ± 23975.58
100.00	2836.38 ± 362.23	165556.67 ± 23814.67	230286.67 ± 27534.74

APPENDIX B

EXPERIMENTAL DATA FOR INTRINSIC VISCOSITY MEASUREMENT

TABLE B1. Intrinsic Viscosity calculation of PLA phase for hydrolyzed starch/PLA blend with different chain extenders

Sample Name	Conc. (g/dL)	Efflux Time ($t_{solution}$) (Sec)			Average (Sec)	η_{rel}*	η_{sp}**	I.V. (dL/g)	Average I.V.***
SP-0.0- CE-TSE	0.210	184.94	184.98	184.87	184.93	1.328	0.328	1.42	1.45
	0.140	168.68	168.95	169.13	168.92	1.213	0.213	1.43	
	0.280	205.81	206.09	205.98	205.96	1.480	0.480	1.50	
	0.198	181.83	181.91	181.48	181.74	1.306	0.306	1.45	
SP-0.5- 4370S-TSE	0.131	170.34	170.61	170.67	170.87	1.227	0.227	1.62	1.62
	0.087	160.14	159.59	160.84	160.19	1.151	0.151	1.65	
	0.226	195.55	195.91	195.98	195.81	1.407	0.407	1.60	
	0.151	176.70	175.11	175.22	175.68	1.262	0.262	1.61	
SP-2.0- 4370S-TSE	0.160	181.59	181.56	181.96	181.70	1.305	0.305	1.74	1.78
	0.107	167.54	167.01	167.08	167.21	1.201	0.201	1.77	
	0.260	213.90	213.78	213.95	213.88	1.536	0.536	1.78	
	0.173	188.36	186.56	188.26	187.73	1.349	0.349	1.82	

* $\eta_{rel} = t_{solution}/t_{solvent}$ ($t_{solvent}$= 139.205 sec)
** $\eta_{sp} = \eta_{rel} - 1$
*** I.V. = Intrinsic Viscosity (dL/g) calculated by using Solomon and Ciuta equation 3.2

TABLE B1. Intrinsic Viscosity calculation of PLA phase for hydrolyzed starch/PLA blend with different chain extenders

Sample Name	Conc. (g/dL)	Efflux Time ($t_{solution}$) (Sec)			Average (Sec)	η_{rel}*	η_{sp}**	I.V. (dL/g)	Average I.V.***
SP-0.5- 4380-TSE	0.201	184.44	184.67	184.09	184.40	1.325	0.325	1.47	1.49
	0.134	168.42	169.12	168.98	168.84	1.213	0.213	1.49	
	0.273	203.26	204.13	204.55	203.98	1.465	0.465	1.50	
	0.182	180.71	180.28	180.39	180.46	1.296	0.296	1.49	
SP-2.5- 4380-TSE	0.107	162.30	162.26	162.30	162.29	1.166	0.166	1.48	1.48
	0.071	154.20	154.27	154.20	154.22	1.108	0.108	1.47	
	0.232	191.43	192.13	191.96	191.84	1.378	0.378	1.46	
	0.155	174.24	174.63	174.44	174.44	1.253	0.253	1.51	
SP-2.5- DGEBA-TSE	0.103	161.67	161.49	161.72	161.63	1.161	0.161	1.49	1.48
	0.068	154.28	154.34	154.26	154.29	1.108	0.108	1.53	
	0.219	188.45	188.25	188.38	188.38	1.353	0.353	1.46	
	0.146	170.83	170.99	170.83	170.88	1.406	0.406	1.46	
SP-0.5- PEG-DGE-TSE	0.135	170.30	170.69	170.85	170.61	1.226	0.226	1.57	1.55
	0.090	159.77	159.81	160.22	159.93	1.149	0.149	1.58	
	0.220	191.41	191.48	191.24	191.38	1.375	0.375	1.53	
	0.147	173.10	172.94	173.24	173.09	1.243	0.243	1.54	

* $\eta_{rel} = t_{solution}/t_{solvent}$ ($t_{solvent}$= 139.205 sec)

** $\eta_{sp} = \eta_{rel} - 1$

*** I.V. = Intrinsic Viscosity (dL/g) calculated by using Solomon and Ciuta equation 3.2

TABLE B2. Intrinsic Viscosity calculation of PLA/AAC phase for Solanyl® blend 30R with different chain extenders

Sample Name	Conc. (g/dL)	Efflux Time ($t_{solution}$) (Sec)			Average (Sec)	η_{rel}*	η_{sp}**	I.V. (dL/g)	Average I.V.***
SL-0.0- CE-TSE	0.140	166.56	166.47	166.36	166.46	1.196	0.196	1.32	1.30
	0.093	157.43	157.55	157.55	157.51	1.131	0.131	1.35	
	0.270	191.53	192.60	192.34	192.16	1.380	0.380	1.26	
	0.180	173.46	173.69	173.68	173.68	1.248	0.248	1.28	
SL-0.5- 4370S-TSE	0.138	168.63	168.14	168.63	168.47	1.210	0.210	1.43	1.44
	0.092	158.47	158.56	158.63	158.55	1.139	0.139	1.45	
	0.254	195.77	196.23	196.20	196.07	1.408	0.408	1.43	
	0.169	175.50	175.98	175.68	175.72	1.262	0.262	1.43	
SL-2.0- 4370S-TSE	0.180	187.51	186.06	186.04	186.54	1.340	0.340	1.71	1.69
	0.120	169.28	169.30	169.31	169.30	1.216	0.216	1.69	
	0.260	208.45	209.22	208.45	208.71	1.499	0.499	1.67	
	0.173	183.57	183.68	183.78	183.68	1.319	0.319	1.68	

* $\eta_{rel} = t_{solution}/t_{solvent}$ ($t_{solvent}$= 139.205 sec)

**$\eta_{sp} = \eta_{rel} - 1$

*** I.V. = Intrinsic Viscosity (dL/g) calculated by using Solomon and Ciuta equation 3.2

TABLE B2. Intrinsic Viscosity calculation of PLA/AAC phase for Solanyl® blend 30R with different chain extenders

Sample Name	Conc. (g/dL)	Efflux Time ($t_{solution}$) (Sec)			Average (Sec)	η_{rel}*	η_{sp}**	I.V. (dL/g)	Average I.V.***
SL-0.5- 4380-TSE	0.199	181.58	180.97	181.19	181.25	1.302	0.302	1.39	1.40
	0.132	166.06	165.90	165.25	165.74	1.191	0.191	1.36	
	0.277	201.99	200.74	201.68	201.47	1.447	0.447	1.42	
	0.185	179.77	178.68	179.19	179.21	1.287	0.287	1.43	
SL-2.5- 4380-TSE	0.121	164.41	164.22	164.32	164.32	1.180	0.180	1.41	1.42
	0.081	156.88	156.57	155.95	156.47	1.124	0.124	1.48	
	0.221	186.57	186.55	186.50	186.54	1.340	0.340	1.39	
	0.185	179.77	178.68	179.19	179.21	1.287	0.287	1.43	
SL-2.5- DGEBA-TSE	0.136	167.66	167.38	167.80	167.61	1.204	0.204	1.41	1.40
	0.091	157.97	157.79	157.95	157.90	1.134	0.134	1.42	
	0.258	194.68	194.96	195.09	194.91	1.400	0.400	1.38	
	0.172	175.80	175.44	175.13	175.46	1.260	0.260	1.40	
SL-0.5- PEG-DGE-TSE	0.128	167.66	167.05	166.95	167.22	1.201	0.201	1.48	1.48
	0.085	157.44	157.56	157.94	157.65	1.132	0.132	1.49	
	0.231	192.95	193.00	193.12	193.02	1.387	0.387	1.50	
	0.154	172.95	173.95	173.12	173.10	1.243	0.243	1.47	

* $\eta_{rel} = t_{solution}/t_{solvent}$ ($t_{solvent}$= 139.205 sec)

** $\eta_{sp} = \eta_{rel} - 1$

*** I.V. = Intrinsic Viscosity (dL/g) calculated by using Solomon and Ciuta equation 3.2

TABLE B3. Intrinsic Viscosity calculation of starch phease for Solanyl blend 30R and hydrolyzed starch/PLA blend with ADR 4370S CE

Sample Name	Conc. (g/dL)	Efflux Time ($t_{solution}$) (Sec)			Average (Sec)	η_{rel}*	η_{sp}**	I.V. (dL/g)	Average I.V.***
SP-0.0- CE-TSE	0.266	232.09	234.29	233.45	133.28	1.338	0.338	1.15	1.11
	0.204	215.54	215.24	215.98	215.59	1.236	0.236	1.08	
	0.166	208.60	208.41	208.98	208.66	1.197	0.197	1.12	
SP-2.5- 4370S-TSE	0.269	231.90	231.27	231.24	231.47	1.327	0.327	1.10	1.10
	0.207	216.61	216.62	216.98	216.74	1.243	0.243	1.09	
	0.168	208.85	208.49	208.97	208.77	1.197	0.197	1.10	
SL-0.0- 4370S-TSE	0.243	232.43	233.56	232.90	232.90	1.336	0.336	1.25	1.24
	0.187	217.66	217.88	217.08	217.54	1.248	0.248	1.23	
	0.152	209.66	208.72	208.98	209.12	1.199	0.199	1.23	
SL-2.5- 4380-TSE	0.253	232.61	232.00	232.92	232.51	1.333	0.333	1.20	1.19
	0.195	218.38	218.52	218.64	218.51	1.253	0.253	1.21	
	0.158	208.20	208.98	208.54	208.57	1.196	0.196	1.17	

* $\eta_{rel} = t_{solution}/t_{solvent}$ ($t_{solvent}$= 174.37 sec)

** $\eta_{sp} = \eta_{rel} - 1$

*** I.V. = Intrinsic Viscosity (dL/g) calculated by using Solomon and Ciuta equation 3.2